Summer 8-22-2019

Novel Configurations of Ionic Polymer-Metal Composites (IPMCs) As Sensors, Actuators, and Energy Harvesters

Seyed Ehsan Tabatabaie
University of Maine, seyed.tabatabaie@maine.edu

NOVEL CONFIGURATIONS OF IONIC POLYMER-METAL COMPOSITES (IPMCs) AS SENSORS, ACTUATORS, AND ENERGY HARVESTERS

By

Seyed Ehsan Tabatabaie

M.Sc. Tarbiat Modares University, 2006

B.Sc. University of Mazandaran, 2003

A DISSERTATION

Submitted in Partial Fulfillment of the Requirements for

the Degree of Doctor of Philosophy

(in Mechanical Engineering)

The Graduate School

The University of Maine

August 2019

Advisory Committee:

Mohsen Shahinpoor, Ph.D., Professor of Mechanical Engineering, Advisor

Vincent Caccese, Ph.D., Professor of Mechanical Engineering

Afsoon Ebrahimi, Ph.D., Harvard-MIT HST, Harvard University, Wyss Institute for Biologically Inspired Engineering Brigham and Women's Hospital

William Davids, Ph.D., Professor of Civil and Environmental Engineering

Xudong Zhang, Ph.D., Associate Professor of Mechanical Engineering

NOVEL CONFIGURATIONS OF IONIC POLYMER-METAL COMPOSITES (IPMCs) AS SENSORS, ACTUATORS, AND ENERGY HARVESTERS

By

Seyed Ehsan Tabatabaie

Dissertation Advisor: Dr. Mohsen Shahinpoor

An Abstract of the Dissertation Presented

in Partial Fulfillment of the Requirements for

the Degree of Doctor of Philosophy

(in Mechanical Engineering)

August 2019

Abstract

This dissertation starts with describing the IPMC and defining its chemical structure and fundamental characteristics in Chapter 1. The application of these materials in the form of actuator, sensor, and energy harvester are reported through a literature review in Chapter 2. The literature review involves some electromechanical modeling approaches toward physics of the IPMC as well as some of the experimental results and test reports. This chapter also includes a short description of the manufacturing process of the IPMC.

Chapter 3 presents the mechanical modeling of IPMC in actuation. For modeling, shear deformation expected not to be significant. Hence, the Euler-Bernoulli beam theory considered to be the approach defining the shape and critical points of the

proposed IPMC elements. Description of modeling of IPMC in sensing mode is in Chapter 4. Since the material undergoes large deformation, large beam deformation is considered for both actuation and sensing model. Basic configurations of IPMC as sensor and actuator are introduced in Chapter 5. These basic configurations, based on a systematic approach, generate a large number of possible configurations. Based on the presented mechanisms, some parameters can be defined, but the selection of a proper arrangement remained as an unknown parameter. This mater is addressed by introducing a decision-making algorithm.

A series of design for slit cylindrical/tubular/helical IPMC actuators and sensors are introduced in chapter 5. A consideration related to twisting of IPMCs in helical formations is reported through some experiments. Combinations of these IPMC actuators and sensors can be made to make biomimetic robotic devices as some of them are discussed in this chapter and the following Chapters 6 and 7.

Another set of IPMC actuator/sensor configurations are introduced as a loop sensor and actuator that are presented subsequently in Chapter 6. These configurations may serve as haptic and tactile feedback sensors, particularly for robotic surgery. Both of these configurations (loop and slit cylindrical) of IPMCs are discussed in details, and some experimental measurements and results are also carried out and reported. The model for different inputs is studied, and report of the feedback is presented. Various designs of these configurations of IPMC are also presented in chapter 7, including their extension to mechanical metamaterials and soft robots.

ACKNOWLEDGEMENTS

There are several entities I would like to thank for their support of my Ph.D. dissertation research and program. First, I would like to thank the work of my Advisory Committee throughout the process, including the reading of this dissertation and making essential suggestions. Special thanks to my advisor Professor Mohsen Shahinpoor, for technical direction, support, and more importantly, for his encouragement in my academic pursuits.

I gratefully acknowledge the support provided by the University of Maine Department of Mechanical Engineering, the University of Maine SJHF and the University of Maine Graduate School. Also, I would like to acknowledge NASA Epscor and Maine Technology Institute for their financial support.

Finally, I would like to thank my family for many ways of supports they provided me during my Ph.D. program.

TABLE OF CONTENTS

LIST OF FIGURES

LIST OF TABLES

CHAPTER 1

1 INTRODUCTION

Ionic polymer metal composites (IPMCs) are a member of electroactive polymers (EAPs) that demonstrate significant bending and flexing deformation under a small imposed electric field. These materials generate electrical fields by deformation, and in case of applying an electrical field, they deform. Because of their response to external stimuli, this group of ionic gels classified as smart materials. The reversible reaction of this material to input stimuli has been popular for many years, and many applications propose to demonstrate the capability of these materials. As it comes to a better understanding regardless of the diverse electromechanical models proposed to define what happens inside the material, the application side of these materials appeared to be more than what presented so far.

There are several descriptions in the pertinent literature on the behavior and characteristics of ionic polymer metal composites (IPMCs). This part covers a selected presentation of the material definition, applications, electromechanical modeling, and experimental reports. The basic understanding of the material involves its chemical structure and manufacturing models. Such information presented much from related research and as concise as possible. The application part of the review mostly involves the actuation and sensing applications. This part categorizes the applications, based on the formation of this material and the number of the elements.

The electromechanical modeling approaches for modeling IPMCs have diverse directions. From the application point of view, these descriptions define the material deformation when exposed to electrical charge and vice versa. Regarding this modeling, one of the straightforward explanation used as the representation to define mechanical deformation presented in the following chapters. Through literature review, regardless of the method of approach of the literature, some of the experimental results were also reported.

Modeling of the IPMC in a mechanical form considered as two individual task one for actuation and the other one for sensing and energy harvesting mode. The modeling for the actuation mode involves a geometric description of the deformation of IPMC, for example in cantilever mode, which is one of the commonly reported deformations. This model defines the geometrical relation as if the material undergoes a uniform bending moment. For this model, geometric constraints of the IPMCs in actuation were derived. The related curve for further applications of the model was presented and based on a series of experimental test results, the know-how of the graph was presented. The modeling for the IPMC, in actuation for other boundary conditions, are in the category of Euler-Bernoulli beam theory for a beam under moments. Mechanical deformations of homogeneous materials for IPMCs are expected to follow this beam theory.

The sensing modeling looks at the material as it undergoes different types of loading application in chapter 4. The beam modeling for post-buckling formation is

the approach used for developing the idea and nature of the deformation. Here the implemented modeling for post-buckling considered to be suitable as the deformations follow the trend of the closed-looped expressions. The other characteristics of the used buckling and post-buckling model are not considered in this dissertation. The derivatives of these functions were used for further definitions. The necessity of considering the full formation of curvature was discussed in this chapter. For the next step based on the variation of curvature as an essential parameter in sensing characteristics of IPMC sensors was derived. In the next part of chapter 4, elastic modeling of elastic material presented, which is expected to be more accurate. This formation ends up being in the form of elliptic integrals while the former model uses trigonometry functions. At the end of this session, a comparison plot of these function was presented. The plot demonstrates that these functions have similar critical points, while the intensity of their behavior is different for the rest of the regions.

The individual modeling approached presented chapter 3, and 4 are the base elements of configurations. In the assembly, some parameters play an important role and make distinguished models. Some of these new elements include types of boundary connections, number of elements, and electrical connections. For the assembly, these parameters and some basic parameters, for example, the complexity of manufacturing as if the manufacturing process involves pattern coating or not, are discussed in chapter 5. This new set of parameters generates lots of possibilities

for actuators, sensors, and energy harvesters while causing complexity for selecting a proper configuration. As a solution, a decision-making algorithm introduced to help the potential user make a logical decision for selection.

As an element for haptic feedback, a looped configuration for IPMC introduced in chapter 6. Characteristic of this element includes a mathematical model of the deformed shape, response to front and side deformations reported in this chapter. The tests also include load-deformation and the response of similar looped sensor on a smaller scale version. Later, a new version for this sensor, which includes test reports, presented at the end of chapter 6. This new formation uses the already introduced configuration as the base element. To cover another part of the promise of this dissertation by introducing the essential elements and their mathematical modeling, some devices based on these elements presented in chapter 7.

CHAPTER 2

2 LITERATURE REVIEW ON IPMCs

2.1 Introduction

This review is directed toward providing the basic understanding of IPMCs' developments and their configurations in the form of actuator, sensor, and energy harvester applications. This chapter presents in the form of "What is IPMC?", "Applications", "Modeling approaches", and "Experiments on IPMC."

The first part will explain IPMC and its mechanism, some information on the IPMC manufacturing process, and essential characteristics of IPMC. Knowing the IPMC, the next session introduces some of the applications for the IPMC. This part is essential to explain the expected domain for these types of materials and a demonstration of possible future advancements. This part covers the sensing, actuation, and energy harvesting applications introduced for IPMC.

By exploring the above part of the literature in a combination of introducing the models and configurations, it is essential to know the proposed modeling approaches for IPMC. This part will connect the practical aspect of the proposed configurations. For this matter, the next part of this literature review covers some of the modeling approaches. The goal is to combine one of the modeling approaches

with the mechanical deformation of the proposed model of IPMC actuators, sensors, and energy harvesters.

2.2 What is IPMC?

Ionic polymer metal composites (IPMCs) are a member of electroactive polymers (EAPs[1]). History of observing ionic material deformation goes back to 1948 and the works reported by Kuhn, W. et al. in "Helvetica Chemical Acta" [2–4]. These materials demonstrate significant bending and flexing deformation under small imposed electric field (a few V/mm), as well as providing sensing and energy harvesting capabilities when deformed. The physical deformation can be due to mechanical and environmental dynamics such as wind or water waves. The deformations can be regulated by other means such as mechanical force and electrical potential[5]. They work both in the air and in polar liquids such as water [2,6,7]. The essential mechanism of actuation and sensing in IPMC demonstrated in Fig. 2.1. When IPMC is at rest, there is no biased of the concentration of the cations in the material molecular structure. However, in the deformed shape, depending on the applied deformation or applied voltage, the charge concentration on each side will be different.

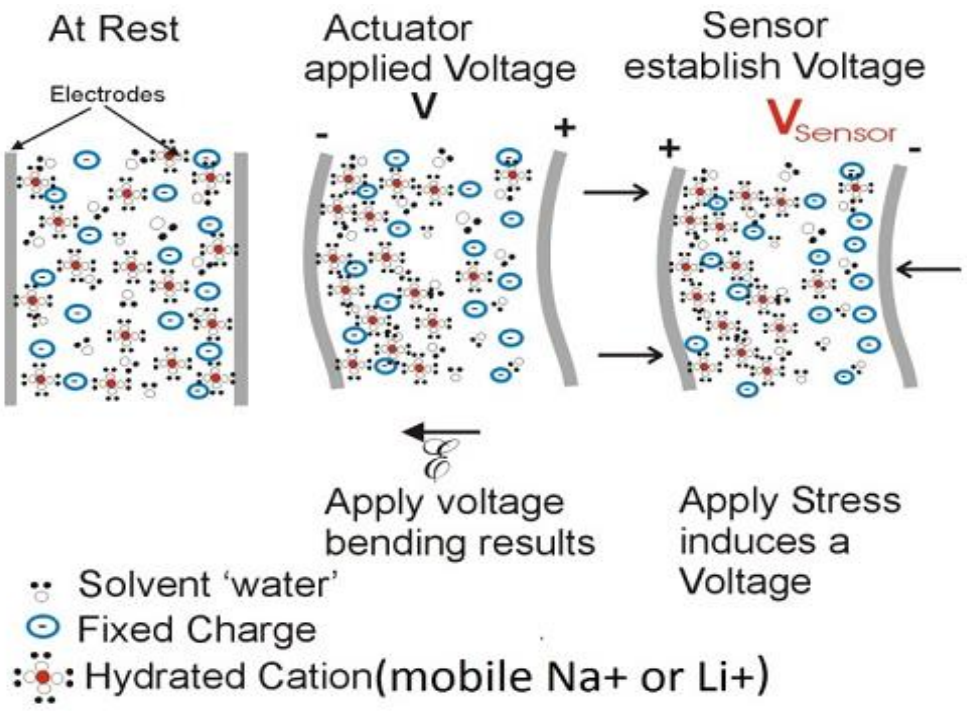

Fig. 2.1 The essential mechanism of actuation and sensing in IPMC

Tadokoro et al. (2002)[8] introduced a categorized mechanical characteristic of IPMC. However, A more comprehensive properties can be found in "Ionic Polymer-Metal Composites (IPMCs)" Shahinpoor et al. (2016)[9]. Some of these properties restated here.

- Their driving voltage for a small sample (1cmx4cmx0,2mm) for maximum force or deflection is about 4 volts. The regular operation voltage is 1 ~2 Volts.
- They have a broad bandwidth in actuation and sensing up to kilo Hz.
- Their elastic modulus is about 1 G Pa.
- Manufacturing in size of less than a millimeter is possible.
- Their durability is more than a million cycles.
- Their force density is about 40.
- They do work in liquids such as water or other polar liquids.

In a comparison review, properties of IPMC, Shape memory alloys (SMA), and Electroactive ceramics (EAC) are discussed by Shahinpoor et al. (1998)[6]. The force density for IPMC believed to be around 40 in a cantilever configuration, which means the material was able to lift a weight 40 time of its own.

2.2.1 Molecular Structure

The base of IPMCs composites is ionic polymers such as perfluorinated sulfonic ionic membranes. Good examples of such materials are DuPont Nafion® and Asahi ACIPLEX®. Also, there are perfluorinated carboxylic ionic membranes such as Asahi Flemion® that demonstrate similar characteristics. The base material is composed of a cross-linked polymeric network Baek et al. (2004)[10]. This network structure imbibes solution and swell. These ionic polymers are produced by copolymerization of a perfluorinated vinyl ether comonomer with tetrafluoroethylene (TFE), resulting in the chemical structure presented in Fig. 2.2 for Nafion® or similar chemical structures such as ACIPLEX®, or Flemion® [11].

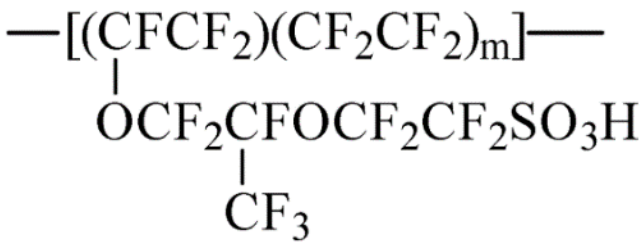

Fig. 2.2 Nafion® chemical molecular structure

The base material depends on their ionic group, is called sulfonate or carboxylate. The one represented in Fig. 2.2 is a sulfonate membrane (it has SO_3^- on its short side termination). In this material, a few fixed ionic group located at the end of side-chain create nano-channels that is referred to as cluster networks Shahinpoor et al. (2003)[7]. One of the theories for micro molecular interaction in IPMCs describes these nano-channels as a gateway for ions displacement inside the Nafion®.

Mojarrad (2001)[4] reported mechanical characteristics of Nafion®-117 as the adopted base material for IPMC manufacturing as a deviation of Nafion®. Nafion®-117 is stiffer with a higher module of elasticity. Following are the characteristics of Nafion®-117 reported in references [12,13].

Table 2.1 Properties of Nafion®-117 [13]

Property	Value
Equivalent weight:	1100 g $gmol^{-1}$ SO_3-
Thickness:	200 micron
Conductivity:	0.1–0.12 S cm^{-1}
Area resistance:	5 Ohm cm^{-2}
Water uptake capacity:	Up to 30% at room temperature
Volume expansion on hydration:	12–15%

The surface of an IPMC is chemically plated or physically coated with a conductor such as platinum, gold, or other noble metals. Because of their response to external stimuli, IPMC is classified as smart materials. This behavior leads the

material usage proposal in a verity of biotechnology and medical applications such as drug delivery, biomimetic actuators and sensors, and chemical valves [14–18]. Such broad and critical applications open the necessity of modeling and prediction of the behavior of ionic polymers in response to stimuli. Hamlen et al. (1965)[19] and Toyoichi & Izumi (1982)[20] are among the earliest reports of these type of ionic polymers responses to an electrical charge. Concerning studying what is happening inside these family of polymers, there are several studies and proposed modeling towards providing a better understanding of these materials [21–25]. One of which is essential is the report by Mojarrad and Shahinpoor (1997) that there is an almost linear relationship between generated voltage and tip displacement in a cantilever beam configuration for these IPMC materials[2].

2.2.2 Manufacturing

Making an IPMC sample is possible in several methods and procedures. Since Nafion® membranes are not melt-processable, Nafion® precursor resins or XR Resins can be used and melted to get a desired shape and geometry for the IPMC actuators and sensors. In this manufacturing processes for IPMC, dry precursor Nafion® granules, which is called the XR Resin, used in a casting or a hot-molding process, as described by Tiwari (2010)[26], Asaka (2009)[27]and Bahramzadeh (2014)[13]. In the process XR Resin pellets are cleaned by hot water for 30 minutes, then the process is followed by cleaning them in 0.5 M sulfuric acid. The dried granules are then heated at about the deformable point temperature at 400^{o} F to the

desired shape and cooled down while it is under mold pressure. In this process, many shapes are possible to form the granules to and coat them with other methods at the next step. After the desired shape created, the XR-Resin material needs to be hydrolyzed. Hydrolyzing XR-Resin involves creating a mixture of 15% KOH weight in pellets (about 30 grams), and 35% Dimethylsulfixides (DMSO) weight in DMSO liquid is about 70 grams and 50% DI water, weight in 100 ccs followed by mixing and heating up to 40 to 50 degrees Celsius for hydrolyzation. Formed XR-Resin objects will be in this solution to be hydrolyzed overnight.

Other processes involve hot pressing of layers of Nafion® film at 180^{o}C and 50 MPa to generate a thicker membrane as Lee et al. (2006) and Bonomo et al. (2010)[28,29] reported. Using Liquid form of Nafion® is another method of manufacturing the desired shapes of IPMCs. This form can be a liquid Nafion® solution[30]. In this process, the solution mixed with boiling water and dried-out to the desired form[31,32].

A more documented report by Kim and Shahinpoor (2003)[33] describes a process to generate the IPMC from Nafion® film. In this process, platinum salt or other metallic salts through a chemical oxidation-reduction process will be plated on the outer surface and to some extent inside the surface of the base material[2]. The chemical plating procedure uses an oxidation-reduction reaction (REDOX) to deposit a metal or a conductor on the macromolecular network of the material. The Nafion® is first oxidized by a water-soluble metallic salt such as tetraamine

platinum chloride hydrate or ($Pt(NH_3)_4Cl_3 + water$) and then reduced by either sodium borohydride ($NaBH_4$) or lithium borohydride or ($LiBH_4$). The chemical reaction can take the following form.

$$LiBH_4 + 4[Pt(NH_3)_4]^{2+} + 8OH^- \Rightarrow 4Pt^0 + 16NH_3 + LiBO_2 + 6H_2O$$

Kim and Shahinpoor explained the manufacturing process of ionic polymer metal composites (IPMCs) (2003)[33] using the Taguchi experimental optimization techniques.

On the group of alternative manufacturing methods, there are some efforts to produce IPMC from other available forms of Nafion® like powder, XR-Resin, and liquid[9]. They generated a thicker IPMC membrane and were able to produce a thick layered laminated of IPMCs and test the sample successfully. In another effort to alternate the base material, Nano cellulose IPMC manufacturing was done[34]. In this effort, by using liquid Nafion® and cellulose nanofiber, a composite material was manufactured and its deformation in response to electrical stimuli demonstrated. This result obtained from a fragile layer of the produced nanocomposite material. The group reported positive expectation in the application of cellulose nanofiber in IPMC production and its applications. In another effort[35] a mixture of Nafion® solution used through casting method. The result demonstrated a %30 reduction in using Nafion® to make the membrane.

Some of the manufacturing processes of IPMCs involve techniques for improving the quality of the final products. Kim and Shahinpoor (2003a, 2001b, 2002c)[32,33,36] and Bonomo et al. (2010)[29] are the examples that provide an overview of some of these parameters towards improving the load and motion range capacity of IPMCs. For example, the sensitivity during the sensing process is observed to be related to the average size of the particle of the reduced metallic part inside the material. The other important characteristic of IPMC is their surface resistance, as based on the experimental results reported in the article by Punning et al. (2007)[37], the inner surface resistance of IPMC in bending decrease while the outer layer demonstrates significant increment in the electrical resistance.

Another manufacturing/post-manufacturing process is to physically load the conductive powder into the polymer network forming a uniform layer before surface electroplating process[36]. This layer function as the primary conductive medium in the composite and helps with reducing the surface resistance and increasing the manufacturing efficiency.

For improving the base material properties, by using liquid Nafion® solution, a porous membrane was produced by Zhao et al. (2016)[38]. The resultant product was able to demonstrate a much more level of deformation under a similar voltage.

A final step in preparing an IPMC sample can be encapsulating the product. This process will preserve the moisture inside the material and support the element

from the operation environment, particularly when it comes to micro size and industrial applications[39]. A downside of the encapsulating, as stated by Rinne et al. (2019), is increasing the young moduli. This downside even may cause the membrane to have lower performance. However, there are some other reports for this post-processing procedure proposal to have more stable feedback from IPMC by Shahinpoor et al. (1998) [6,40–42] and Lei et al. (2014)[43]. In an experiment done by Barramba et al. (2007)[40], the group successfully encapsulated a sample, and the results demonstrate better achievement in maintaining actuation displacement for the encapsulated IPMC. Lei et al. (2014)[43] reported more stable sensing results from encapsulated IPMC in sensing mode as well. In the result, they demonstrated variation in normalized sensing result of IPMC has a direct relation with increment in relative humidity.

2.3 Applications

The primary characters of IPMCs are surface charge differential due to deformation and deformation due to an applied electrical charge. These responses classified these materials as actuators, sensors, and energy harvesters. The actuation characteristic of these materials will cause variation in the shape of the base material Punning (2004)[44], Yamakita (2005)[45], and Paquetre (2004)[46] or a pattern forming. On the other hand, the sensing and energy harvesting of the IPMC material collect dynamic inputs of arbitrary environmental deformations and convert it to electricity. These deformations can be changing the shape of the

material or its thickness. An early example of variation in thickness and receiving feedback can be introducing the application of these materials named ion-exchange-membrane metal composite (IEMMC) as vibration damper and accelerometer by Sadeghipour et al. (1992)[47]. Another similar application introduced by Mojarrad (2001) and Ferrara et al. (1999)[4,48] to measure pressure in the human spine. In addition to this, the energy harvesting characteristics of IPMCs, Tiwari et al. (2010)[26] uses a disc-shaped IPMC object for energy harvesting application. Their results demonstrate a direct relation between charge generation and the coated area for implementing the bending concept to the disc-shaped IPMC sample. In this concept, deformation of the material is related to its physical connection with other components. Another example of energy harvesting introduced by Martin et al. (2005)[49]. In their device, a weight used as a head mass with a pair of IPMCs used as the legs attached to the base mass. The system had an operation frequency of 0.2 to 4.2 Hz and lateral acceleration of about 1g. There are some other applications for these materials like water electrolysis[50], humidity sensor[51,52], and a reflective device by Chen et al. (2015)[53].

2.3.1 Sensor Applications

Sensor applications of IPMCs are generally based on their bending behavior as they generate voltages when deformed. In some other cases, researchers measured the capacitance and electrical resistance properties of the IPMC as a way towards feedback measurements reported by Smoukov et al. (2016) and Nakabo et al.

(2007)[54] [55]. Here some of the ideas presented by researchers for sensor applications of the IPMC are listed.

Using a single cantilever beam formation, Mojarrad et al. (1997)[2] demonstrated linear relation between the generated signal and applied deformations on an IPMC. The active part of the IPMC was 25 mm x 5 mm with the thickness was around 200 microns. Tip displacement was up to 16 mm to generate maximum differential voltage up to 35 mV. With a linear arrangement of the cantilever beams formation, Abdulsaddat et al. (2012)[56] used a linear array of IPMC in a cantilever configuration. They implemented a neural network to predict the fluid movement with the assistance of received signal from IPMCs. They demonstrated by increasing the number of sensors and training points the error will decrease.

Considering the input deformation from a particular source as acceleration, Ando et al. (2013)[57] proposed a configuration to measure seismic behavior by implementing IPMC and Ferrofluids. Interaction of Ferrofluids and IPMCs in a cantilever configuration is the base of their design. They proposed a tuning scenario for the system with the application of an external magnetic field to change fluid viscosity behavior. In another configuration by using a lumped mass attached to the end of an IPMC strip in a cantilever configuration, Paola et al. (2008)[58] proposed a vibration sensor model. In their concept, the mass will generate the corresponding force/displacement due to vibration and movement of the end of the IPMC.

Using the bending characteristic of IPMC, Bonomo et al. (2008)[59] measured the tip displacement of another IPMC in actuation mode. Further, Brunetto et al. (2008)[60] designed a small scale viscometer by stacking two IPMCs strips, one as a sensor and the other one as an actuator. They both developed a mathematical model for their device.

In another biomimetic soft configuration, by considering mid-plane of a conventional IPMC rectangular form as a fixed plane, Ming et al. (2018)[61] used the bending characteristic of IPMC to predict bending angle of joints in a glove as a wearable smart material. In their smart glove system, they were trying to detect cardiovascular pulses and read Braille language. Seidi et al. (2015)[14] used IPMC as impact sensor in headgear to detect the severity of the impact in case of an accident. For a study of the electrometrical and morphological characteristic of IPMC, Hong et al. (2017)[62] used a test methodology to apply compression stress on the material surface.

In application of IPMC for haptic feedback sensor in a looped configuration Shahinpoor et al. (2018)[15] is an excellent example of the possible use of these materials in soft biomimetic robotics. In the proposed application, they used a looped IPMC striped. The model by receiving deformation generates a voltage signal with a linear relation to the input deformation. They demonstrate a linear relationship between the applied displacement deformation and the generated

voltage. They demonstrated the possibility of using looped IPMC for future haptic feedback application.

An omnidirectional, tubular IPMC sensor was introduced by Lei et al. (2016)[63]. In the design concept, a tubular Nafion® used to make a tubular IPMC then the external coated layer divided into four separate strips. A common electrode used for the inside surface. Later they demonstrated an electromechanical model and obtained some of the modeling constants through experimental measurements. They were able to successfully predict the generated signal based on the position of the tip of the sensor. Introducing this type of sensor and actuator goes back to the works done by Tsugawa (2014)[64]. They proposed, designed, and made the tubular IPMC and tested for actuation and sensing characteristics.

Gudarzi et al. (2017) demonstrated a linear relationship between pressure and generated signal using the bending characteristic of IPMC in a disc shape configuration[65,66]. In this configuration, the pressure will deform an IPMC sample in diaphragm shape. In addition to the bending characteristic of IPMC used in the above sensors, IPMCs used for shear and compression sensing. In their sensing procedure, the capacitance and resistance of the IPMC samples were measured.

Based on the damping properties of IPMC, Sadeghipour et al. (1992)[47] introduced a vibration sensor to be one of the earliest reports of sensing application

of this material[67]. In their design proposal, they modeled the system as a damped cantilever and proposed an accelerometer.

Bahramzadeh et al. (2011)[68] tested IPMC in a dynamic curvature sensing. The results demonstrate a nonlinear relation between curvature and the generated voltage. They utilized a cantilever beam form to experiment with the curvature sensing of a deployable structure. In 2017 Song et al.'s reports represent almost a linear relation between curvature and sensing signal for sensing signal vs. curvature and bending angle[69].

On the aspect of energy harvesting of IPMCs, Cellini et al. (2014) used a cantilever beam configuration for interacting in a fluid environment[70]. The IPMC strips were attached to a turbine blade underwater to generate electric voltage as turbine rotated them. As a more general form, a linear arrangement of these cantilever beams was considered to serve as the energy harvester. The energy harvesting considered to be possible for the range of 10-100Hz with maximum potential power density from 0.5 to 100 mW/cc for a range of vibration from 50 to 350 Hz[71].

Table 2.2 represents a comparison for generated power of different transducers. These materials are IPMC, piezoelectric ceramic PZT (lead zirconate titanate), and PVDF (polyvinylidene difluoride). Patel et al. (2018)[71] concluded the parallel

electrical configurations of harvester has a significant impact on the amount of harvested energy.

Table 2.2 Comparison of generated power of different transducer materials[71]

Material	Applicable Frequency	Order of Generated Power	Form
IPMC	Less than 100	Micro-Watt	Flexible
PZT	More Than 100	Milli-Watt	Stiff
PVDF	Less than 100	Micro-Watt	Flexible

IPMC in the form of tubular was used to sense a torsional input by Sharif et al. (2018)[72]. During the experiment, a pure torsion was applied to the tip of a tubular IPMC demonstrating a pick pulse at the beginning of the applied torque and when the direction of the torque changes in the opposite direction.

Ming et al. (2018) considered the sensing characteristics of this material a reason to embed them into a glove to measure the pressure in a biomimetic application for smart gloves[61]. Ming et al. (2018) anticipated reading body pulses in medical applications and reading the Braille alphabet.

Giacomello et al. (2011) studied a large flag hosting IPMC for energy harvesting of IPMC[73]. The study involved fluid-structure interaction analysis ending a closed-looped form of expression.

2.3.2 Actuator Applications

In contraction to the sensing application of IPMC in actuation or as an actuator, there are more possibilities and proposed applications. The large displacement in actuation is an important outcome of these materials that caused to be patented (1993)[74] as an actuator element, later (2002)[75] as sensor and actuator element, and later in 2007 in a method of fabrication[76]. However, introducing the actuator element can be traced back to 1992 as the work by Masao Dot (1992)[77]and the letter to Nature[78] that contained more than a 40-year-old reference[20].

Some of these applications are integrated systems[79] [60,80], and some others used the IPMC as an actuator for autonomous swimming device[81]. Here the aim is to demonstrate the actuation application in order of the number of components used for a mechanism. Most of the actuators in these configurations are made by using the conventional ~0.2 mm Nafion® unless otherwise stated.

2.3.3 Cantilever IPMC actuators

Using the activation characteristic of IPMC to move a fish like a robot or floating object reported by several groups with different applications [4,82,83]. Their robot was less than two inches in length. They concluded that the speed of the device is controllable by adjusting the amplitude and frequency of the input voltage.

The maximum speed of 0.8 in/second achieved for a floating object. In their design, they used a pair of IPMC with fin-shaped components attached to their ends. They developed a mechanism to control the direction of the swimming device for forward, right turn, and left turn. In another concept, Kim et al. (2005) and Jung et al. (2003)[84] [85] used the undulating motion to present a wireless tadpole robot. The frequency of input was less than 10 Hertz. The size of the device was less than 100 mm in length with the actuator part to be almost 20 mm by 4 mm and 200-micron thickness. They present an analysis of the fin motion and based on the experimental results at a frequency near 1 Hertz device had the maximum thrust amplitude while demonstrating a linear relationship between maximum tip displacement of the actuator and the input frequency. Paquetre (2005)[46] introduced IPMC for aquatic robotic propulsor. In their experiment, they recorded the generated thrust vs. voltage for a sample size of 30 mm by 4 mm and 0.15 mm for thickness. They recorded the maximum thrust pulse for the input frequency of 4.0 Hertz. The maximum trust was 6.5mN, causing the speed of 23 mm/second. Chu et al. (2012)[86] represent a review for the proposed application of smart materials, including IPMC for underwater locomotive where different material classified for their application and ability for underwater locomotive devices.

Arena et al. (2006) designed a worm-like robot utilizing an assembly of several bending actuators[87]. The system was equipped with a high-level controller and was able to move along a line.

For medical applications, Gua et al. (2002) and Fango et al. (2010) proposed a catheter device[88] [80]. The devices had two active bending directions. In these configurations, the tip of the catheters had an IPMC material as the bending actuator. For their devices, they tried to resolve the issues like heating up and electricity leakage and response time. Both were able to demonstrate the practical aspect of their design proposal.

Lumia et al. (2008) introduced a micro-gripper model by using a pair of IPMC samples. In this application, the samples were cut to form a sharp tip of the microgripper. The test results demonstrate the ability to lift a weight of 15mg[89] and being able to lift as small as 0.63mm (weight 0.45mg) up to 2.34mm (weight 75.8mg)[90]. In another study, a more theoretical approach of this device was studied[91].

A pair of cantilever IPMC used to work alternately and rotate a rotor by Aw et al. (2014)[92]. The article also demonstrated an alternative form of the motor by incorporating more actuators to get a smoother rotation.

In a more complex application, a strip of IPMC embedded into a soft tube to control the direction of the tube[93]. They used IPMC strip with cross-section 1mm by 1mm on four side of a silicon tube. The setup was able to generate up to 0.5 mm tip displacement under 2-volt input.

Mojarrad and Shahinpoor (2002, 2008)[94,95] developed a biomimetic robotic propulsion device. They used two samples 2 X 0.25 in^2 attached to a floating object on water and discussed the undulating motion of the IPMC. They demonstrated a linear increase in the speed of the device (from 0.2 to 0.8 in/Sec) by increasing the input frequency to the system (1 to 5 Hertz). The proposed model extended to a more underwater application as a fish fin. In another floating object application by Ymakita et al. (2005)[45], the actuation properties of IPMC are used to produce a snake-like swimming robot. Their model consists of three blocks attached by IPMC strips. Each IPMC actuator strip acts like a rotary joint between blocks. They provide an experimental result for speed vs. consumed power and speed vs. input frequency. Their maximum speed reached when the input pulse had a frequency less than a Hertz. They demonstrated these test results for different ionic materials (sodium, cesium, and tetraethylammonium). Their result indicated a higher speed for sodium actuator in both cases. Similar to this application, Olsen et al. (2018)[96] used a pair of bent IPMC actuators for each joint. In terms of land robots, a single walking mechanism proposed by using two IPMC strips in a cantilever configuration parallel to each other by Moghadam et al. (2015)[97]. In the proposed structure, two parallel IPMC samples control a mutual point. The group demonstrated kinematic of their model and through simulations were able to meet any point inside a hypothetical circle. Their mechanism is in its early stage of the experiment to demonstrate the simulation results. They proposed an updated version of their device with 6 degrees

of freedom. They concluded that the capability of their micromanipulator is applicable for dynamic micromanipulation in soft robotics.

Extending the number of actuators provide more power and possibility for complex movements. Jellyfish made as a biomimetic object, by placing four IPMC actuators around a disk in a cantilever configuration. The setup used 5 cm by 0.8 cm (200-micron thickness) samples and was able to move at 1.5 mm per second[98]. Total generated force vs. different input frequency was measured and resulted in changing the input frequency from 1 Hertz to 2 Hertz, which decreases the generated force from 0.879 g-forces to 0.544 g-forces[99].

In another biomimetic concept[44], eight pairs of IPMC used to mimic an African ray. They attached the actuators to the sides of a floating object. The other end of the actuators was attached to an IPMC strip film. This film gives more support for a smoother motion of the system. This concept repeated in a process to fabricate a mold around the membrane in another research inspired by manta ray Chen et al. (2011)[100].

In a similar concept to what this manuscript is trying to present, Yamakita et al. (2004)[101] introduced a unit liner actuator based on a combination of four IPMC that demonstrates a linear displacement actuation. They provide a larger size of the actuator by combining several individual units. This concept is an excellent example

of the actuators made with IPMCs for biomimetic applications. Their design intended to provide the possibility for manufacturing a walking robot.

Chen (2017)[102] presents a review on robotic fish enabled by IPMC. One of the significant characteristics in this application is the large deflection of these materials. They reviewed a theory on the model of the fin tail beam and beam dynamics in a fluid and presented an application of IPMC used as the fish caudal fin and tail by presenting several models of underwater fishlike objects.

In a different configuration, Shahinpoor et al. (1998)[6], extended the applications by modifying the cantilever beam. By adding a hook to the end of a single IPMC and arranging the IPMCs in a circular configuration, the group demonstrated the possibility of using these materials in soft biomimetic robotics to grip and hold weights relying on the base material mechanical properties. Another concept was using deformed striped that can get the input signal from a platform connected to each end. They involved flexible material in addition to the IPMC for the tail and fin they designed.

Nguyen et al. (2015)[103] introduced a configuration for a walking robot using the cantilever concept of IPMC actuators. In this configuration, four sets of IPMC actuators were used to move two active legged of a four-leg robot. The proposed concept illustrates the possible movement of the actuators and the possibility of programming these types of robotic devices. Similar to their mechanism, by using

two active polymers, a two-link manipulator introduced by Kim et al. (2016)[104]. The manipulator intended to mimic an index finger to pick or hold objects. They were able to generate 20 gram-force.

A Venus flytrap model was subject of biomimetic applications of IPMC for several studies by Shahinpoor (1995) and Shahinpoor et al. (2011) [105],[106]. These design extended to a walking base robot for a flytrap by incorporating 8 IPMC actuators by Shi et al. (2016)[107]. The actuators' size was 24 mm by 3 mm and 0.2 mm thickness with input frequency between 2.5 Hertz to 3.5 Hertz was able to have a maximum speed in movement and rotation.

In a drug delivery device, a system proposed to use IPMC actuator and remotely controlling the device[108]. This device consisted of a drug capsule closed by IPMC sample and a power generator that produce signals by receiving magnetic resonance field. This combination introduced a wireless activation mechanism. The device with input frequency around 13.6 MHz was able to generate 1.89V. In a similar approach, 2.2V with 25Mhz reported by Cheong at al. (2018)[109]. The mechanism was able to lift the actuator 0.1 millimeter. Wireless IPMC actuation was used in a microgripper device design by Cheong at al. (2018)[110].

An excellent example of an underwater vehicle design application is the design of Propulsion and Maneuvering in Bio-Inspired Underwater Systems[111]. This design

studied the bending/flapping and twisting of the actuator for the proposed design concept.

2.3.4 Addition to Cantilever IPMC actuators

In the previous session, actuators had a cantilever beam formation. In a different configuration, Tadakoro et al. (1998)[112] bent the IPMC sample to form semicircular formation and controlled the actuator from both ends. By placing several of these individual components, they demonstrated a platform equipped with a series of bent IPMCs sample to move the object. In a similar application by using the bent formation, they demonstrated a possibility to have palm manipulation hand. The design supposed to be able to hold and move objects by working on both sides of the object.

Shahinpoor (2008)[95] proposed different shapes of IPMC actuators for biomimetic applications. The shape is an eight-finger made of a unit sheet to represent an artificial muscle. This shape can be a jellyfish or gripping tool if the arm strips are around an axis. The other form is coil-type artificial muscle. A linear actuation response from this muscle expected. Also to the extent of using these materials as biomimetic, a folded form of this material used to reproduce the Venus flytrap[106]. The system tried to incorporate the trigger mechanism of what is in Venus flytrap. An alternative version of this fly trap recently introduced by Shi et al. (2016)[107]. The design consists of two separated actuator sample parallel to each

other equipped with a proximity sensor in the middle. The sensor will detect the object and send actuation signals to the IPMC lobes. The article proposed for an updated version to include a three lobes IPMC.

In a micro-pump design Tadokoro et al. (1998) [113] used IPMC actuator as a diaphragm for a micro-pump chamber, and by using active one-way valve were able to demonstrate the application of IPMC in the pump chamber and the active valves. For a biomimetic design, a shark's gill jet orifice made with actuation properties of this materials by Du et al. (2018)[114]. In a biomedical application, Sherif et al. (2009) and Shahinpoor et al. (2009)[115] [116] proposed pump to support heart function.

An application of IPMC for miniaturized five-finger hand tested in a cantilever configuration by Chattterjee et al. (2013)[117]. In this form, a flat IPMC sample cut into a five-finger shape for the experiment. The experiment demonstrates an increase in the level of the received signal as the number of bent fingers increases.

Using two crossed and bent pairs of pre-bent IPMC strips, Tadokoro et al. (2003)[118] demonstrate a soft micromanipulator. They used an independent controller for each side input and used dynamic force balance to describe the motion and positioning of their device.

In 2001, a space-related application for IPMC by Steve et al. (2001)[119] demonstrated a sophisticated design for MEMS sensor. Their design consists of various electromechanical components into a multichip module. In this design, they

proposed a patterned electrode placing. The goal for patterned electrode placing was to generate patterned local deformation on the electromechanical module. In another practice for pattern coating [120], a sample with the weight of 85mgram was able to lift a 129mgram weight for 14.5 mm demonstrated by Chang et al. (2018).

2.4 Electromechanical Modeling Approaches

Understanding and prediction of the mechanism of Nafion® in actuation and its feedback to mechanical stimuli require knowing the material in-depth. In order to cover this part of the material, several modeling approaches by the researcher were proposed[22–24,67,121–127]. Some of these approaches are in actuation or sensing, and some have a more general concept as they are looking at the base material and derive expressions for the material behavior in general.

The proposed modeling methods can be categorized into different groups based on their approaches[128] and presented modeling approaches for each category. A broader method to categorize these materials started from black box modeling and gray box modeling towards white box modeling. In the black box modeling, the system is a box with some inputs, and work is to guess the output. This type of modeling mostly relies on experimental results and are mostly limited to particular configurations. This type of modeling can be calibrated to adopt the manufacturing deviation of newly produced materials. However, this approach does not provide much information regarding what is happening inside the material [121,129,130] [121]. In

addition to these types of modeling as the knowledge related to these materials grows, the gray box modeling starts to develop toward involving more detailed information related to the material characteristics and its components in a continuum mechanical investigation. In a more detailed description of this modeling of micro molecular models toward providing the white box modeling adopted. It is tried to provide actuation and sensing results by adhering to the relevant physics laws or internal structure of the IPMCs. These approaches even based on opposite assumptions [8], [131] reach a confirmation of the expected result from their simulations Branco et al. (2006)[132]. Here we are trying to present one of the most generally applicable of the modeling approaches presented in the pertinent literature.

By considering the static electric field, homogeneous presence of sodium ions, and make some simplification assumptions De Gennes et al. (2000)[22] tries to demonstrate the basic principle of actuation and sensing by a description of deformation based on linear irreversible thermodynamics and standard Onsager relations. They considered the following equations for current density and flux density.

$$\mathrm{J} = \sigma E - L\nabla p \tag{2.1}$$

$$\mathrm{Q} = \mathrm{LE} - \mathrm{K}\nabla p \tag{2.2}$$

where J is the ionic current flow rate, σ is the membrane conductance, E is the electric field, L is the Onsager coefficient, Q is the actual solvent rate, and Δp is the

pressure gradient across the IPMC strip, K is Darcy's diffusion permeability coefficient.

For actuation when an electric potential exists on the membrane surfaces and material reaches its electromechanical equilibrium, they assumed there is no flux in the material and based on this assumption the pressure gradient is calculated based on the following expression.

$$\nabla p = \frac{L}{K}\mathrm{E} \tag{2.3}$$

under applied deformation when there is no current in the system J = 0 and the electric field calculated based on the following equation.

$$E = \frac{L}{\sigma}\nabla p \tag{2.4}$$

In another approach the above modeling used and by considering small deflection of the corresponding Euler-Bernoulli beam for the IPMC strip monument, the deflection equation for cantilever beam configuration for sensing solved by Newbury et al. (2002)[129].

A gray box modeling for a cantilever beam sensor configuration is as presented in eqn. (2.5) by Bonomo et al. (2006) [130].

$$\frac{i}{\delta} = s\frac{3dt\omega Y}{4L_s} \tag{2.5}$$

where i, δ are sensing current, tip displacement, respectively, and ω, t, are the dimension of the beam, L_s length to the displacement point, s is the Laplace variable, Y and d are complex functions to be found.

For the next step through experimental results, they introduce a procedure to the identification of the sensor parameters.

2.5 Experiments on IPMC

There is ongoing research on different characteristics of IPMC. For example, Chang et al. (2018)[133] study the effect of different sanding parameter on IPMCs and Shen et al. (2019)[134] study the shape memory effect of the IPMCs. In this part, a report of some of the researchers' results IPMC presented.

Mojarrad (2001)[4] reported Nafion®-117 as one of the adopted material for IPMC and reported the mechanical characteristics of it within the application for sensing and actuation properties as well as the manufacturing process. Further, Mojarrad et al. (1997)[2] reported their methodology of converting a Nafion® to an IPMC membrane and the measurement of the signal. Their experimental result demonstrates a linear relationship between tip displacement and the sensing signal. These results again obtained by Bonomo et al. (2006)[130] in experiments as they demonstrate the almost linear sensing behavior of IPMCs as well as their durability. An additional outcome of their experimental result was that the sensing applications of IPMCs are better when IPMCs are in equilibrium with air. On the actuation part of

the IPMC back relaxation is related to the humidity of the environment, and it decays as the humidity decreases [135].

Mojarrad (2001)[4] reports on IPMC actuation response for an improved IPMC model and reports on indicate increasing the actuation stress by %50 of the original value of the manufactured IPMC. In their report on the membrane with 200-micron thickness by applying 4 volts, they were able to increase the actuation stress from 10 to 15 MPa. In another experiment, dry IPMC holds the stress up to two times of a wet one while the wet ones had the ultimate strain two times of the dry IPMC[13]. Also in similar experiments by Ansaf et al. (2018) and Zhu et al. (2016) [136,137] on the effect of humidity on this material, an increase of stiffness observed by decreasing the humidity.

In some study achieving higher force density for IPMC and reducing water leakage from the membrane become possible[138]. As a result of the experiment done by Shahinpoor (1998)[6], they considered water to be the element causing pressure gradient and actuation to form a curvature. In experiments, samples were soaked in water beforehand. They observed the degradation of the displacement at the voltage higher than 2 volts. The other parameters, Shahinpoor and Kim (2005)[138] considered in their study, were particle size, penetration, and distribution. In their experiment, they achieved a sharper response and increment in the force density by 100%.

Dominik et al. (2016)[139] reported endurance sensing capability of IPMC. The experiment was on two IPMC samples; one was a used sample while the other one was newly made. Their test involves simultaneous bending of samples and measurement of signal. They reported more than 21% drop of generated voltage through an endurance test. Their report also indicates a more stable generated voltage for higher displacements.

Asaka et al. (2000) observed an increment of curvature by increment in current density and a decrement of curvature by decrement in current density[124]. The group observed the back relaxation in material, as after reaching its maximum deformation, the material slowly bent back to the cathode. Also, the concept of time dependence IPMC in actuation was demonstrated. The report indicates the resultant displacement will be less as the frequency for the applied voltage increases[6].

Combination of palladium and platinum as a coating material for electroless plating demonstrates a worthy improvement of actuation of IPMC, reported by Palmre et al. (2014)[140]. In this experiment, palladium particle penetrated more in-depth into the material, causing the blocking force for a 1mm thickness membrane at 4V be a little more than 0.3N.

CHAPTER 3

3 MODELING OF IONIC POLYMER-METAL COMPOSITES (IPMCS) IN ACTUATION

3.1 Introduction

When a voltage is applied to IPMC, depends on the intensity of the voltage, the material undergoes different variations of deformations that depends on the microstructural of the base material and coating process. A deformation response presented in Fig. 3.1 as the applied voltage is at upper limits of the conventional values.

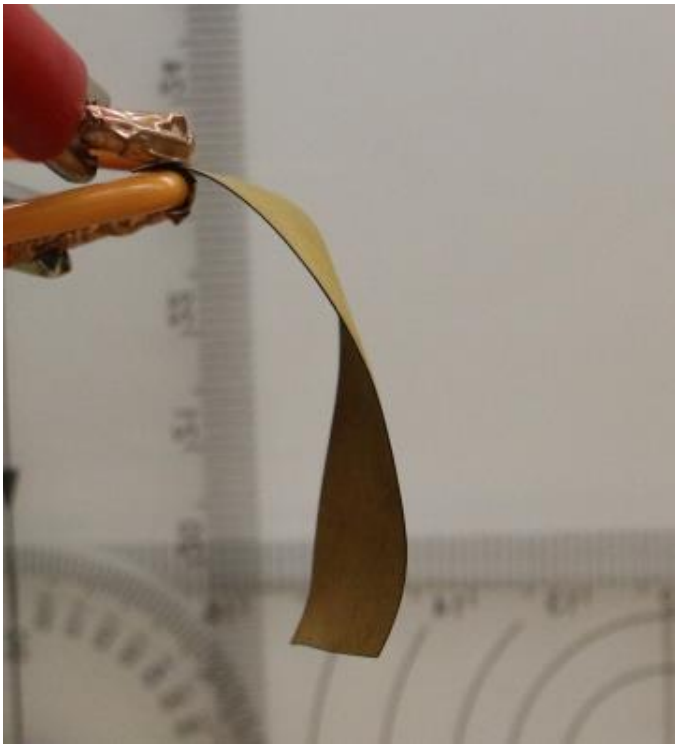

Fig. 3.1 Bending and Twisting Deformation of an IPMC sample

Assuming the IPMC material receives a conventional operation voltage (around 1~2 Votes for the sample in Fig. 3.1) and has an isotropic structure. Such IPMC will have a uniform deformation. This part explains a geometrical relation of Ionic Polymer-Metal Composites (IPMCs) in actuation mode.

De Gennes et al. (2000)[22] presented the fundamental theory for sensing and actuation in ionic polymer metal composites using irreversible thermodynamics and Onsager's formulations. A simple description of the electromechanical effects in IPMCs is possible based on two forms of transport: ion transport and ionic solvent transport. The conjugate forces include the electric field E and the pressure gradient Δp.

$$J(x,y,z,t) = \sigma E_e(x,y,z,t) - L_{12}\nabla p(x,y,z,t) \quad (3.1)$$

$$Q(x,y,z,t) = L_{21}E(x,y,z,t) - K\nabla p(x,y,z,t) \quad (3.2)$$

where J is ion transport current density normal to the material, Q solvent transport, E_e electric field equal to V/t, ∇p pressure gradient, σ and K are the material electric conductance and the Darcy permeability, respectively, and the Onsager's symmetric material coefficients $L_{12} = L_{12} = L$.

Assuming 1D form of the equation, in quasi-static actuation Q = 0 which gives the following expression.

$$\nabla p(s,t) = \frac{L}{K} E_e(s,t) \tag{3.3}$$

where s is a space variable and t is time.

The $\nabla p(s,t)$ will induce a curvature k which is proportional to $\nabla p(s,t)$ on the IPMC membrane. Expecting the shear deformations to be not significant, the deformations remain within the Euler-Bernoulli beam theory. In Fig. 3.2, when an electrical charge is applied to an IPMC, ion movements generate a pressure gradient across the IPMC strip and causes the material to expand on the cathode (side I), and shrink on the anode (side II), which then causes the strip to bend towards the anode side.

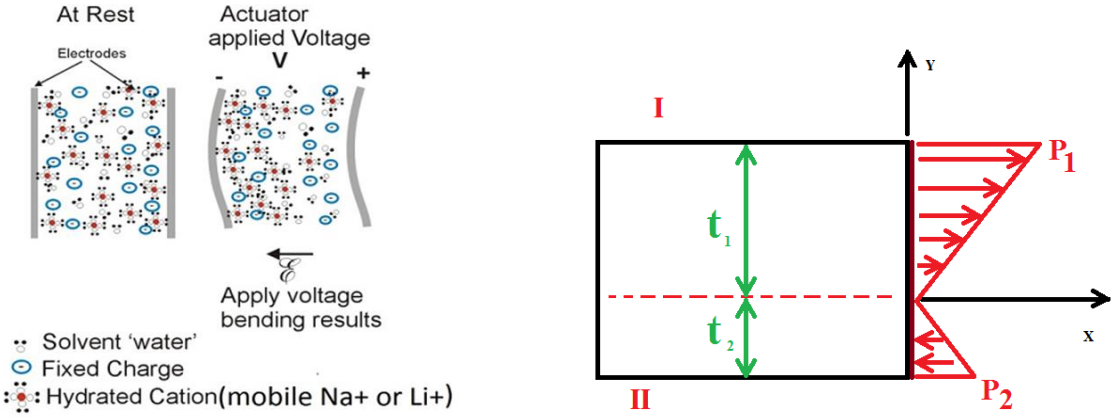

Fig. 3.2 Essential mechanism of actuation in IPMC

With the assumptions of having linear elastic behavior for ion displacement's results, stress-strain relation in engineering form, and constant curvature, Hooke's law can be introduced here as.

$$P_1 = Y\varepsilon_I = \frac{Y\, t_1}{\rho} \tag{3.4}$$

$$P_2 = Y\varepsilon_{II} = \frac{Y\, t_2}{\rho} \tag{3.5}$$

where P_1 and P_2 are pressures on each side, Y and ε are young modulus and strain, and t and ρ are thickness and radius of curvature of the material. Combining eqn. (3.4), and eqn. (3.5) relate the pressure gradient and curvature such that.

$$\nabla P = Y\varepsilon = \frac{Y(t_1 - t_2)}{\rho} = Ykt \tag{3.6}$$

Combining eqn. (3.3) and (3.6), and rewriting electric field as $E_e = V/t$, the curvature will be expressed by input parameters to the IPMC material from which defines the shape of the material.

$$k = {}^{L\,V}/_{Y\,K\,t^2} \tag{3.7}$$

Assuming the cross coefficient, young modulus, and Darcy permeability be constant during actuation effect of voltage variation for different thickness is demonstrated in Fig. 3.3. In this figure, voltage variation considered to be (0~1) Volts, and for the thickness variation is between (0.001~1) mm.

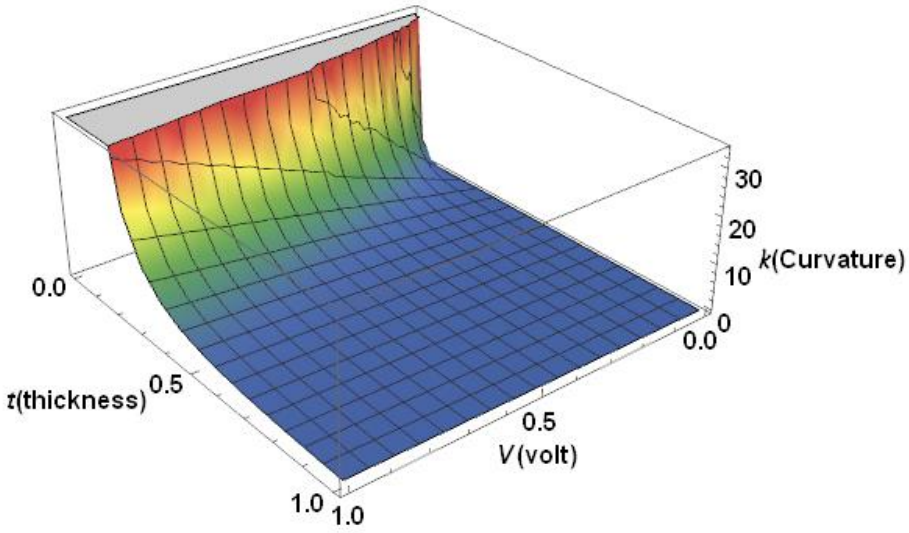

Fig. 3.3 Variation of curvature vs. applied voltage for different thickness

As demonstrates, the curvature has a linear relation with applied voltage and has a nonlinear relation with the material thickness. Also, the limitations of these parameters are verifiable by experiments. In a more general form eqn. (3.8)will be

$$k_s = {}^{L_s V_s}\Big/_{Y_s K_s t_s^2} \tag{3.8}$$

An application of this form of defining the curvature is when considering L, Y, and K as constants, changing the voltage by introducing surface resistance and material resistance. The curvature along the IPMC strip from the contact point will be:

$$k = {}^{L (V_0 - V_{d(s,time)})}\Big/_{Y K t^2} \tag{3.9}$$

$$V_{d(s,time)} = R_{d(s)} I_{d(s,time)} \tag{3.10}$$

Where $V_{d(s, time)}$ is the voltage drop along the strip from the contact point, $R_{d(s)}$ is the surface resistance along the strip regarding the contact point, $I_{d(s, time)}$ is the surface current along the strip. The surface current, $I_{d(s, time)}$, has variation due to the internal electric discharge that happens due to ion movement and the IPMC internal resistance. This time-dependent value will reach its equilibrium value and will be $I_{d(x)}$ as the strip reached its maximum possible deformation under current condition.

Eventually, the voltage drop will be uniform along the membrane surface. Removing the time constants and controlling the voltage drop by surface resistance variations on an IPMC actuator strip, the curvature will vary. As this uniformly variable voltage gradient will introduce the osmotic pressure gradient alongside the IPMC material, the curvature *k* is related to the applied voltage, and it is changing uniformly (Fig. 3.4). As a result of this curvature variation, forms like swirling actuators will be possible. Another way of having voltage variation on an IPMC surface is introducing voltage density concept. Based on this condition, ion concentration on the surface will not be uniform and will vary due to possible arrangements of coated electrodes on each side. This variation of the voltage will cause the variation in the electric field in IPMC base material and as a result on the material curvature.

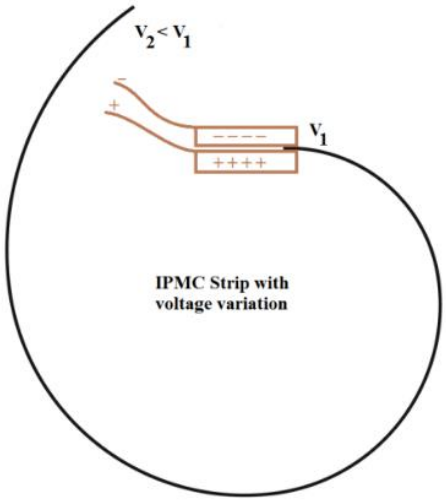

Fig. 3.4 Graphical representation of a spiral IPMC sensor/actuator

3.2 Geometrical Modeling of IPMC in Actuation

Considering eqn. (3.7) and the assumption of a uniform curvature for the IPMC in actuation, the expected bending will be a circular arc as the curvature is constant, Fig. 3.5.

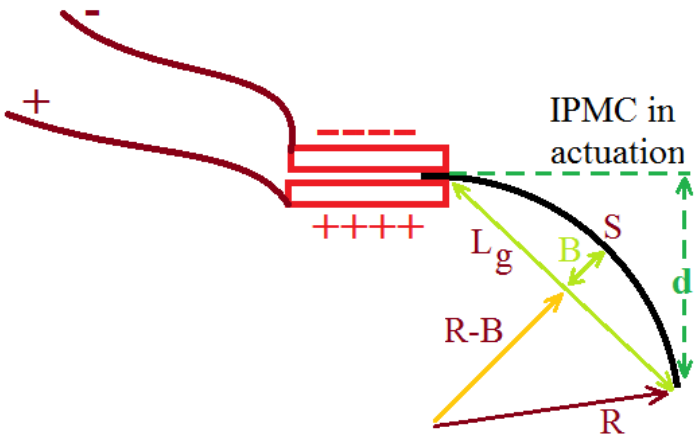

Fig. 3.5 Dimensional representing IPMC in actuation

With the assumption of constant curvature, the dimensions in Fig. 3.5 are geometrical relations as expressed in the following expressions.

$$d_v = 1/k(1 - \cos Sk) \tag{3.11}$$

$$d_h = S - \frac{\sin Sk}{k} \tag{3.12}$$

$$B = 1/k - \sqrt{1/k^2 - \frac{{L_g}^2}{4}} \tag{3.13}$$

Rewriting eqn. (3.13) for curvature

$$k = \frac{8\,B}{4\,B^2 + {L_g}^2} \tag{3.14}$$

where S is arc length or initial length of an actuator, and k is curvature. Rewriting the curvature based on electromechanical inputs for the IPMC, d_v *and* d_h will be:

$$d_v = \frac{Y\,K\,t^2}{L\,V}\left(1 - \cos\frac{S\,L\,V}{Y\,K\,t^2}\right) \tag{3.15}$$

$$d_h = S - \frac{Y\,K\,t^2}{L\,V}\,\sin\frac{S\,L\,V}{Y\,K\,t^2} \tag{3.16}$$

where S is arc length or the initial length of the actuator, L is cross coefficient, V is the applied voltage, K is Darcy permeability, Y is Young's modulus of the IPMC strip, and t is material thickness. This ratio of tip displacement presented in Fig. 3.6 for a constant length of the IPMC actuator (here length considered to be unit)[141].

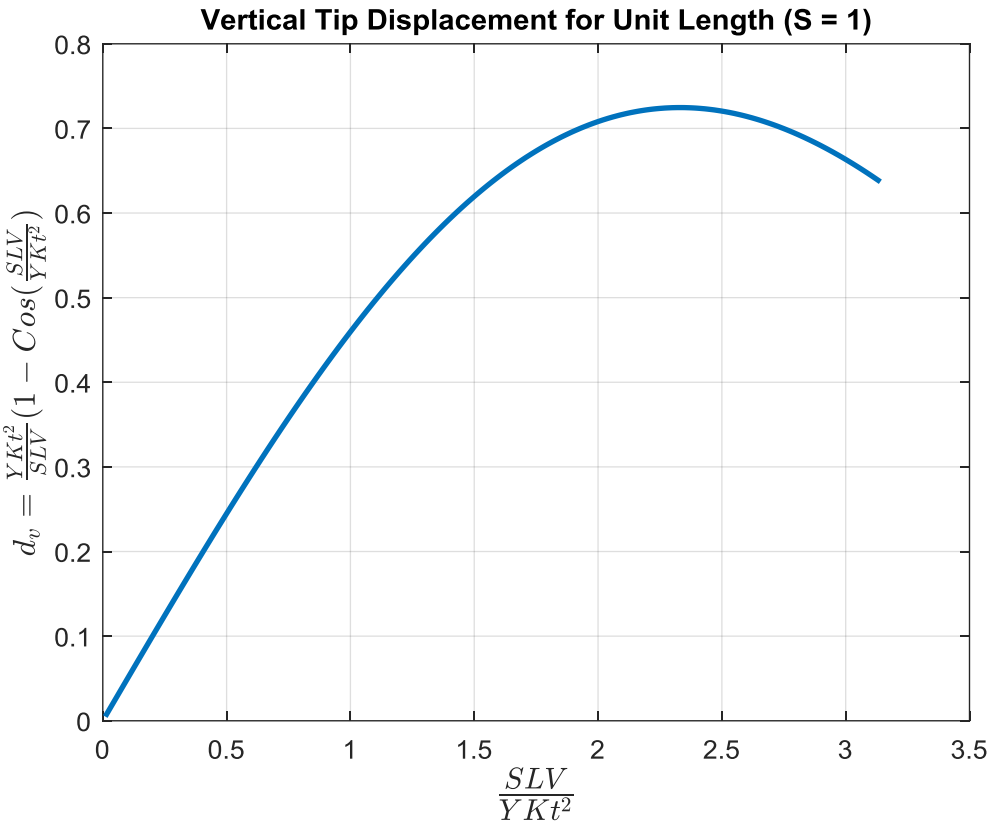

Fig. 3.6 Vertical Tip Displacement Ratio vs. Input Voltage Ratio

In the case of having a variable voltage along the IPMC, the tip displacement ratio will be different. An example is a model presented in Fig. 3.4 in which maximum tip displacement due to voltage variation is higher than a uniform curved form.

Referring eqn. (3.15), values for $\frac{S\,L\,V}{Y\,K\,t^2}$ will be between 0 and π resulting in deformation from a straight line to a half-circle. Solving $\frac{\partial d_v}{\partial V} = 0$ for V, Gives

$$\frac{S\,L\,V}{Y\,K\,t^2} = 2.33\ rad \tag{3.17}$$

This result is the value for maximum possible vertical deflection of an IPMC sample with a uniform bending curvature. From which, one can calculate optimum length, voltage, or thickness for maximum vertical deflection, in case of having a uniform curvature. A relation between the curvature ratio and input ratio of IPMC sample in actuation demonstrated in Fig. 3.7. In this plot, constant length of the IPMC actuator considered to be unit (S=1).

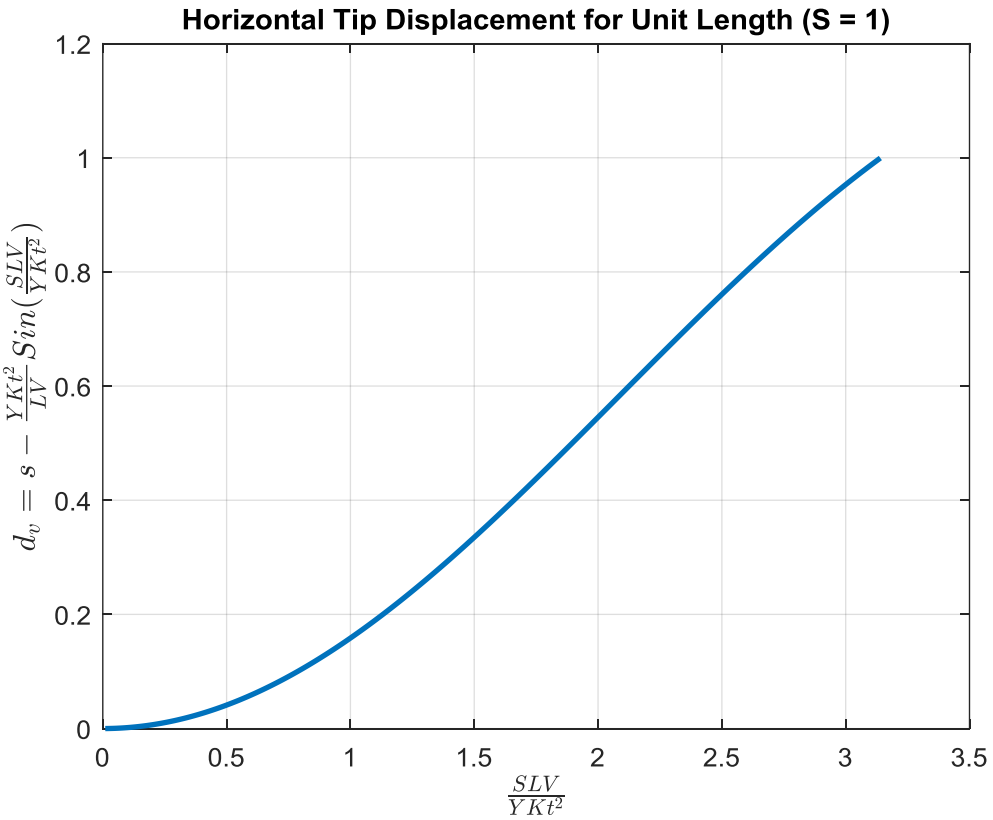

Fig. 3.7 Horizontal Tip Displacement Ratio vs. Input Voltage Ratio

3.3 Experimental test Result

On a sample with the dimensions 40mm by 11mm by 0.2mm in Fig. 3.8, the voltage variation for the test was between 0.07 volts and 3.59 volts.

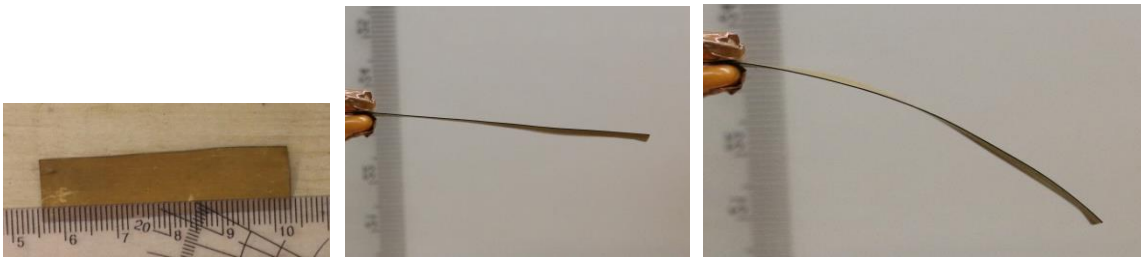

Fig. 3.8 IPMC sample in actuation with voltage 0.55 Volts and 2.16 Volts

In Fig. 3.8, IPMC sample is on the left side, the middle picture shows deformation at 0.55 Volts, and the right-side picture showed deformation at 2.16 Volts. The variation of the twist angle of the strip is noticeable when voltage changes in these pictures. Fig. 3.9 and Fig. 3.10 demonstrate the test results for this sample. A comparison of Fig. 3.9 and Fig. 3.6 for vertical tip displacement, and Fig. 3.10 and Fig. 3.7 for horizontal tip displacement demonstrate conformity of the trend of the recorded results. Also calculated curvature for each deformation derived in Fig. 3.11. The curvature for the sample at the beginning of the test was not detectable, but as voltage increased the material started to follow the expected deformation for tip displacements and curvature.

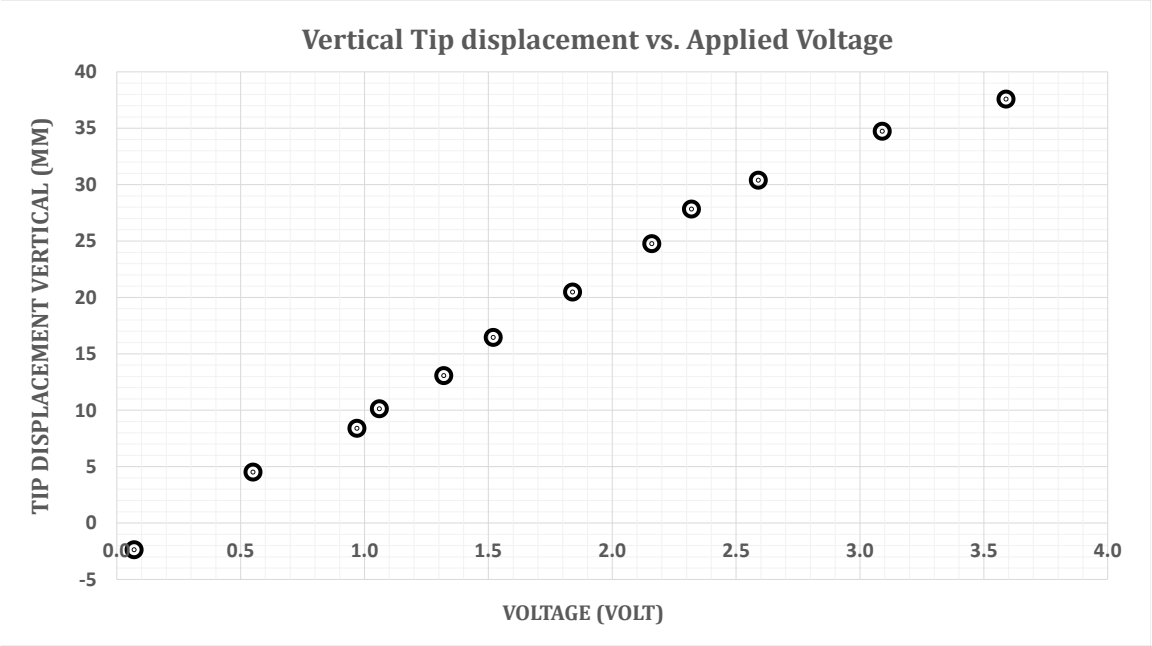

Fig. 3.9 Vertical Tip displacement of IPMC sample vs. applied voltage

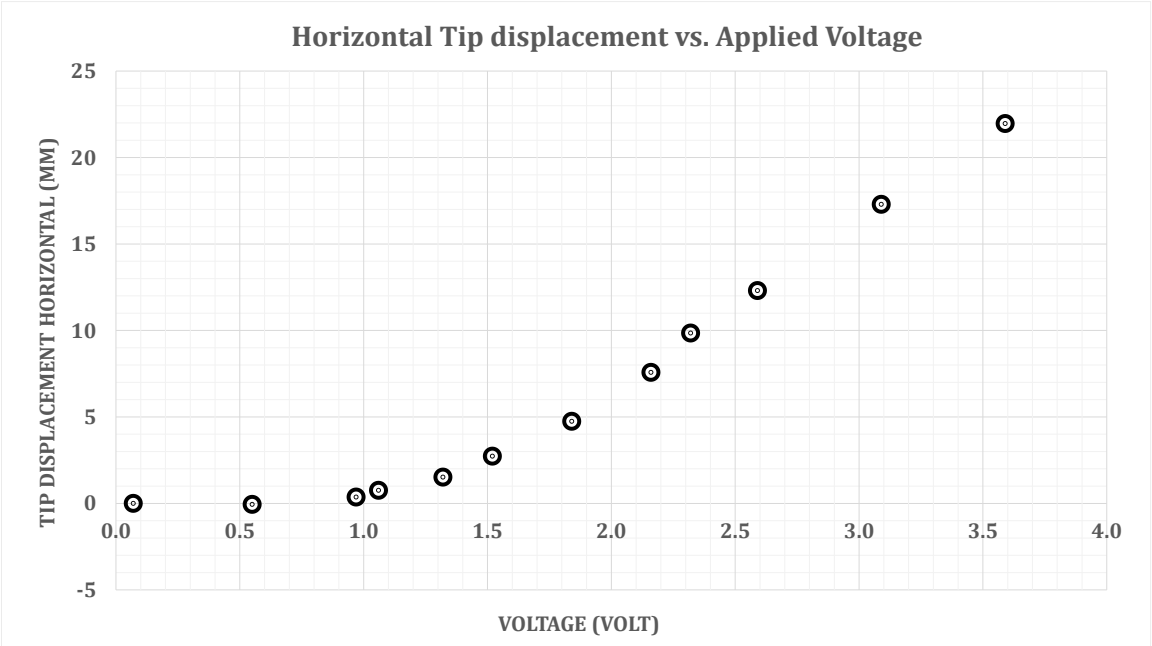

Fig. 3.10 Horizontal Tip displacement of IPMC sample vs. applied voltage

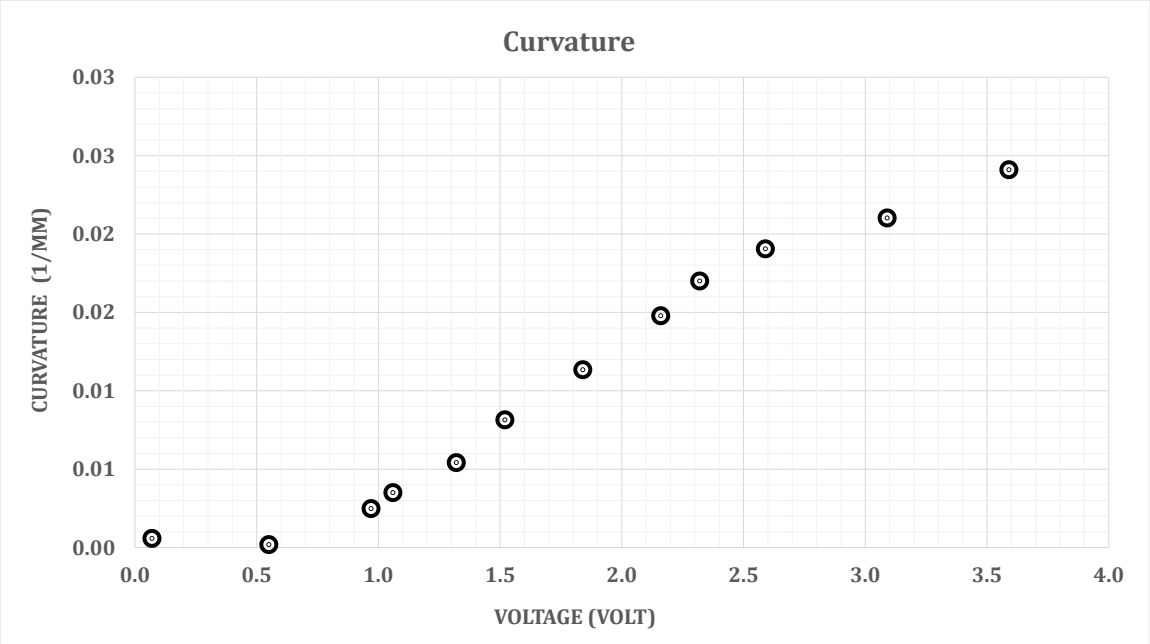

Fig. 3.11 Curvature of IPMC sample vs. applied voltage

In another similar setup with a larger sample test was performed. In this test, the size of the tested part sample was 73 mm. length, 13 mm. width, and 0.3 mm. thickness. Deformation of the sample presented in Fig. 3.12. In this test, the material demonstrates a much smother deformation in comparison with the previous sample.

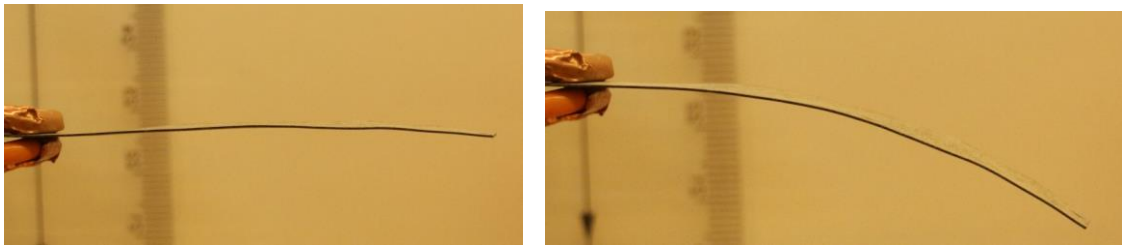

Fig. 3.12 IPMC sample in actuation with voltage variation

Test results demonstrated in Fig. 3.13 and Fig. 3.14 are for tip displacements. In this test, the sample was much larger (170mm) than the part of it was tested and higher voltage required for the actuation in comparison with the previous sample.

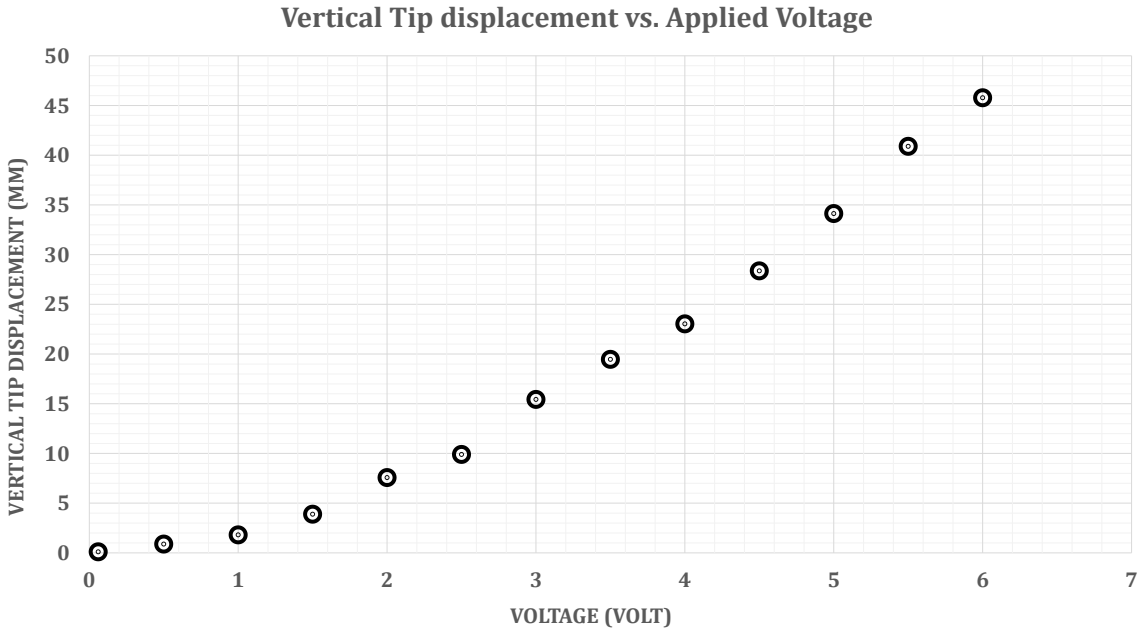

Fig. 3.13 Vertical Tip displacement of IPMC sample vs. applied voltage

Curvature and its variation demonstrated in Fig. 3.15. As it is noticeable from this figure, the curvature has a smooth increment variation as voltage increases.

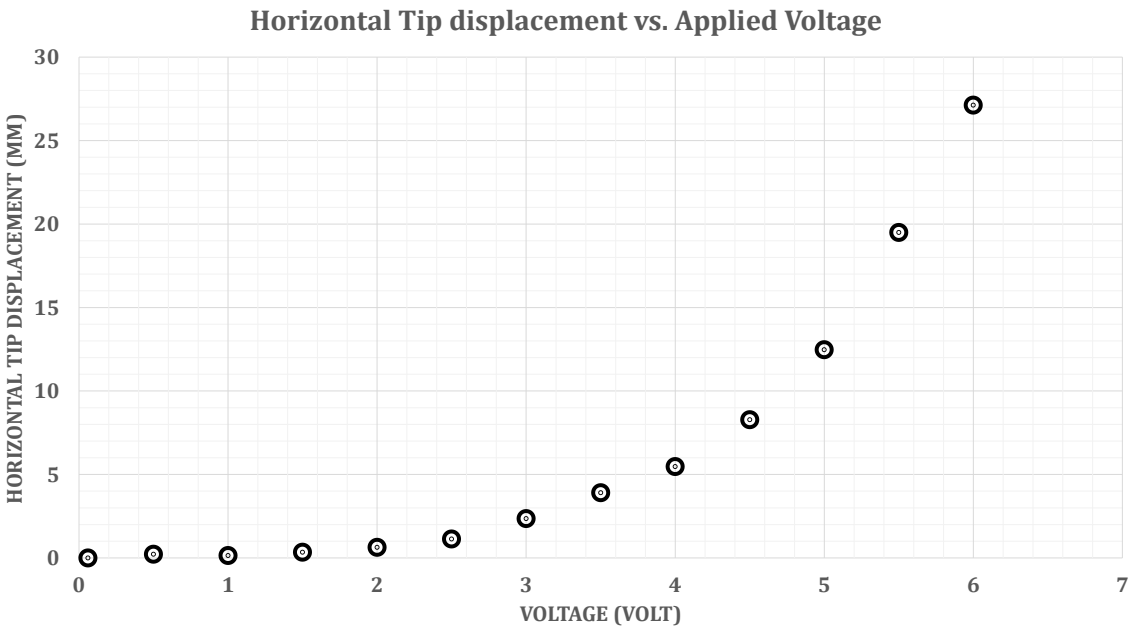

Fig. 3.14 Horizontal Tip displacement of IPMC sample vs. applied voltage

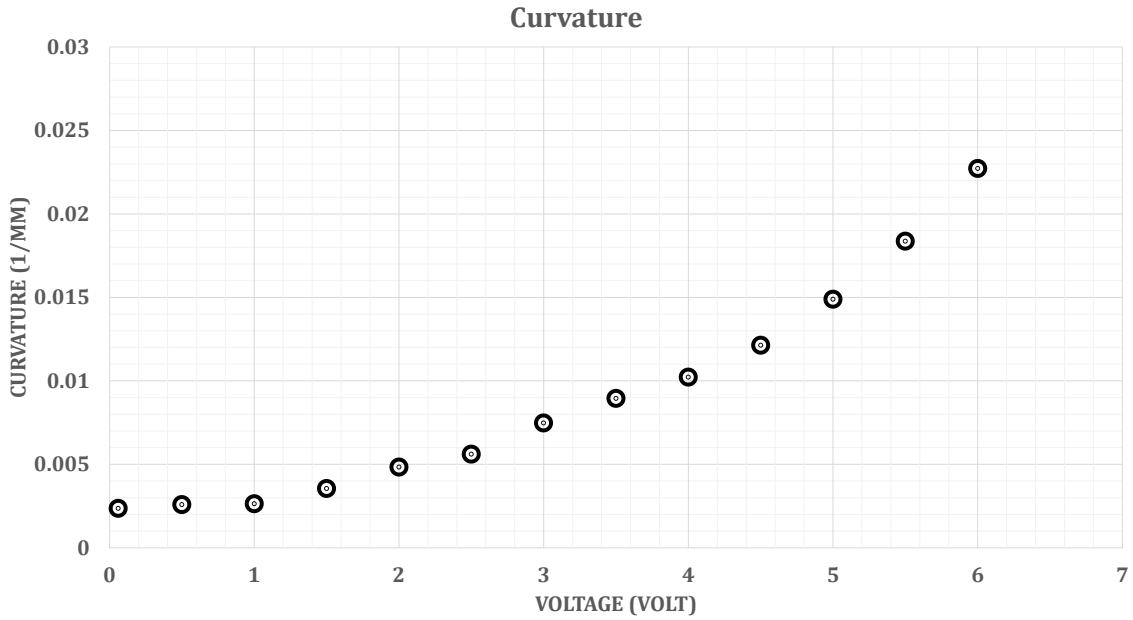

Fig. 3.15 Curvature of IPMC sample vs. applied voltage

Note that if the computed curvature, from eqn. (3.7), equates to the beam curvature equation or $k = \frac{M}{EI}$, applied moment across the IPMC sample under the applied voltage will be $M = \frac{E\ I\ L\ V}{Y\ K\ t^2}$. Having $\mathrm{U} = \frac{1}{2}\theta\mathrm{M}$ as the energy equation for a beam under a bending moment, the mechanical energy in an IPMC sample in actuation will be $\mathrm{U} = \frac{1}{2}\frac{\mathrm{E\ I\ L^2\ V\ k}}{\mathrm{y\ K\ t^2}}$. Having electrical energy as $\mathrm{U} = \mathrm{V\ I}$, the Variation of the current consumption of IPMC actuators will be:

$$i = \frac{1}{2}\frac{\mathrm{E\ I\ L^2\ k}}{\mathrm{y\ K\ t^2}} \tag{3.18}$$

Based on eqn. (3.7) and (3.18), the curvature of IPMC in actuation is controllable by electrical current consumption of the IPMC actuator.

3.4 Actuator linear models

One way to make a linear actuator is to have a pair of an already discussed form of IPMC Fig. 3.16 and pair them back to back. Similar to this form already introduced by Yamakita et al. (2004)[101]. In this format variation of the length is possible by actuation or changing the distance as a sensor.

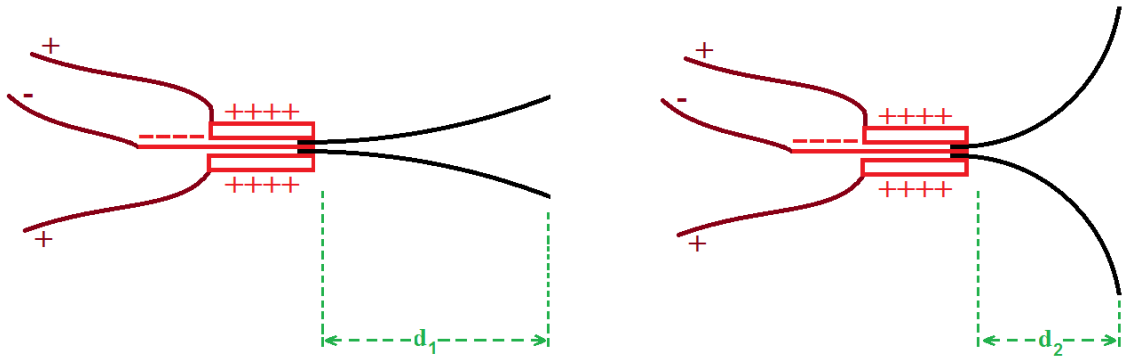

Fig. 3.16 IPMC actuator with Clamped-Free boundary configuration

In addition to the above formats pairing two IPMCs with other types of boundary configurations also gives new linear actuators. These configurations will use a pair of IPMCs to cancel out their side deformations and have more axial deformation. These forms presented in Fig. 3.17 to Fig. 3.19.

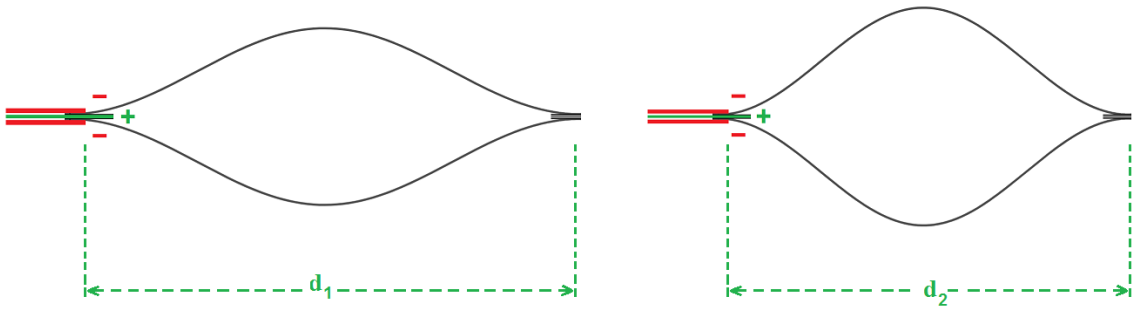

Fig. 3.17 IPMC actuator with Clamped-Clamped boundary configuration

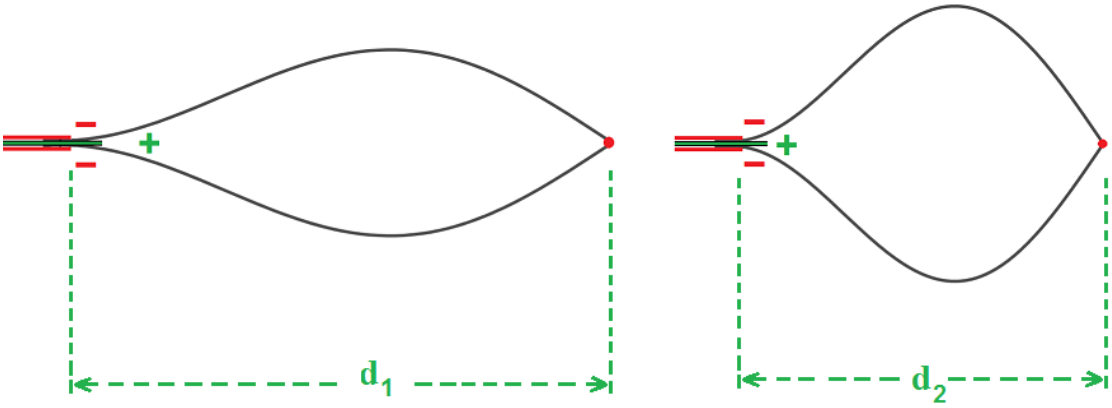

Fig. 3.18 IPMC actuator with Clamped-Hinged boundary configuration

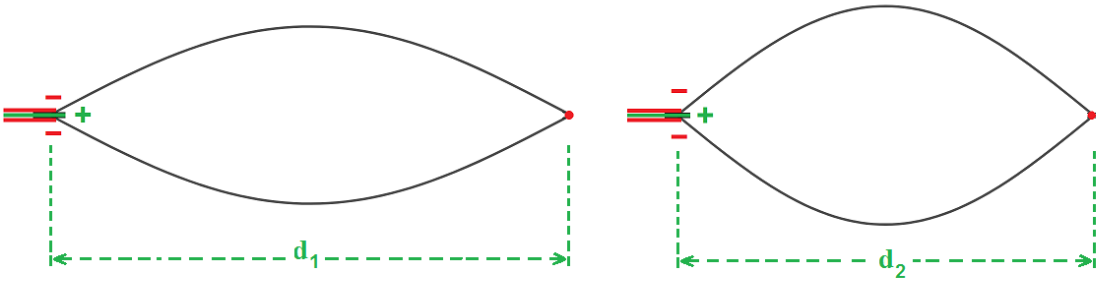

Fig. 3.19 IPMC actuator with Hinged-Hinged boundary configuration

CHAPTER 4

4 MODELING OF IONIC POLYMER-METAL COMPOSITES (IPMCS) IN SENSING

4.1 The basic form of the linear sensors

Here, by attaching two similar IPMCs strips end-to-end, it is expected the pair lead displacements in a more linear or guided manner. As Fig. 4.1, Fig. 4.2, and Fig. 4.3 illustrate by adjoining IPMC strips end-to-end with a slightly pre-bent configuration, the assembly will work along its axis with expected deformation directions.

The imposed displacement deforms the samples and generates electrical charges bringing the possibility of linear sensor applications. The concepts formed in three categories and their derivatives. The formulation for these concepts considered to be within the scope of an elastic beam with boundary conditions of hinged, clamped, and free. The rest of the concepts can be formulated based on these main configurations. In this chapter, the basic beam modeling formulations discussed. Although these models introduced as a sensor and energy harvester, they can be used for actuation purposes as well.

In Fig. 4.1, Form A on the left side illustrates the concept in extended and compressed mode. The samples have pre-bending, so the imposed force/displacement will cause the expected deformation. This concept has the IPMC

with Clamped boundary condition on both ends. Form B on the right side is half of what is in form A as one side has the Clamped boundary condition, and the other side is perpendicular to the base similar to what is in the middle of form A.

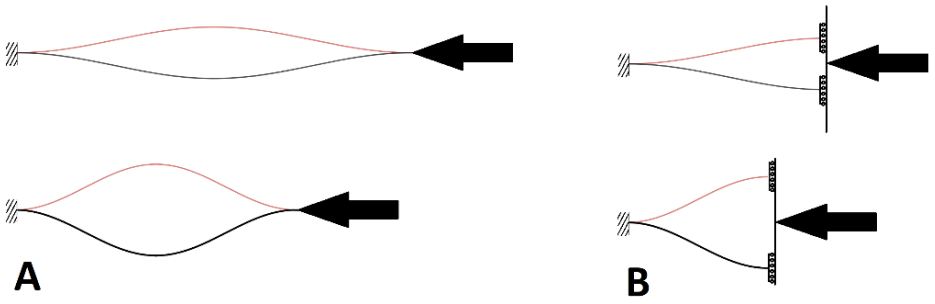

Fig. 4.1 Clamped-Clamped concept configurations

In Fig. 4.2, Form C on the left side illustrates the concept in extended and compressed mode. The samples have pre-bending, so the imposed force/displacement will cause the expected deformation. This concept has the IPMC with Hinged boundary condition on both ends. Form D on the right side is half of what is in form C as one side has the Hinged boundary condition, and the other side is perpendicular to the base similar to what is in the middle of form C.

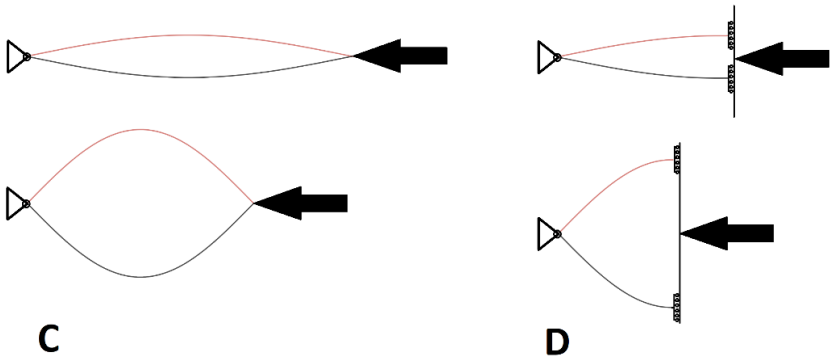

Fig. 4.2 Hinged-Hinged concept configurations

In Fig. 4.3, Form E on the left side illustrates the concept in extended and compressed mode. The samples have pre-bending, so the imposed force/displacement will cause the expected deformation. This concept has the IPMC with Clamped boundary condition on the left ends, and Hinged boundary condition on the right ends. Forms F and G on the right side is half of what is in form E as one side has the Hinged or Clamped boundary condition, and the other side is perpendicular to the base similar to what is in the middle of form E. These forms are similar to what presented in form B and Form D.

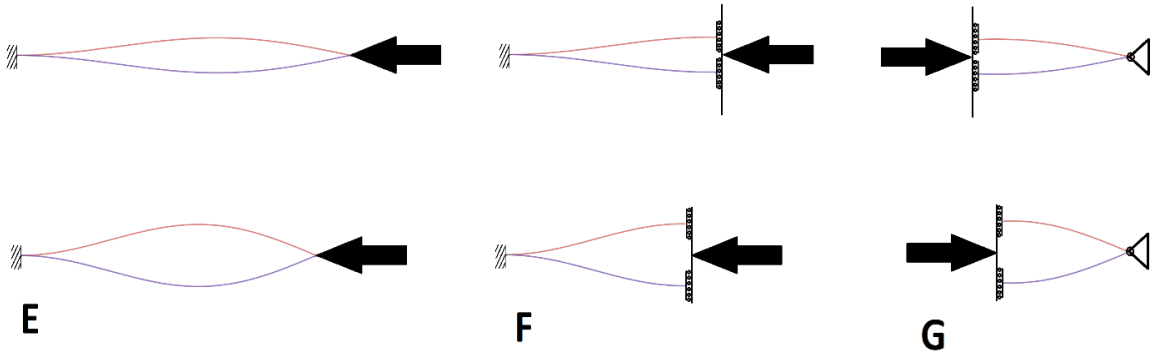

Fig. 4.3 Clamped-Hinged concept configurations

The above configurations are the base elements for some of the proposed concepts. Next will discuss the curvature as the parameter to define the shape of the above configurations.

4.2 Curvature and sensing

Assuming an IPMC sample in the proposed assembly unit follows a beam model in beam eqn. (4.1) and (4.2), the curvature of the deformed shape has a direct relation with the applied moment, and with the IPMC osmotic pressure gradient. This curvature imposes pressure gradient to the material, which causes the deformation. In Fig. 4.4, curvature variation on a deformed beam presented for Clamped-Clamped and Hinged-Hinged boundary condition. In this figure, Left-side is for Hinged–Hinged boundary condition, and the right side is for Clamped-Clamped boundary condition. The red color is associated with higher curvature value, while the green and blue area have lower or close to zero curvature value.

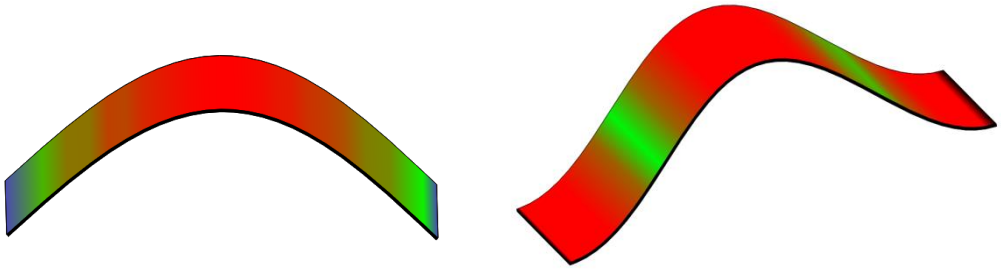

Fig. 4.4 Variation of curvature for a deformed IPMC strip

$$k = \frac{M}{EI} \tag{4.1}$$

$$\sigma_{max} = \frac{Mc}{I} \tag{4.2}$$

where k is curvature, M is the applied bending moment, E and I are Elastic Modulus and moment of inertia, c is half of the beam thickness, and σ is the stress in the beam.

De Gennes et al. (2000)[22] model of IPMC in a sensing mode relates generated the electric field to the pressure gradient.

$$E = \frac{L}{\sigma}\nabla p \tag{4.3}$$

where E is the generated electric field, L is the membrane cross coefficient, σ is the membrane conductance.

Next step is introducing the mechanical modeling approaches to define the mechanical deformation of the material. This mechanical deformation with the electromechanical model introduced above, or other approaches by several scholars are helpful to get a better electromechanical model of the proposed IPMC sensors configurations.

The assumption here is that an IPMC (strip) under axial load deforms similarly to a mechanical beam[57,142,143] under axial load. Figure 4-5 demonstrates a familiar load-displacement curve when the material can accept large deformations without having the plastic phase. The first part of deformation is a straight line as the load is less than the buckling load. The second part of the graph related to where load passed the buckling load, and it is related to the proposed sensor concepts. In this

concept, when load passed the buckling load value, the column will continue deforming at a faster pace. These configurations are about the material as they already deformed under a load and is not going to involve the buckling, post-buckling, and other related concepts related to buckling. Other than deformation trend concept, there is not much of a relation with buckling concept here.

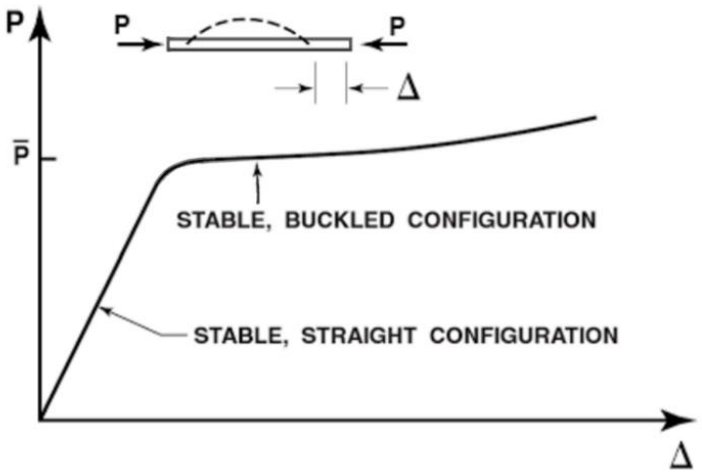

Fig. 4.5 IPMC axial load variation under axial compression load

In the beginning, sensors have small curvature or imperfection to guide the deformation outward. This pre-bent configuration does not affect the modeling since the sensing mechanism is based on feedback variation and the sensing equations discussed earlier for the electromechanical modeling. The results reported by Mehran Mojarrad (1997)[144] demonstrates there is a linear relationship between the generated signal and the applied deformation, which provide support for the feedback variation concept. The variation of the load is not significant as the change is much smaller than what was before the buckling load and at most will be

less than two times of buckling load factor[145]. From another point, the increment of load ensures the tendency of material returning to its original formation and keeping the contact with the target.

The model used for post-buckling of the IPMC is the work done by Nayfeh and Emam (2008)[145]. They presented a closed form solution for post-buckling of a beam subjected to diverse combinations of fixed and hinged boundary conditions. These expressions are used to demonstrate the nature of the deformations. Expressions for the first buckling mode shapes for unit length are in Table 4.1. These expressions relate the force and amplitude of the mode shape of the IPMC and considered for the concepts in Fig. 4.1 and Fig. 4.2 in Table 4.1.

Table 4.1 Equation for the 1st Buckling mode shape of columns

Boundary conditions	Deformation configuration
Clamped – Clamped	$\psi(x) = 2\sqrt{P/_{4\,\pi^2} - 1}\,[1 - \cos(2\pi x)]$
Hinged – Hinged	$\psi(x) = 2\sqrt{P/_{\pi^2} - 1}\,\sin(\pi x)$
Clamped – Hinged	$\psi(x) = 2\sqrt{P/_{\lambda^2} - 1}\,[1 - x - \cos\lambda x + \frac{1}{\lambda}\sin\lambda x]$

$\psi(x)$ *is lateral displacement along y axis*, $P = \frac{\hat{P}L^2}{EI}$, *where* $\hat{P}$ *is the* applied load ,

$x = \frac{\hat{x}}{L}$ *where* $\hat{x}$ *is the length of the beam along x axis,*

and λ *is the first root of* $tan(\lambda) = \lambda$, $\lambda \cong 4.4934094$

The expression for Clamped–Hinged (Fig. 4.3) is similar to the one expressed in the source with a slight variation for sin function multiplier. This expression is next to other expressions from the same sources in Table 4.1.

Various deformations demonstrated in Fig. 4.6 for a beam with definite length under different boundary conditions. This figure demonstrates the shape with maximum considered deformation from the expressions in Table 4.1. The right side is related to what the expressions are describing. In this case, the formation is related to Clamped-Clamped expression in Table 4.1.

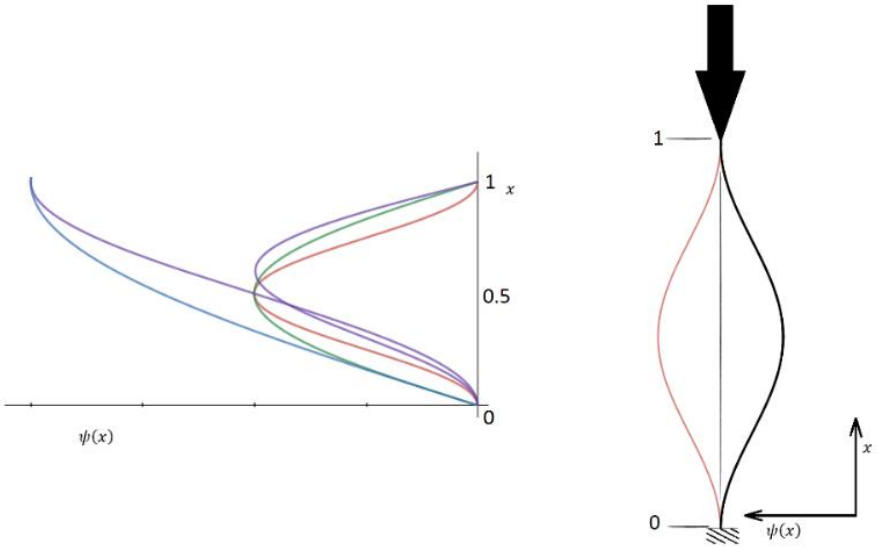

Fig. 4.6 Beam 1st Buckling mode's concepts.

4.3 Curvature and Its role in the IPMC sensing

When the deformation is large, the response of IPMC is more noticeable. The error associated with the simplified curvature equation for large deformation expressed in the below equation.

$$\frac{M}{E\,I} = \frac{v''}{(1-v'^2)^{3/2}} \tag{4.4}$$

In the above equation v' is the slope of the beam that considered to be less significant in most simplified linear solutions. Error for such assumption expressed below.

$$\%\ error\ (k) = \frac{k-k_s}{k} = 1-(1+y'^2)^{3/2} \tag{4.5}$$

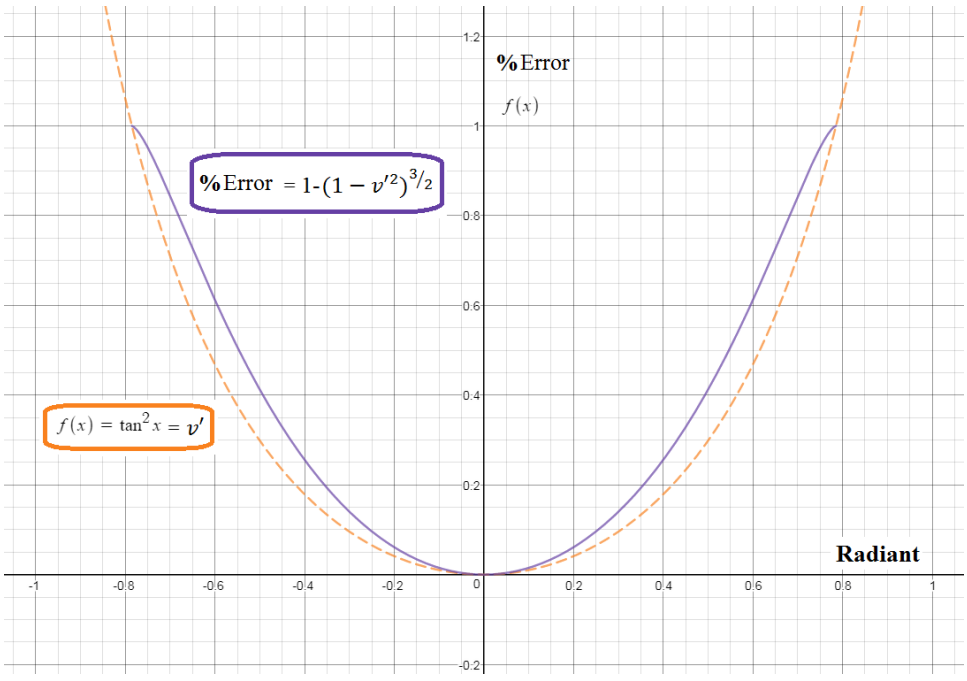

Fig. 4.7 Variation of error for simplified curvature equation

When $v' < 0.2\ rad$ results in less than 6% error. This error will reach 14% when the deflection angle reaches 0.3 radian that is around 17 degrees, and for 20 degrees the error will be around 20%, so it is essential to consider the nonlinear form of the curvature in the beam theory.

From a mechanical perspective, IPMC samples under axial force behave like a beam or other mechanical structure like tube under axial force. This deformation will define a local curvature k for membrane, and the local curvature related to local pressure by eqn. (4.3).

Table 4.1 presented the definition of deformations in a Cartesian coordinate system and the eqn. (4.6) gives the curvature expressions for the proposed concepts for unit length, as presented in Table 4.2.

$$k = \frac{y''}{(1+y'^2)^{3/2}} \tag{4.6}$$

In Table 4.2, critical points are where the value of curvature is maximum or zero. Fig. 4.8 represents the variation of the curvature along the curve for different boundary configurations. The thickness of the curved line is proportional to the value of curvature and the generated signal. This figure demonstrates curvature, and its related charge varies along the IPMC in these configurations in Table 4.2.

Table 4.2 the curvature of columns in 1st Buckling mode

Boundary conditions	**Curvature Expression**	**k value at Critical points**
Clamped - Clamped	$k(x) = 2\sqrt{{}^{P}/_{4\,\pi^2} - 1}\,[\frac{4\pi^2 \cos 2\pi x}{(1 + 16\pi^2({}^{P}/_{4\pi^2} - 1)\sin^2 2\pi x)^{3/2}}]$	$k(x = 0.25) = 0$ $k(x = 0.75) = 0$ $k(x = 0) = max$ $k(x = 0.5) = max$ $k(x = 1) = max$
Hinged – Hinged	$k(x) = 2\sqrt{{}^{P}/_{\pi^2} - 1}\,[\frac{-\pi^2 \sin \pi x}{\left(1 + 4\pi^2({}^{P}/_{\pi^2} - 1)\cos^2 \pi x\right)^{3/2}}]$	$k(x = 0,1) = 0$ $k(x = 0.5) = max$
Clamped - Hinged	$k(x) = 2\sqrt{{}^{P}/_{\lambda^2} - 1}\,[\frac{\lambda^2 \cos \lambda x - \lambda \sin \lambda x}{(1 + (4({}^{P}/_{\lambda^2} - 1)(-1 + \lambda \sin \lambda x + \cos \lambda x)^2)^{3/2}}]$	$k\left(x = \frac{\lambda - \pi}{\lambda}\right) = 0$ $k(x = 1) = 0$ $k(x = 0) = max$ $k\left(x = \frac{2\lambda - 2\pi}{\lambda}\right) = max$

where λ *is the first root of* $tanc(x) = 0$, $\lambda \cong$ 4.4934094,
$P = \frac{\hat{P}L^2}{EI}$, *where* $\hat{P}$ *is the applied load* and $x = \frac{\hat{x}}{L}$ *where* $\hat{x}$ *is length of the beam along x axis*

Referring to Fig. 4.8, for the concepts discussed in Fig. 4.1-B, and Fig. 4.2-D, note that most of the sensing signals generated near the boundaries, and for concepts in Fig. 4.2-C the middle part is the signal generator. Also, the concept in Fig. 4.3-E has a mixed region of signal generation area. From another point of view, the Clamped-Clamped concept has curvature in two directions with the same level and intensity.

This condition leads to having net zero curvature. As a result, charge for the concept introduced in Fig. 4.1 should be zero unless the strip has a gap or discontinuity for these regions at the areas with almost zero/unnoticeable curvature (Table 5).

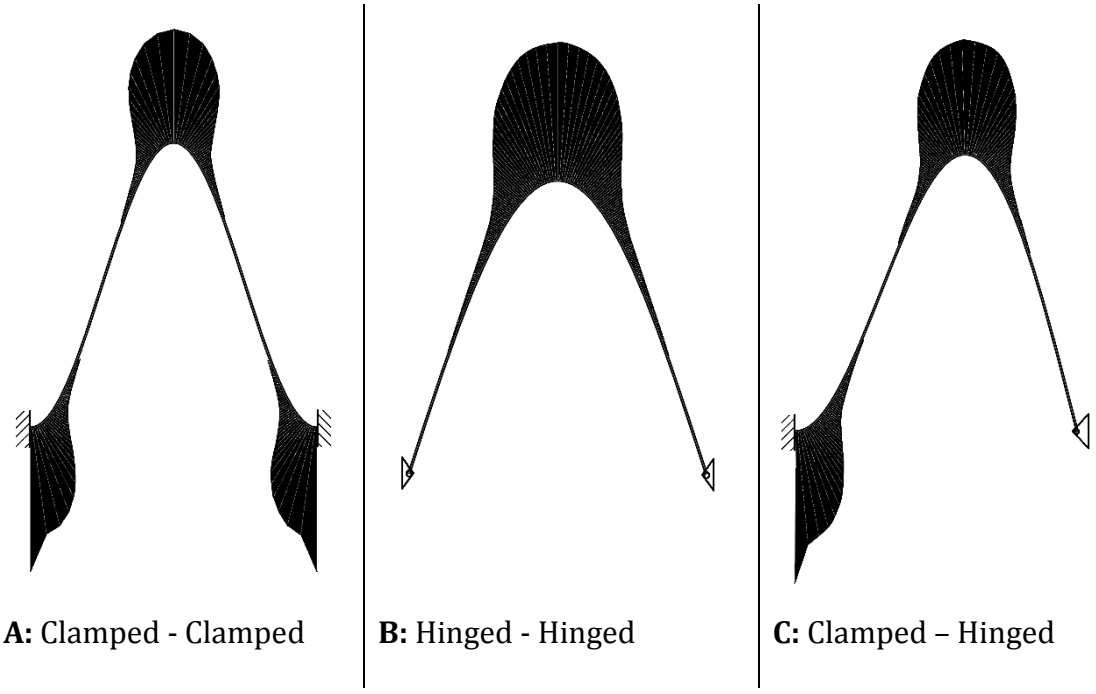

A: Clamped - Clamped | **B:** Hinged - Hinged | **C:** Clamped – Hinged

Fig. 4.8 Variation of curvature for different boundary conditions

Assuming almost zero stretch or compression in the length of the IPMC strip, eqn. (4.7) is the expression for the arc length in the Cartesian coordinate system. Based on the calculation of arc length and its variation with P (Table 4.1), the following expressions in Table 4.3 are for the length of the strips from which the axial displacement of the tip of the strip can be calculated.

$$s = \int_a^b \sqrt{1 + y'^2}\,dx \tag{4.7}$$

Table 4.3 Length of a Beam in 1st Buckling mode from Geometry perspective for unit length

Sensor Concept	Length of the strip [a]	Max Lateral amplitude	Load Range
Fig. 4.1-A	$S = 2 * e^{0.14(P-40.75)} - \frac{3}{16} * e^{-P+40.75}$	$2\sqrt{P/4\,\pi^2 - 1}$	$4\,\pi^2 < P < 4.25\,\pi^2$
Fig. 4.2–C	$S = 2 * e^{0.14(P-11.14)} - \frac{3}{16} * e^{-P+11.14}$	$2\sqrt{P/\pi^2 - 1}$	$\pi^2 < P < 1.25\,\pi^2$
Fig. 4.3–E	$S = 2 * e^{0.13(P-21.5)} - \frac{3}{16} * e^{-P+21.5}$	$2\sqrt{P/\lambda^2 - 1}$	$\lambda^2 < P < 1.127\lambda^2$

[a] Expressions obtained by curve fitting, minimum Goodness of fit: R^2: 0.9998, SSE: 9.5e-4 which is related to the case "Fig. 4.3–E", and for the other ones: R^2: 1, SSE: 1.8e-4

In Table 4.3, the axial load range for each concept considered to be between the value of the buckling load as the minimum and the value of the same sample fit unit distance as the maximum load. In other words for three IPMC sensor samples with boundary conditions defined in Table 4.3, in order to have the same amount of axial (tip) displacements, they should receive the maximum load defined in the load range of Table 4.3. These extreme cases are in Table 4.4 for all of the cases and calculations of average curvature and a helpful hint for sensor and IPMC coat segmentation pattern.

In Table 4.4, the active regions for each design configuration are defined. First, by using eqn. (4.8) and (4.9), the average curvature calculated. By using eqn. (4.10) and the local average curvature value for each design concept, active regions are defined. Another set of the active regions also calculated based on the minimum average curvature in order to have similar design criteria. For "Active regions 1" maximum value for k is the local one and for "Active regions 2" maximum value for k is 0.41, which is related to Fig. 4.2-D in Table 4.4. Active regions are for the unit length of an IPMC strip.

$$Ave.(k) = \frac{1}{S}\int_0^1 \frac{y''}{(1+y'^2)^{3/2}} \tag{4.8}$$

$$Ave.|k| = \frac{1}{S}\int_0^1 \left|\frac{y''}{\left(1+y'^2\right)^{\frac{3}{2}}}\right| \tag{4.9}$$

$$\left|\frac{y''}{\left(1+y'^2\right)^{\frac{3}{2}}}\right| \leq Ave.|k| \tag{4.10}$$

Table 4.4 Geometric properties of an IPMC sample with different boundary conditions

Sensor Concept (BC)	Deformation Equation:	Ave. |k|	Ave. k	Active Regions 1 [a] for Unit Length	Active Regions 2 [b] for Unit Length
Fig. 4.1–A	$Y(x) = 0.5\,[1 - \cos(2\pi x)]$	1.65	0	[0, 0.1], [0.4, 0.6], [0.9, 1]	[0, 0.1], [0.4, 0.6], [0.9,1]
Fig. 4.1–B	$Y(x) = [1 - \cos(\pi x)]$	0.83	0	[0, 0.1], [0.9, 1]	[0, 0.2], [0.8, 1]
Fig. 4.2–C	$Y(x) = \sin(\pi x)$	0.83	-0.83	[0.4, 0.6]	[0.3, 0.7]
Fig. 4.2–D	$Y(x) = 2 * \sin(0.5\pi x)$	0.41	-0.41	[0.7, 1]	[0.7, 1]
Fig. 4.3–E	$Y(x) = 0.71\,[1 - x - \cos\lambda x + \frac{1}{\lambda}\sin\lambda x]$	1.23	-0.42	[0, 0.1], [0.4, 0.6]	[0, 0.1], [0.4, 0.7]

Ave. |k|: Average Curvature Ave. k: Average Net Curvature

[a)] Areas with curvature larger than their average curvature considered to be active regions.

[b)] Areas with curvature more substantial than the average curvature in Fig. 3–D formation.

Fig. 4.3–F: Similar to Fig. 4.1–B, and Fig. 4.3–G: Similar to Fig. 4.2–D.

Table 4.4 provides a base for area segmentation, as discussed earlier. The surface segmentation for this case is possible even by scratching the coated metal from the surface in regions with almost zero curvature.

A closer look at the "Active regions 2" in Table 4.4 shows the intensity of curvature variation along the strip in the Clamped-Clamped (Fig. 4.1-A) configuration when compared with the Hinged-Hinged (Fig. 4.2–C) configuration. In connection with the graph in Fig. 4.8, curvature near the boundaries and bent areas changes rapidly in a small region from minimum to maximum values. The rapid variation of curvature values also showed in the Clamped-Hinged (Fig. 4.3–E) concept. The variation was less than 10% and on the hinged side variation of the threshold changed more than 10% along the strip.

When the criteria for active region changed from 1.65 to 0.41 for Fig. 4.1–A, the active region did not change much (variation was less than 10%, so it did not change the range). That demonstrates that the majority of curvature and sensing signals of IPMC in Clamped-Clamped configuration are from the boundaries and the middle part and the rest of the sensor is not active in generating sensing signals.

Table 4.3 and Table 4.4, along with Fig. 4.8, provide some general guidelines to select a proper coating pattern for specific samples. Also, the distribution of generated electrical charge will not have much of actuation effect on the IPMC as it is in the order of 1e-3 in comparison with the actuation voltage.

4.4 Experimental Results

For experimental results, a pair of IPMC samples (5 mm by 50 mm and 0.2mm thickness) configured for the Clamped-Clamped, Hinged-Hinged, and Clamped-Hinged configurations correspond to Fig. 4.1–A, Fig. 4.2–C, and Fig. 4.3–E. Three 5mm displacements applied to each sensor configuration, tests repeated five times, and the results are in Fig. 4.9 - Fig. 4.12. The test carried out at 73^{o}F, and relative humidity of 16% and using a program written in LabVIEW and using DAQ NI9219 to filter and scale the signals. During the tests at times t = 15 Sec., t = 25 Sec., and t = 35 Sec. +5 mm displacements applied to the end of the sensor, then at each 15 Sec. -5 mm displacements applied. The output voltage signals recorded for each unit of the applied displacement. The time accuracy of the manually applied load is better than 1 Sec.

Figure 4.9 shows the result for the Clamped-Clamped configuration. The probe for this concept was in the middle of the IPMC strip. The results obtained are from 5 sequences of tests. In some of the results at t = 5 Sec., one can detect the increase of the charge as it rapidly canceled within the next few seconds. Although the applied displacements were similar to other tests, there is not a clear relation between applied deformation and observed signal. As a result, these responses considered to be noise.

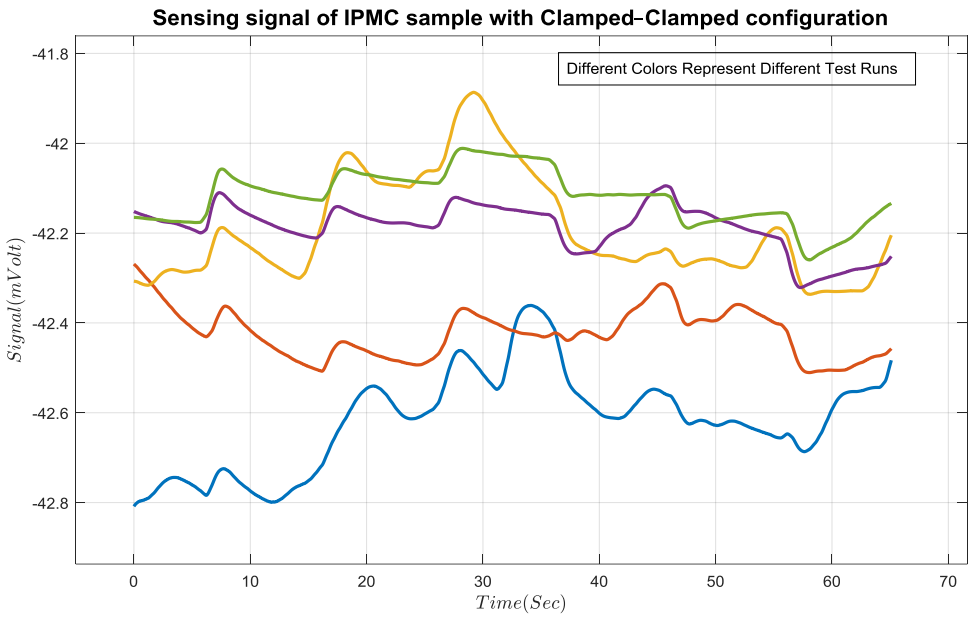

Fig. 4.9 Sensing signal of IPMC sample with Clamped–Clamped configuration

These test results also show the importance of surface conductivity and regional segmentation concepts introduced in Table 7 as when a local charge imbalance cancels out with other regions charges. The reason for having a slope after some of the pulses can be the electrical resistance of the IPMC. Note this slows the movement of the charges along the sensor membrane.

In Fig. 4.10, sensing signal of an IPMC sample in the Hinged – Hinged configuration is reported. The left side, the probe is on the low curved region. For the right side, probe on the high curved region. This results obtained for a Hinged-Hinged configuration, as for this concept, the average curvature is not zero (Table 7, Fig. 4.2-C). In these set of tests, sensing signal from two different regions have a

similar strength. In this figure, different colors demonstrate different runs of the described tests.

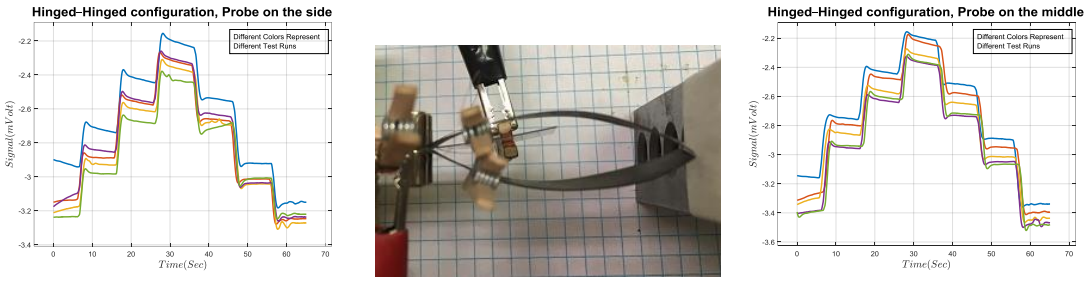

Fig. 4.10 Sensing signal of IPMC sample with Hinged–Hinged configuration

Fig. 4.11 represents the test results obtained from the sample in Clamped-Hinged configuration. These results are from areas with the lowest possibility for curvature and the middle area with high curvature. These test results also demonstrate what is being observed is the average sensing signal during these deformations (Table 7, Fig. 4.3-E). In this figure, for the left side results, the probe is on the low curved region. For the right side results, the probe is on the large curved region. The different colors related to different test runs in each figure.

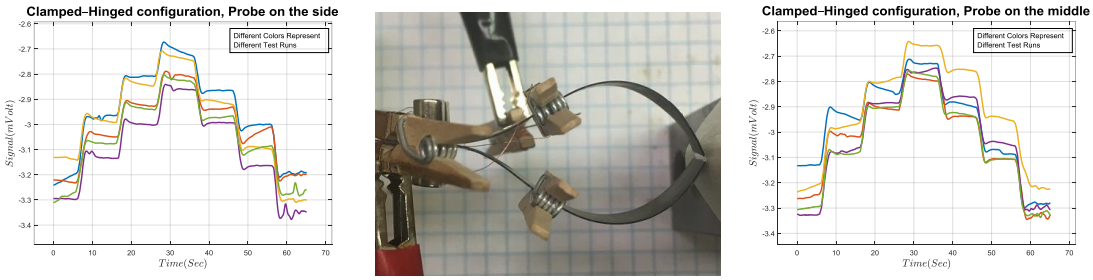

Fig. 4.11 Sensing signal of IPMC sample in a Clamped–Hinged configuration

The other observation is the variation of the charge for each displacement shown in Fig. 4.12. This Figure combined the test results of Fig. 4.10 and Fig. 4.11. In this figure, one can distinguish the two group of the received signal with the ratio of 2. Referring to Table 4.4, net curvature for the concept "Fig. 4.2–C" is almost two times what is in the concept "Fig. 4.3–E "which is another way of describing linear relation between curvature and sensing signal for IPMC. Comparison Sensing signal of Clamped-Hinged and Hinged-Hinged configuration. The graphs demonstrate two groups with a ratio of almost 2 for the generated signal.

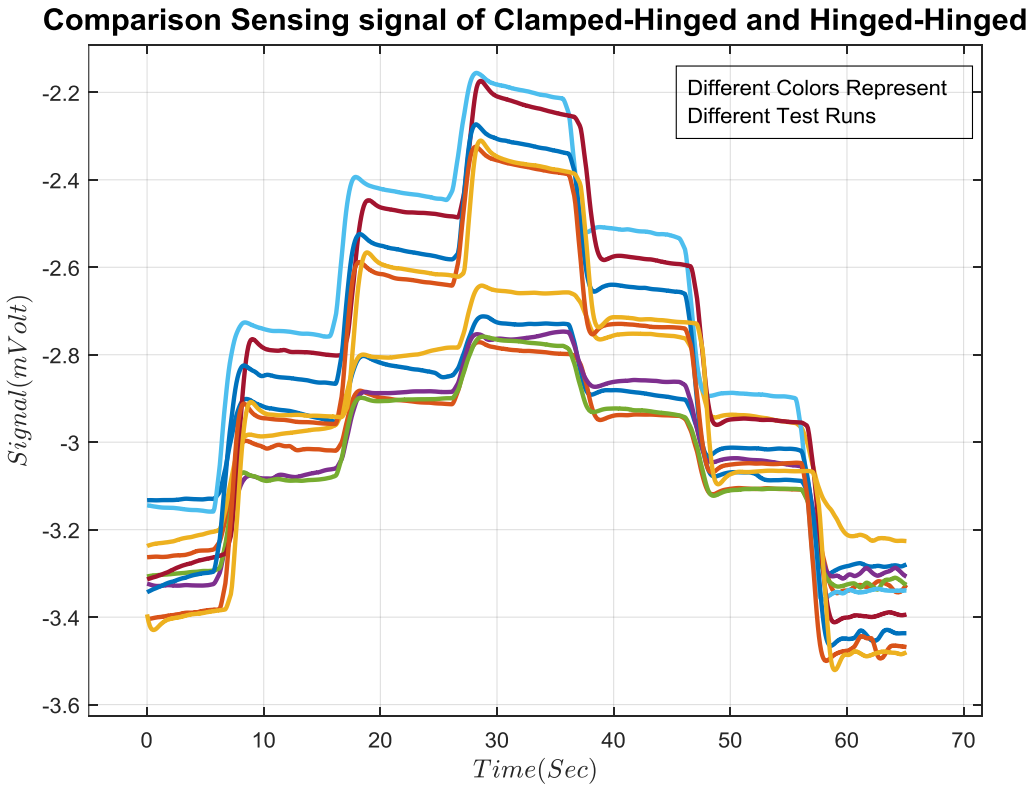

Fig. 4.12 Comparison Sensing signal of Clamped-Hinged and Hinged-Hinged

In this part, a new linear sensor configuration using the IPMC strip is introduced. The concept of post-buckling behavior of beams was employed to demonstrate the deformation of the IPMC beam. Graphic and expressions for the curvature provide a guideline for the practical applications of the IPMCs in the proposed configurations. The tests result demonstrate and confirm that the proposed linear sensing configurations based on the behavior of IPMC strips are a promising sensing scenario for IPMCs as linear displacement sensors. A linear relation between curvature and the generated signal in IPMCs is demonstrated.

The modeling approach presented in the next section for hinged-hinged and clamped-clamped configurations are expected to find the deformations more accurately.

4.5 Hinged-Hinged configuration

Figure below present an elastic beam under axial load with Hinged-Hinged boundary condition.

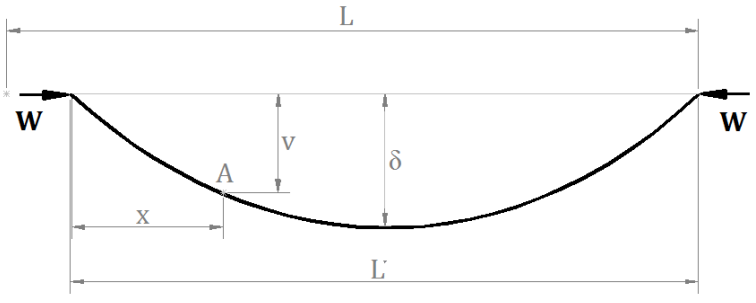

Fig. 4.13 An elastic beam material under axial load-deformation

Following equations applied for an elastic membrane under axial load. Parameters are defined in Fig. 4.13.

$$\left(\frac{2W}{EI}\right)^{1/2}.x = -\int_{\alpha}^{\emptyset}\frac{\cos\emptyset}{\sqrt{\cos\emptyset-\cos\alpha}}d\emptyset \tag{4.11}$$

$$\left(\frac{2W}{EI}\right)^{1/2}.v = -\int_{\alpha}^{\emptyset}\frac{\sin\emptyset}{\sqrt{\cos\emptyset-\cos\alpha}}d\emptyset \tag{4.12}$$

$$\left(\frac{2W}{EI}\right)^{1/2}.s = -\int_{\alpha}^{\emptyset}\frac{1}{\sqrt{\cos\emptyset-\cos\alpha}}d\emptyset \tag{4.13}$$

Above equations for maximum lateral deflections will be:

$$\left(\frac{2W}{EI}\right)^{\frac{1}{2}}.\frac{L'}{2} = \int_{0}^{\alpha}\frac{\cos\emptyset}{\sqrt{\cos\emptyset-\cos\alpha}}d\emptyset = \sqrt{2}\,(3E\left(\sin\left(\frac{\alpha}{2}\right)\right) - K\left(\sin\left(\frac{\alpha}{2}\right)\right)) \tag{4.14}$$

$$\left(\frac{2W}{EI}\right)^{\frac{1}{2}}.\delta = \int_{0}^{\alpha}\frac{\sin\emptyset}{\sqrt{\cos\emptyset-\cos\alpha}}d\emptyset = 2\sqrt{2}\sin\frac{\alpha}{2} \tag{4.15}$$

$$\left(\frac{2W}{EI}\right)^{\frac{1}{2}}.\frac{L}{2} = \int_{0}^{\alpha}\frac{1}{\sqrt{\cos\emptyset-\cos\alpha}}d\emptyset = \sqrt{2}\,K\left(\sin\left(\frac{\alpha}{2}\right)\right) \tag{4.16}$$

where K and E are complete first and second kind elliptic integral, L, L', and δ are the initial length, length of the deflected, and max lateral inflation for the IPMC sensor.

Solving the above set of equations gives the basic parameters of the IPMC in sensing. The solutions will be lateral inflation vs. axial deflecting, which is important for placing several sensors in a limited space.

Having the base equations for the shape of the deformed sample, and using the parametric equations for the curvature. The curvature for such a shape can be defined in the following form.

$$k = \sqrt{\cos \emptyset - \cos \alpha} \tag{4.17}$$

4.6 Clamped-Clamped configuration

Consider Fig. 4.14 for the clamped-clamped case. Assuming an elastic polymeric beam with under axial deformation and using the general format of Euler beam equation the following equations are valid.

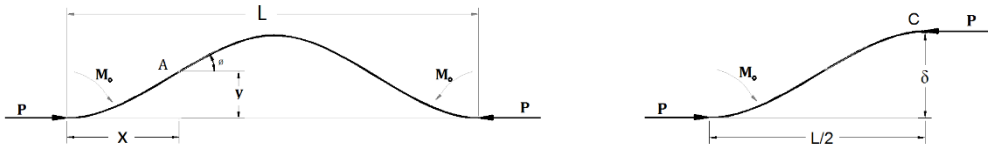

Fig. 4.14 An elastic clamped-clamped beam, axial load-deformation

$$M = \frac{EI}{R} \tag{4.18}$$

$$M = M_0 - Pv \tag{4.19}$$

$$ds = R\, d\emptyset \tag{4.20}$$

$$dx = \cos \emptyset\ ds \tag{4.21}$$

$$dv = \sin \emptyset\ ds \tag{4.22}$$

where E is elastic modulus and I is the moment of inertia of the elastic beam. At equilibrium, for a point like A will be:

$$\frac{EI}{R} = M_0 - Pv \tag{4.23}$$

Taking the derivative of eqn. (4.23) and integration leads to the following expression for the local radius of curvature.

$$\frac{1}{R} = \sqrt{\frac{2\,P}{EI}(\cos\emptyset - c)} \tag{4.24}$$

The general form of the curve presented in Fig. 4.14 defines changes in the curve direction. Solving for positive values of c yields the following value for θ ($0 \le \theta \le \pi$).

$$\emptyset_{max} = \cos^{-1} c \;\; for\; 0 \le c \le 1$$

Solving the above expression for point length, x, and y give the following expressions.

$$S = \sqrt{\frac{EI}{2P}} \int \frac{1}{\sqrt{\cos\emptyset - C}}\, d\emptyset = \sqrt{\frac{EI}{2P}}\, \frac{2F\left(\frac{\emptyset}{2}\middle|\frac{2}{1-c}\right)}{\sqrt{1-c}} + Const1 \tag{4.25}$$

$$x = \sqrt{\frac{EI}{2P}} \int \frac{\cos\emptyset}{\sqrt{\cos\emptyset - C}}\, d\emptyset = \sqrt{\frac{EI}{2P}}\, \frac{2\left[c\,F\left(\frac{\emptyset}{2}\middle|\frac{2}{1-c}\right) + (1-c)\,E\left(\frac{\emptyset}{2}\middle|\frac{2}{1-c}\right)\right]}{\sqrt{1-c}} + Const2 \tag{4.26}$$

$$v = \sqrt{\frac{EI}{2P}} \int \frac{\sin\emptyset}{\sqrt{\cos\emptyset - C}}\, d\emptyset = \sqrt{\frac{EI}{2P}}\, (-2)\, \sqrt{\cos\emptyset - c} + Const3 \tag{4.27}$$

$$M = \sqrt{2PEI}\sqrt{(\cos\emptyset - c)} \tag{4.28}$$

In the above set of equations, the moment equation can be used at the boundaries. Also, parameter c defines when and where the curvature changes its direction.

Solving moment equations for the left side and middle of the deformed shape ends up having the following equations for the moments at the boundaries.

At x = 0	At x = L/2
$M_{v=0} = M_0 - 0$	$M_{v=\delta} = -(M_0 - P\delta)$
$M_{\emptyset=o} = \sqrt{2PEI}\sqrt{(1-c)}$	$M_{\emptyset=o} = \sqrt{2PEI}\sqrt{(1-c)}$

$$M_o = \frac{P\delta}{2} \tag{4.29}$$

Using the above equations define the parameter C based on the applied force and lateral deflection.

$$c = 1 - \frac{P\delta^2}{8EI} \tag{4.30}$$

Above set of equations are sufficient to solve the deformation of IPMCs and its relation to the sensing signals. A graphical comparison between the beam post-buckling modeling, which is following the trigonal function and the model presented

in this session plotted in Fig. 4.15. The Figure demonstrates that the utilized beam model for post-buckling, in comparison with the approaches based on Euler beam, less intensity for curvature, and follows the same behavior in term of variations and critical points. This comparison gives justification for using closed-form equation of the selected post-buckling modeling approaches as they provide a similar characteristic for the critical points. In this figure for each pair of curves, the thinner line is trigonometry function, and the thicker line is from the solution to the elliptic integral presented in this session.

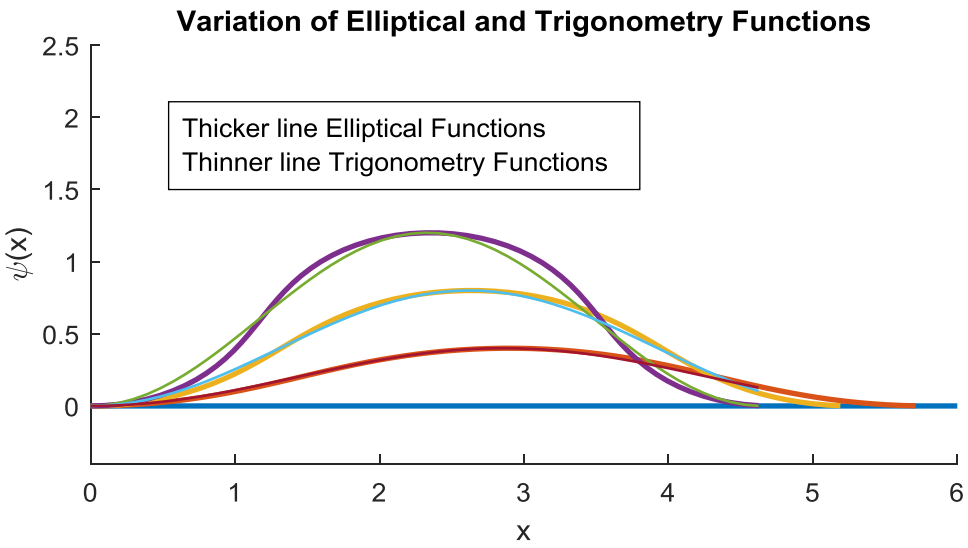

Fig. 4.15 elastic beam deformation of elliptical and trigonometry functions

CHAPTER 5

5 BASE CONFIGURATIONS OF ACTUATORS AND SENSORS

5.1 Basic elements

The major elements of IPMC configurations demonstrated in Fig. 5.1 were discussed in previous chapters. Base configurations: Cylindrical, Tubular, Linear, Slit, Helical, and Torsional for actuators and sensors will be discussed in this chapter. These elements are a single strip of IPMC with clamped, hinged, or free boundary conditions based on what presented in the previous chapters.

Having multiple of each of these components in an assembly, the load capacity of the sensor/actuator will increase in the assembly. For example here by a combination of 5 pairs of connected IPMC strips, load range will be $5 * 2 * (4\,\pi^2 < P < 4.25\,\pi^2)$ for a similar displacement range.

In Fig. 5.1, the basic pairs demonstrated as the upper left is Clamped-Clamped, the upper middle is Hinged-Hinged, upper right is Clamped-Hinged, and the lower row is their half model.

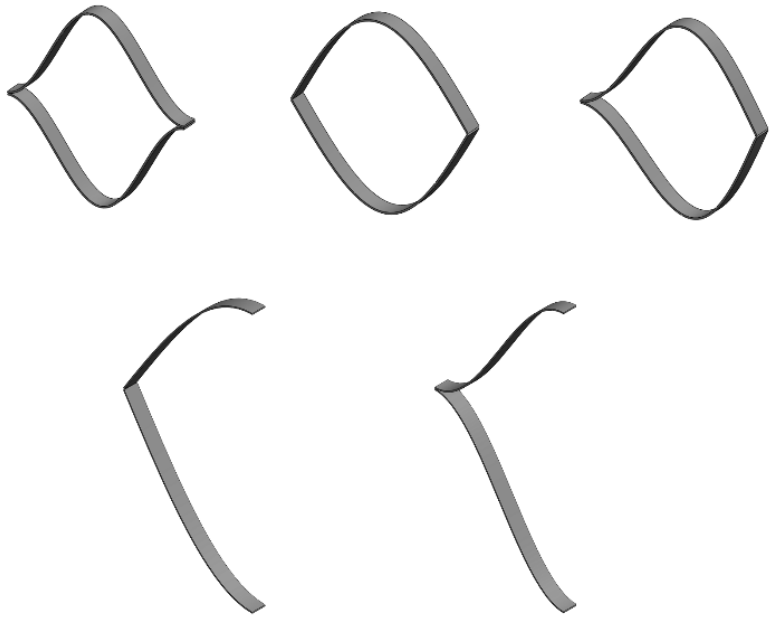

Fig. 5.1 Basic configurations of pairs of IPMC sensors

When it comes to the assembly configurations, the boundary connections will be a new parameter in defining the sensors and actuators. As mixed boundary connections give more flexibility to control the endpoint of the assembly. Figure 5.2 demonstrates a possible combination of these mixtures.

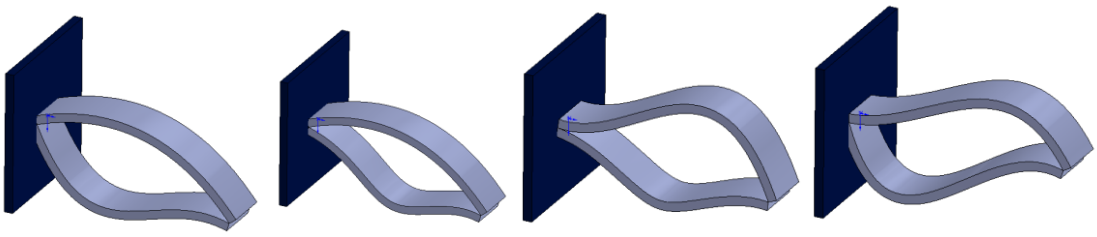

Fig. 5.2 Combination of the different boundary conditions IPMC actuators

5.2 Boundary connections

For the boundary conditions of these pairs of attached IPMC strips, the following configurations are considered to be possible, as shown in Fig. 5-2 regardless of the type of the boundary conditions. This figure presents the formation of pairs to each other. These are the boundary connections to define the distance between the individual membranes as an example, type C' presented in Fig. 5.4. This parameter generates the assembly of IPMC derivatives based on the type of boundary connections. Type A': placing the individual pairs next to each other. Type B': stacking the membranes. Type C': making of a flat piece of material.

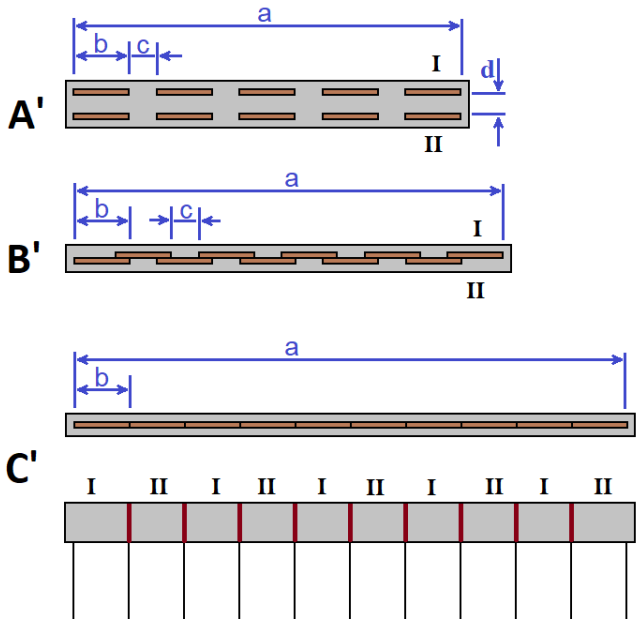

Fig. 5.3 Boundary connections of IPMC assembly

Figure 5.4 presents type C'. An Assembly of IPMC Strips with Clamped ends and Hinged ends. The right side picture describes the active area as they deform in two different directions.

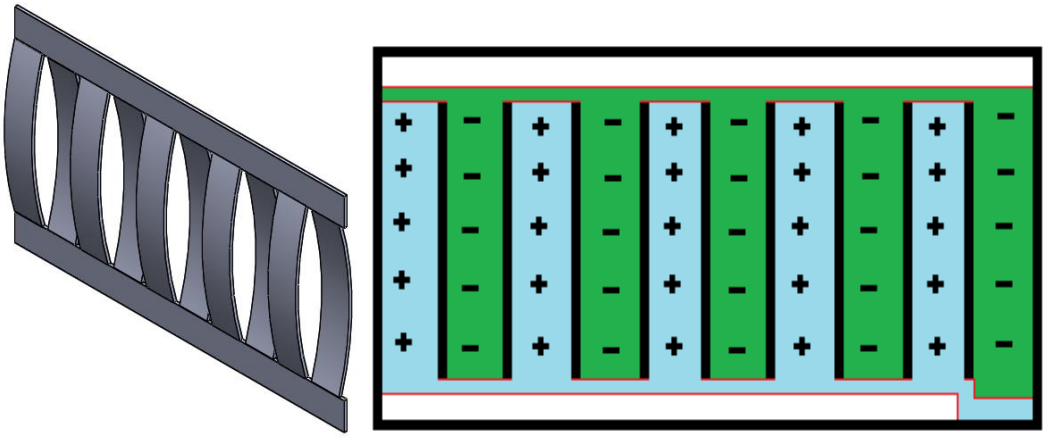

Fig. 5.4 - Two Assemblies of IPMC Strips

Each of these boundary connections has its characteristics and properties. For Type A', following characteristics considered to be possible:

I. Simple assembly effort, since it made of placing individual sensors/actuators next to each other with individual connection for every single pair.

II. Compact form, the width of the assembly depends on the gap between each pair "c". This gap can be almost zero resulting in the total width "a" be a summation of the width of each sensor/actuators. In this case a = 5*b.

III. Moderate complexity of wiring.

IV. It has the possibility for individual activation/sensing signals.

For type B', samples have a similar distance to type A'. In this formation, the mirrored membrane shifted to one side to share a contact point with its neighbor. This formation provides more simplicity in term of electrical connections as the first pair will be connected to output/input, and the rest of the assembly's electrical connection will be within the assembly structure. The following characteristics considered to be possible:

I. Moderate assembly effort, since it is made of connected individual sensors/actuators to the adjacent and neighboring element. This assembly formation might cause some complexity in terms of mechanical connection.
II. The compact form of IPMC elements, such that the width of the assembly depends on the gap between each pair "C" and half of a single strip. The gap can be almost zero resulting in the total width "a" to be a summation of the width of each sensor/actuators plus half of the last one, In this case, a = 5*b + 0.5*b.
III. The simplicity of wiring as the first pair needs wiring out to get or receive electrical signals.
IV. Individual activation/sensing signal is not possible.

Figure 5.5 presents a combination of these three formation concepts for a single sensor/actuator in term of Clamped-Clamped boundary condition. The schematic wiring for bending directions describes the divers wiring complexity for each concept.

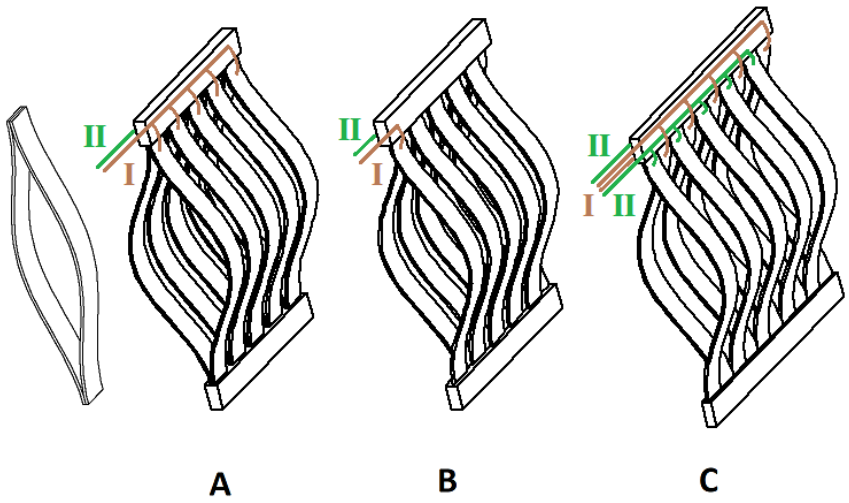

Fig. 5.5 Example of attaching multiple sensors

In Fig. 5.5, there is an example of attaching multiple sensors. On the left, a single pair of a sensor, A through B: multiple configurations of 5 pairs. These patterns have similar load capacity. However, their manufacturing is different. Also, for this concept, a more straightforward connection is possible with pattern coating.

5.3 Platform Arrangement

The assembly in these concepts is along a straight line. This sensors/actuators assembly can be around a circular or rectangular boundary. By this, the whole assembly has a more compact form and more stability. A schematic of this formation is presented in Fig. 5.6. This combination provides stability in comparison with the one along a straight line.

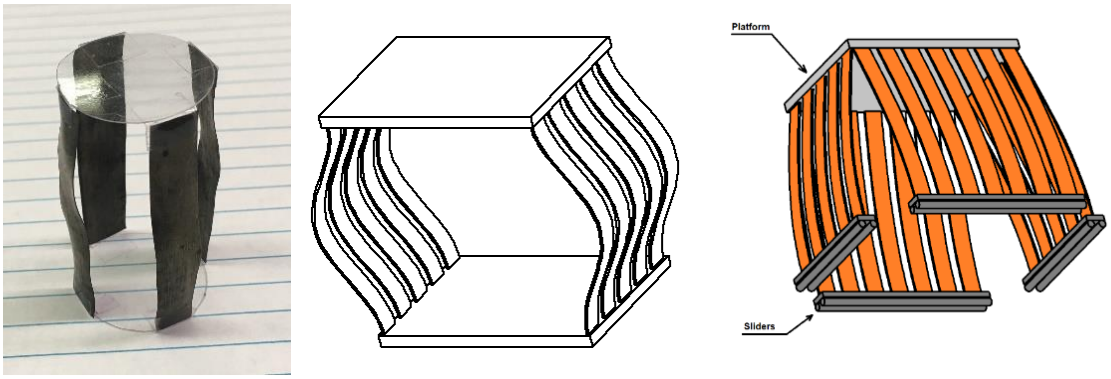

Fig. 5.6 Circular and rectangular assembly of IPMC sensor/Actuators

Examples of circular and rectangular assembly of IPMC sensors/actuators are in Fig. 5.6. The assembly might fully cover the surrounding area of the platform or partially cover the sounding area of the platform. An example of linear actuation presented in Fig. 5.7. In this configuration, all of the IPMC membranes used the common electric connection of the slit cylindrical IPMC actuator. The deformation obtained with 15 Volts actuation voltage[141].

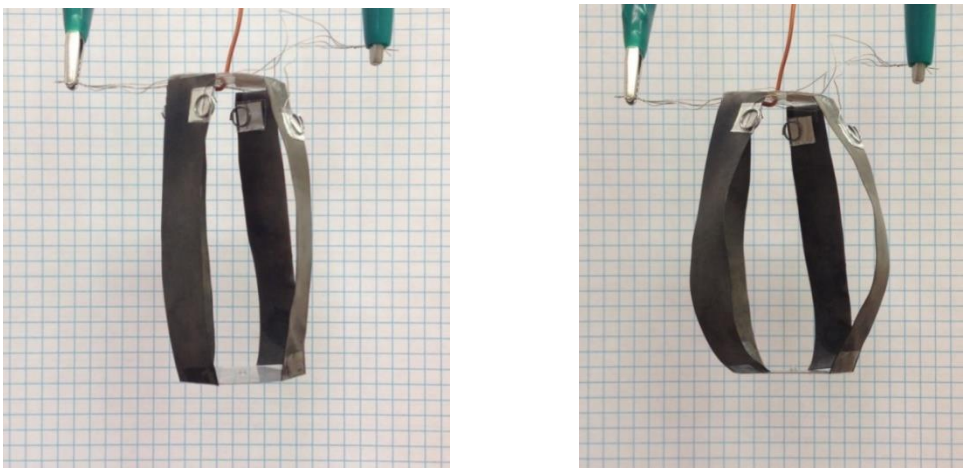

Fig. 5.7 Actuation of a slit cylindrical IPMC actuator

5.4 Directional Arrangement

So far, the sensor/actuator direction was along a primary axis. An alternative to this formation is considering the assembly at an angle other than 0 or $\pi/2$ radian with respect to a primary axis. This formation gives an alternative possibility of sensing and actuation. In term of sensing, the linear assembly can sense the horizontal and vertical displacements simultaneously. The circular formation can sense the axial and rotary inputs. In term of actuation, these formations will be able to impose these characteristics as their outputs. Various combination arrangements of IPMC strips presented in Fig. 5.5 through Fig. 5.7. Particularly Fig. 5.8 and Fig. 5.9 demonstrate prototypes for the directional arrangement of IPMC elements in circular and linear assembly and an assembly of straight IPMC strips are also shown.

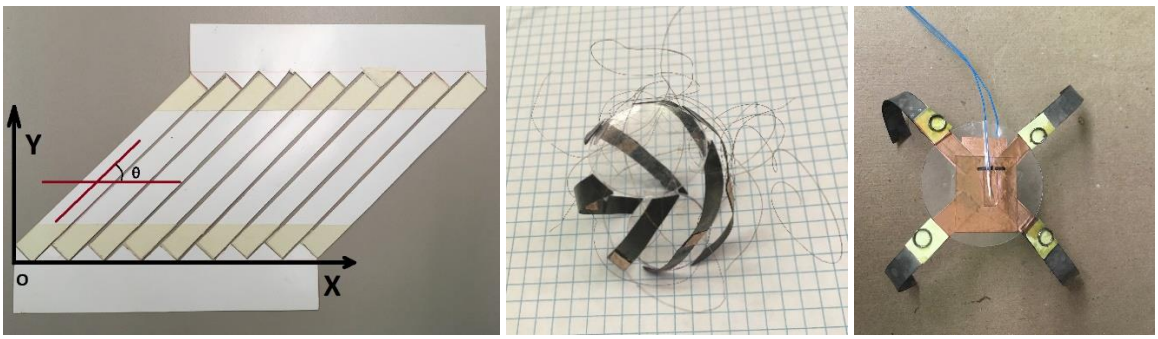

Fig. 5.8 Prototype models for assembly of IPMC sensor/actuator

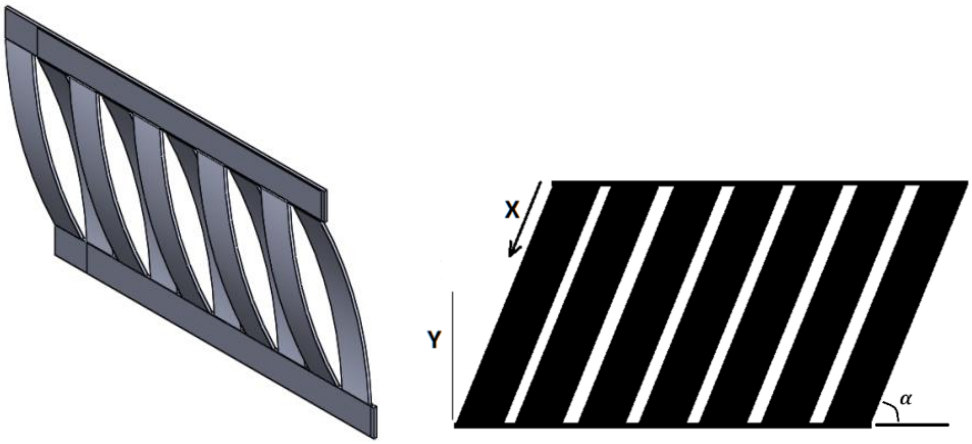

Fig. 5.9 Angled arrangement concept of IPMCs membrane

In Fig. 5.8 for the angles arrangement of the IPMC strips at the boundaries, the ending can be perpendicular to the direction of the individual strip sample (similar to the linear prototype) or the ending can be to the platform (similar to the cylindrical version). Considering and using the one with rectangular end-cut makes the equation and formulations much easier. Based on this configuration, each strip will follow the formulation along its axis. Moreover, rectangular end-cut torsion for the helical version has a much simpler definition.

In actuation, the following relations are considered to be valid for displacement ∇ along the IPMC membrane, and for angle Θ in Fig. 5.8 (or angle α in Fig. 5.9) of the membrane slope with respect to the x-axis.

$$\textit{Actuation displacement} \text{ along x axis } = \nabla \cos \Theta \tag{5.1}$$

$$\textit{Actuation displacement} \text{ along y axis } = \nabla \sin \Theta \tag{5.2}$$

And in sensing following relations are considered to be valid.

$$\nabla = \text{(sensing displacement along x axis)}/\cos\theta \tag{5.3}$$

$$\nabla = \text{(sensing displacement along y axis)}/\sin\theta \tag{5.4}$$

For the case of the circular platform, this deformation interprets in the form of axial displacement and angular rotation. Considering θ be the pitch angle of IPMC strips, in actuation.

$$Axial\ actuation\ displacement = \nabla \sin\theta \tag{5.5}$$

$$Angular\ actuation\ rotation\ (Radiant) = {}^{\nabla \cos\theta}/_{2\pi\, r} \tag{5.6}$$

5.5 Cylindrical and Helical form of IPMC actuator/sensor

Arranging IPMC membrane around a circular object or just around the linear arrangement of the IPMC membrane in a circular form gives a new formation of actuator/sensors. The force capacity will be the summation of the number of membrane capacity.

In addition to the above configurations, another configuration of actuator element will be using the IPMC strip at an angel or role the IPMC strips around a circular object mantle as shown in Fig. 5.10 through Fig. 5.14 to have a helical arrangement.

In Fig. 5.10, assembly of collinear IPMC strips actuators going through a cycle of deformations depicted. This assembly is a prototype of cylindrical IPMC actuator/sensor under various endpoint displacement.

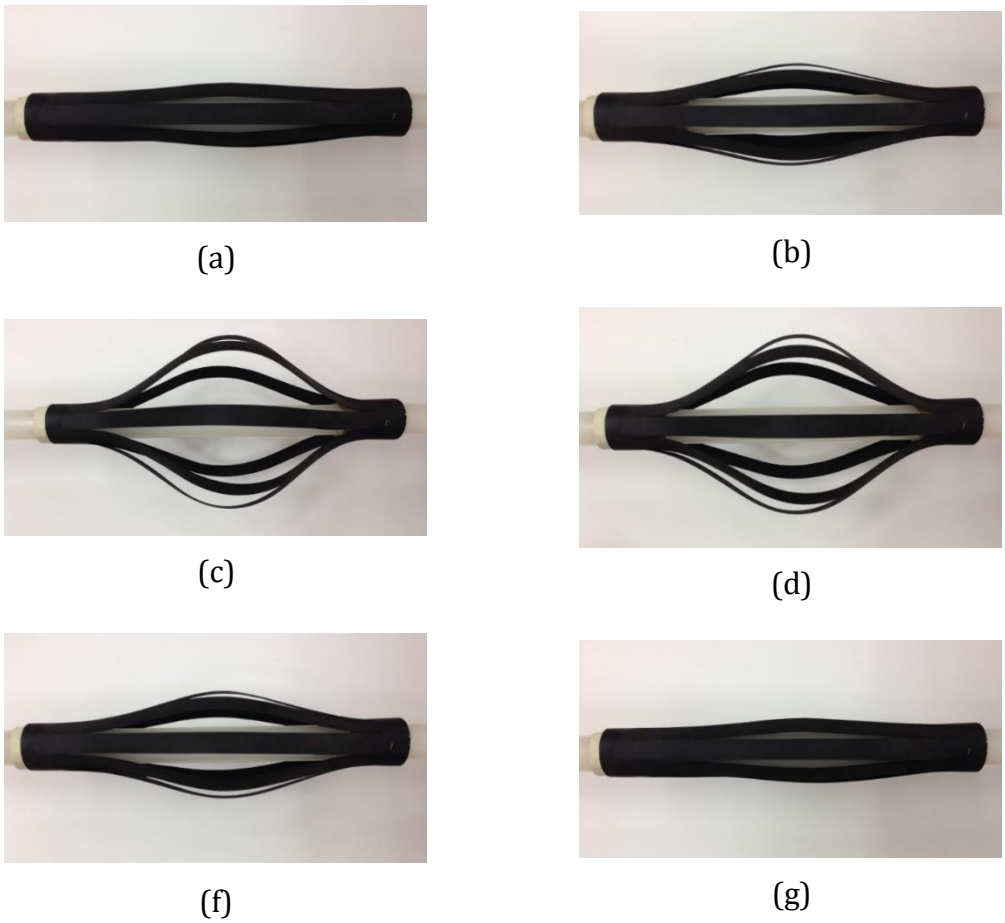

(a) (b) (c) (d) (f) (g)

Fig. 5.10 Prototype of cylindrical IPMC actuator/sensor

(a) (b) (c)

Fig. 5.11 Cylindrical, and Helical form of IPMC actuator/sensor

In Fig. 5.11 and Fig. 5.12 some concepts and prototype of Cylindrical, and Helical geometry form of IPMC membrane of actuator/sensor presented. Formations in Fig. 5.11 and Fig. 5.12 are complex geometries in the analysis as being helix[146], [147] or a twisted geometry, but for the prospect of actuation and sensing, they are a group of pre-bent and pre-twisted strips IPMC strips placed at an angle. Angel of the twist reduces as the bending increases and vice versa. Twist angle depends on the revolution of the strip around the circle.

In Fig. 5.11, The left side is slit cylindrical formation, the middle row is the helical version with strips goes to touch the circular platform, and the right side represents a version with rectangular IPMC strips placed around a cylinder. A

prototype form of this form presented in Figure 5.12. These figures demonstrate the concept of twisting in this group of actuation and sensors.

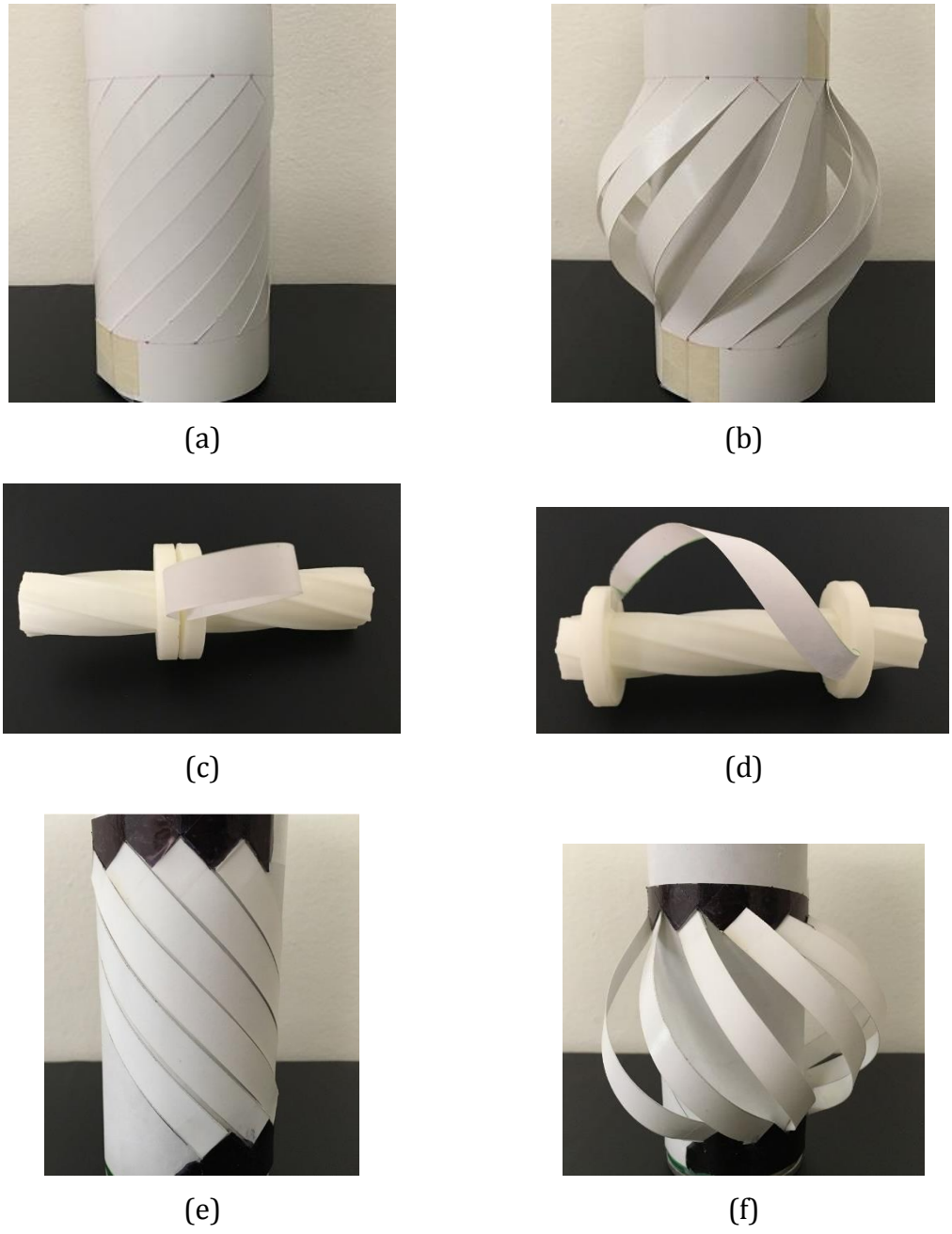

(a) (b)

(c) (d)

(e) (f)

Fig. 5.12 Deformations and twisting of IPMC as helical actuator/sensor.

In Figure 5.12, (a) demonstrates IPMC as helical actuator/sensor at rest. (b) demonstrate the twist-helical as the sample deformed, (c) (d) demonstrate a single strip at full deformed and expanded along the helix, (e) another helical with a different connection at rest and deformed are in the formation(f).

In Fig. 5.13, The test carried out for a hypothetical sample being around a cylindrical object (a), in this form, the IPMC sample can be considered a single strip in space (Fig. 5.14-d), while it is deformed, it will not follow the straight line connected its original ending and follow the helix curve. This constraint caused the IPMC strip to experience a twisting as it deformed Fig. 5.13-b. The twisting will be zero when the strip has fully collapsed where its end reaches the straight line connects its end in the rest formation.

(a) (b) (c)

Fig. 5.13 Deformation of IPMC in a helical configuration.

In Fig. 5.13, deformation of IPMC in a helical configuration demonstrated as at the beginning (a), and at full collapse (c) there is no twist.

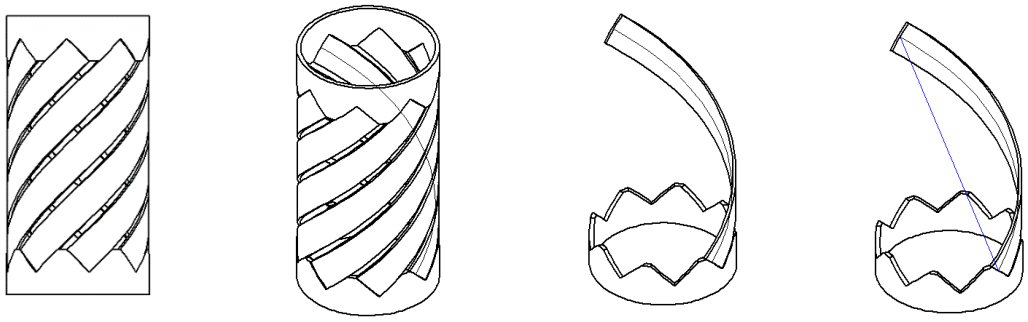

(a) (b) (c) (d)

Fig. 5.14 IPMC model in a helical slit configuration

In Fig. 5.14, IPMC model in a helical slit configuration showing the IPMC strips and how they are the individually arranged wrap of IPMC strips around a cylindrical mantle in (a), (b) and (c). Following is a set of equations considered for a helix in the Cartesian coordinate system.

Using a set of the equations in Table 5.1 gives the necessary component to simulate the deformation of the membrane at each point.

Table 5.1 Helix equations in a Cartesian coordinate system for the initial parameter of IPMC in helical actuator/ sensor configuration

$x(t) = r * \cos(t)$	$k = \frac{r}{r^2 + c^2}$
$y(t) = r * \sin(t)$	$s = \sqrt{r^2 + c^2}\, t$
$z(t) = c * t$	$\tau = \frac{c}{r^2 + c^2}$

for $0 \leq t \leq \pi$ where r is the radius of the helix, x, y, and z are coordinate system axis, k, s, τ are curvature, arc length, and torsion.

Arc length gives the initial length of the IPMC strip, coordinates at the beginning define the shape of the IPMC membrane and end points of the membrane. Knowing the endpoints and torsion at endpoints in connection with boundary condition, one may derive the deformation definition equations for various boundary conditions.

The Helical assembly will rely on the displacement of the endpoints along the helix curve, so axial deformation and rotation of the helical assembly are related based on the following equations.

$$\text{Rotation of one end (radiant): } ds * \frac{\cos(\alpha)}{2\,\pi\,r} \tag{5.7}$$

$$\text{Axial displacement of one end: } ds * \sin(\alpha) \tag{5.8}$$

5.6 Electrical connection

Each of these IPMC strips in the sensing mode act as a source of potential energy. These IPMC strips can be added in a series of electrical connections to generate more stable output. Since the signal will be the average output of all IPMC sensors together or they can be attached in series to sum the values and generate a higher signal. This way, it is expected that the assembly sensor had a higher sensitivity as the output of all individual sensors is summed to generate a higher voltage. In Fig.

5.15, schematic of the electrical connection for slit pattern coated cylindrical IPMC demonstrated for two types of boundary condition.

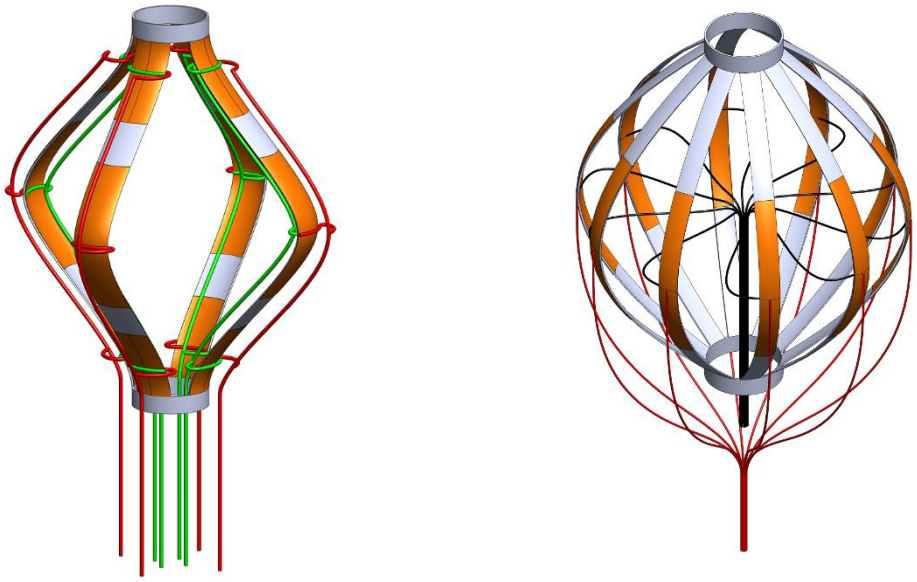

Fig. 5.15 Demonstration of wiring for slit cylindrical IPMC actuator/sensor

5.7 Selection of a proper configuration

Combinations of variations presented above provide possibilities for actuation and sensor configurations. Each of the above deviations for various configurations has some advantage over the others. The above concepts have 5 x 4 x 2 x 2 x 2 = 160 variations, besides the number of actuators/sensors and with the assumption of having two variations for the platform arrangements. One way to find an optimum configuration for a simple actuation/sensing application is to look at the expected outcome and decide based on those parameters. Some of the parameters that may

be interesting are **A:** load consideration, **B:** displacement range, **C:** compactness, **D:** signal stability, and **E:** Sensitivity.

Each parameter has a different value for different applications, and several configurations are possible, as discussed earlier. Each configuration has different value points related to an application. This complexity makes choosing the proper concept of a new task difficult. There are many algorithms to enhance such a selection. One is a decision algorithm by Nategh et al. (2008)[148]. This algorithm, based on the different value sets for different application scenarios, will sort out these configurations. This algorithm initially introduced to enhance defining priority of design factors based on customer requirement in a machine tool design procedure. The scenario is useful if these design configurations are considered as the factors to be prioritized, and the sensing and actuation application requirements by the customer requirements. Here is an example list of parameters related to each variation described in section 2.

Table 5.2 Design Configurations multiplier list

Formation:	Boundary Connection:	Load Capacity:
- Clamped –Clamped - Hinged – Hinged - Clamped – Hinged - Clamped – Free	- Connection Type A' - Connection Type B' - Connection Type C'	- 1 pair - 2pairs - 3 pairs - 4 pairs

Platform:	Arrangement:	Direction:	E-Connection:
- Rectangular - Circular	- Linear - Circular	- At angle - Straight	- Series - Parallel

Each of the above design multipliers has some advantages and disadvantages when they come to choose their subcategory. Some of the parameters that define these advantages and disadvantages are Load capacity, Displacement, Operational space, Stability, Sensitivity.

For a particular application, one may define their priority of these parameters and using a decision-making algorithm to sort the priority of the Design Configurations multiplier.

CHAPTER 6

6 IPMC LOOP AS ACTUATOR, SENSOR, AND ENERGY HARVESTER

6.1 Introduction

This group of sensors and actuators is made by bending and looping an IPMC strip to make an end-to-end cross and form a looped haptic feedback sensor/actuator. The sensing characteristics as a soft biomimetic haptic feedback sensor are shown to have an excellent potential for ubiquitous Robot-Human Interactions (RHI) as well as providing haptic feedback for robotic surgery. The new family of Ionic Polymer-Metal Composites (IPMCs) sensors and actuators in the form of a loop, made by bending a strip of IPMC around to make an end-to-end cross and form a looped haptic robotic feedback sensor/actuator.

The looped cantilever IPMCs is shown to be capable of bending and sensing characteristics upon various types of deformations. They are shown to generate unique output voltage signal and transient current correlated to the haptic feedback force. Furthermore, the looped IPMC haptic feedback sensor can enable a new advanced technology in robotic surgery by providing surgeons efficient routines for kinesthetic and softness inquiry of organs and tissues during robotic surgery. They can be actuated simultaneously on the fly for reconfiguration of looped IPMC feedback sensors for normal grasping and manipulation of bodily organs and tissues. Also, looped IPMC haptic force feedback sensors have potential as a smart

skin for the development of human-like dexterous and soft manipulation and haptic/tactile sensing.

Operationally they will be used either as haptic feedback sensors in robotic surgery or haptic feedback sensor in determining the softness of the materials or organ the surgeons are performing surgery. Also, these soft looped IPMC sensors and actuators can be in robotic automation and manufacturing in which delicate parts need to handle softly. Looped IPMCs can be tactile sensors as well as haptic feedback sensors. Various configurations of looped IPMCs depicted in Fig. 6.1 and Fig. 6.2, providing haptic feedback sensing signal by contacting and pressing over various organs or bodies.

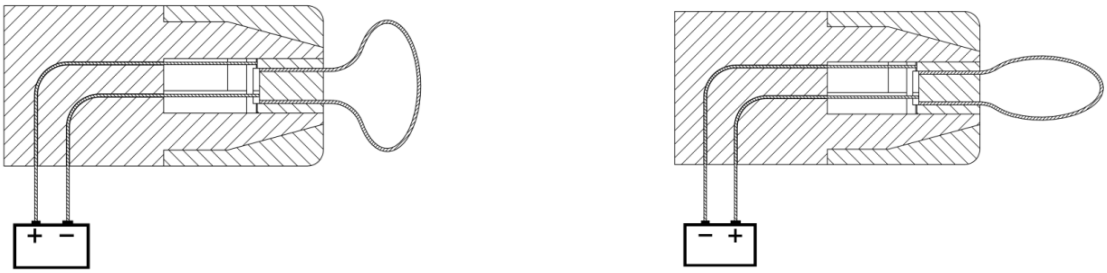

Fig. 6.1 Looped IPMCs actuator with different configurations

Looped IPMCs sensor generating haptic feedback signal as pressing on or sliding over the surface of an organ in Fig. 6.2.

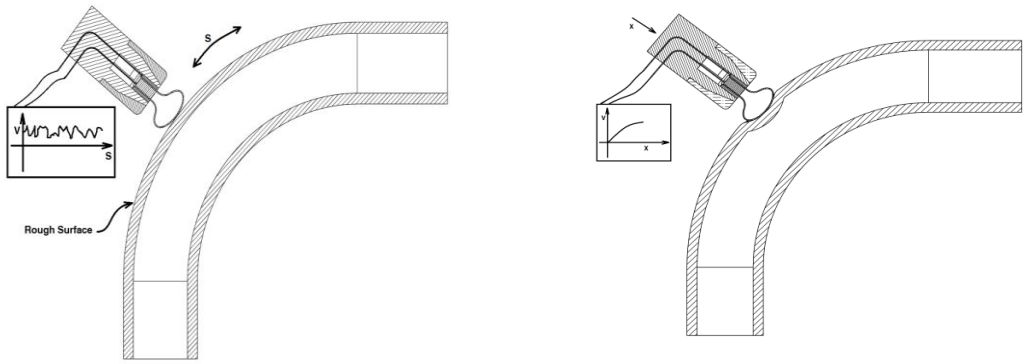

Fig. 6.2 Looped IPMCs sensor generating a haptic feedback signal

6.2 Model descriptions

A conceptual design for a looped haptic feedback sensor made with IPMCs is similar to the graphic shape in Fig. 6.4. The looped configurations IPMCs can interact with organs and tissues. They provide the relevant kinesthetic force signal based on the bending of IPMC strips or deformation of the loop. This signal can be correlated to the force exerted. The looped IPMCs is capable of actuation and haptic feedback sensing simultaneously through proper design and configuration.

Since the procedure for this configuration is bending a straight sample to get the model, results of a deformed beam under similar condition considered for the analysis, looped IPMCs assembled in the form of a cantilever loop by bending a strip of IPMC around to reach itself end-to-end and form a looped haptic feedback sensor and looped actuator. The looped cantilever IPMCs are capable of bending and twisting actions as well as soft sensing.

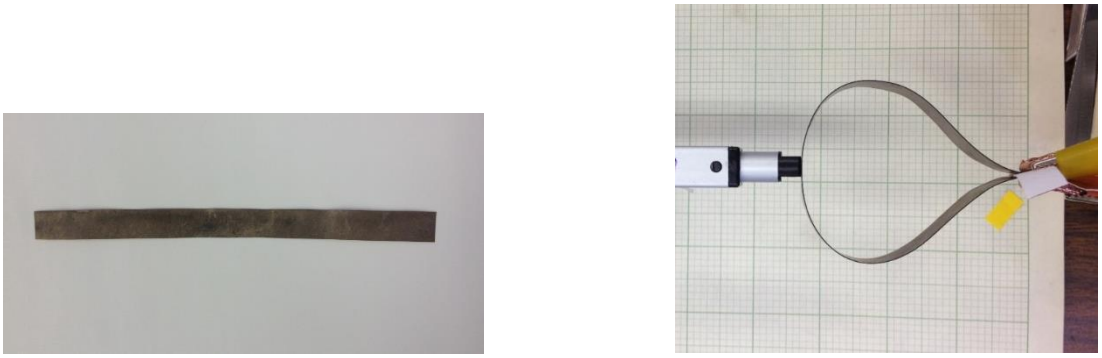

Fig. 6.3 IPMC sample original form and the looped form

One way to present the shape of this loop is to follow the procedure introduced for flexible link mechanisms[149]. This procedure is based on Euler-Bernoulli law and some mathematical manipulation expressing the curvature based on its actual mathematical value. The work eventually presents a system of 7 equations to find ten unknowns. Later the study presents two expressions to define the shape of the elastica as below expressions.

$$x_i = \frac{P\sqrt{EI}[2E(k,\phi_i)-2E(k,\phi_1)-F(k,\phi_i)+F(k,\phi_1)]}{\sqrt[4]{P^2+Q^2}^3} + \frac{2Qk\sqrt{EI}(\cos\phi_i-\cos\phi_1)}{\sqrt[4]{P^2+Q^2}^3} \quad (6.1)$$

$$y_i = \frac{Q\sqrt{EI}[2E(k,\phi_i)-2E(k,\phi_1)-F(k,\phi_i)+F(k,\phi_1)]}{\sqrt[4]{P^2+Q^2}^3} + \frac{2Pk\sqrt{EI}(\cos\phi_1-\cos\phi_i)}{\sqrt[4]{P^2+Q^2}^3} \quad (6.2)$$

In the above expressions E, and I are elastic modulus and moment of inertia of the material. P and Q are axial loads and lateral load on each side of the membrane. Functions F and E are elliptic integrals of the first and second kind, and parameters ϕ and k can be found by inspection of the shape and nature of the undulating elastica.

Using these expressions for an elastica under unit force and considering $\phi_1 = 0$ with a different value for parameter k the following shapes generated in Fig. 6.4.

Fig. 6.4 Generated deformed shape for elastica under axial load

In Fig. 6.4, the left side represents different shape forms based on the parameter k. the right side generated by considering parameter k = 0.73 and scope of the elliptic integral 0.3π~1.7π radian for the sets of equations eqn. 6.1 and 6.2.

6.3 Testing the looped IPMC in haptic sensing

In this experiment, a single 14 mm wide strip of IPMC was bent to create a looped sensor with the length of 73 mm between the surface of IPMC at the endpoints in the loop electrode was placed and the other side as the electrode clamp was holding the assembly. Then, the IPMC loop placed in front of the tip of a linear actuator. LabVIEW software with a data acquisition card and signal generator card used. A pre-test was done to have a better understanding of the effect of noise filtering on the collected data. In this pre-test, different filtering scheme applied to a

5cm range of displacement during data collection Fig. 6.6. For this concept, data passed through a 0.5 Hz filtration are considered to have a proper portion of clarity and data.

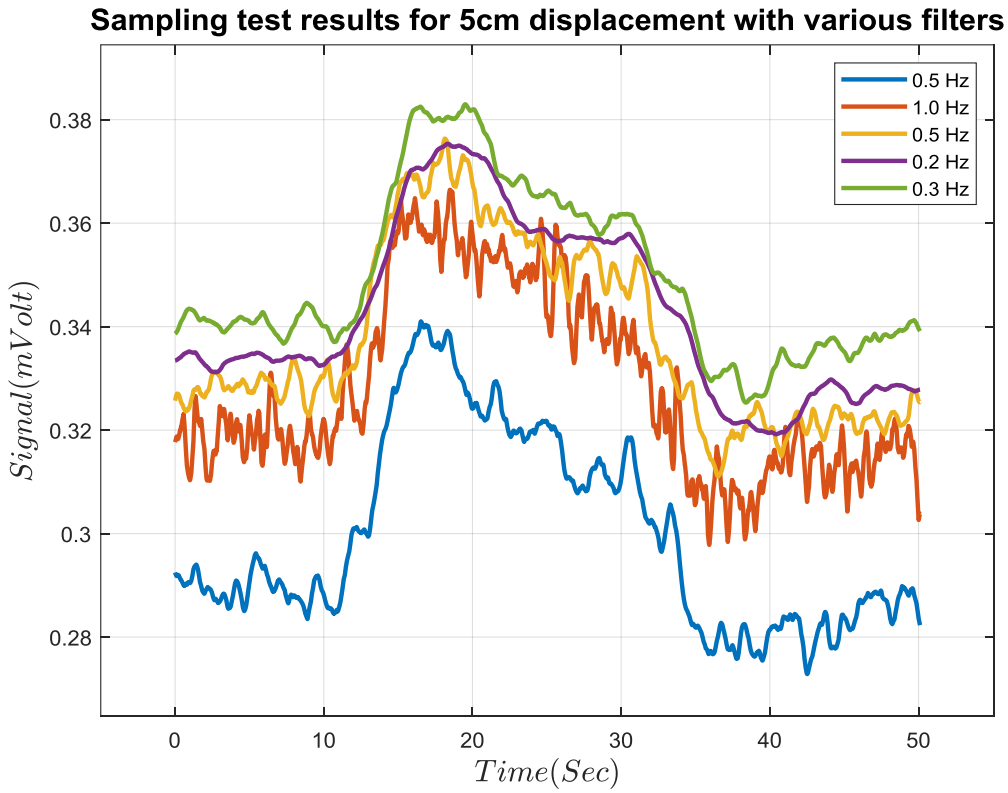

Fig. 6.5 IPMC sensing results for a 5cm displacement with various filters

Experiments for the case in which a frontal tip force pushed the looped IPMC sensor presented in Fig. 6.6. Fig. 6.10 and Fig. 6.12 depict the experimental set up in which the looped haptic sensor deformed in a direction directly and the shape of the looped sensor under full frontal deformation. In Fig. 6.6 IPMC loop sensor is in its initial surface contact on the left side, and reshaping to 5 cm deformation on the right side in haptic feedback sensing

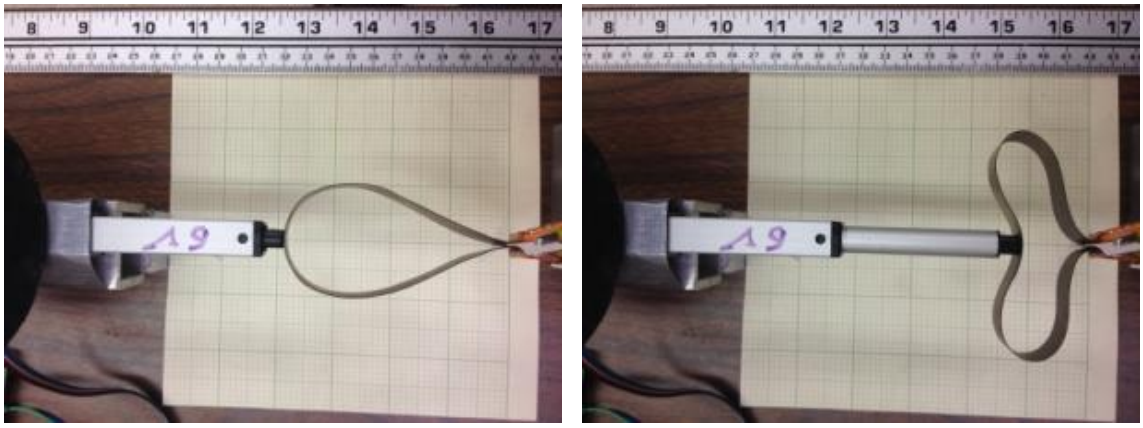

Fig. 6.6 IPMC loop sensor in haptic feedback sensing

In Fig. 6.7 sensing experimental results for a 5 cm displacement of tip force presented. The result consists of 10 experimental measurements for 5 cm displacement. The test continued for less displacements 4 cm, 3 cm, 2 cm, and 1 cm.

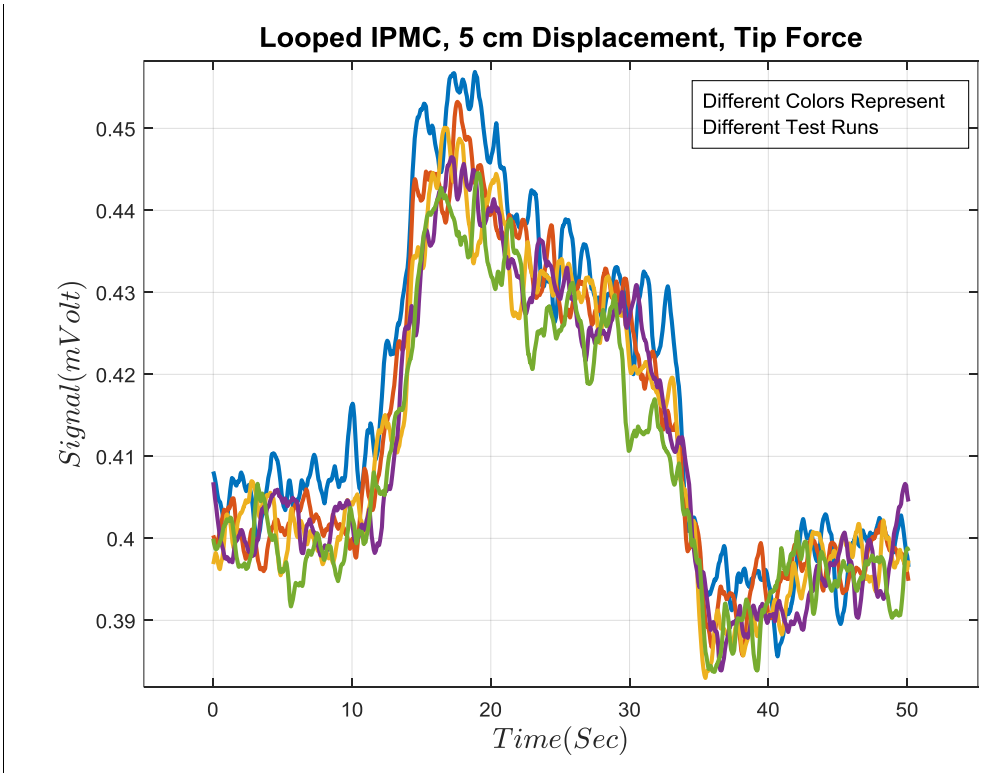

Fig. 6.7 IPMC sensing experimental results for a 5cm displacement

In Fig. 6.8 variations of charge level on the sample for a 1 cm deformation reported. Charge variations for 1cm displacement are not as clear as they were for other levels of deformations. Additional tests were performed by applying lower filtering frequencies. However, the results did not change very much, as shown in the figures. As a result, this 1 cm displacement considered the limits of this test setup.

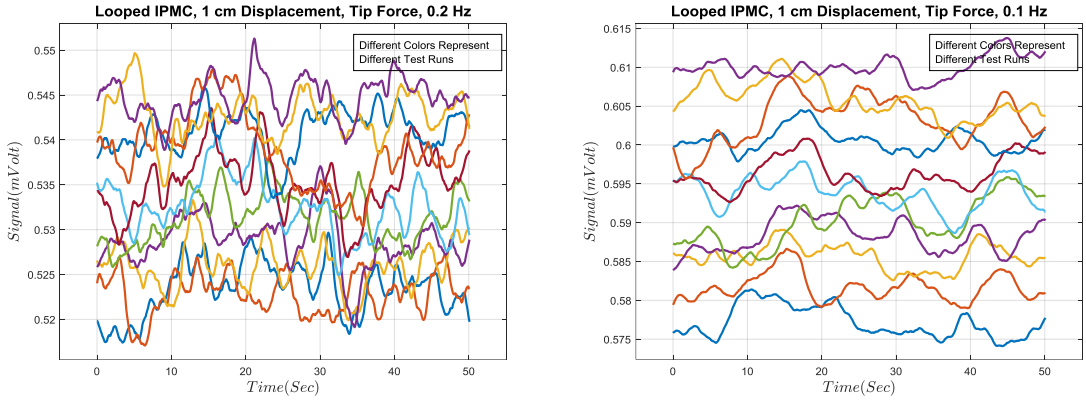

Fig. 6.8 IPMC sensing test results for 1cm displacement

For setting the minimum and maximum displacement for the test setup and other parameters, many tests performed. Tests repeat for displacements 1 cm, 2 cm, 3 cm 4 cm, and 5 cm are shown in Fig. 6.9.

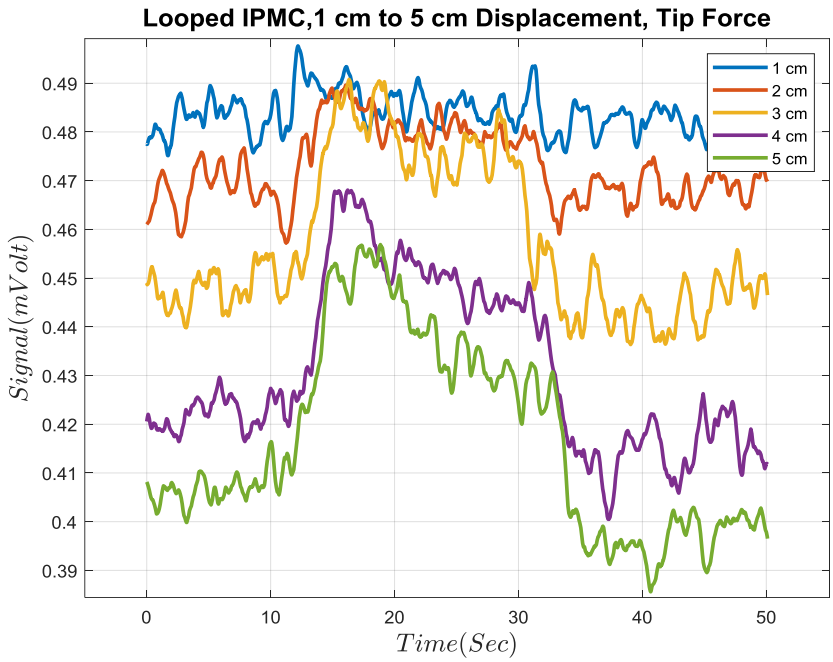

Fig. 6.9 Looped IPMC response voltage signal to tip point force

In Fig. 6.10, test results of the deformations for various applied displacement are reported. This figure contains test results for applied deformations from 1 cm to 5 cm to the linear actuator. Each test contains several consecutive test results demonstrating the consistency of the responses. There is 10 second missed from each 1 minutes recorded data. This time length considered to be used by system at the beginning of the recording to gain enough data for the utilized filtering system.

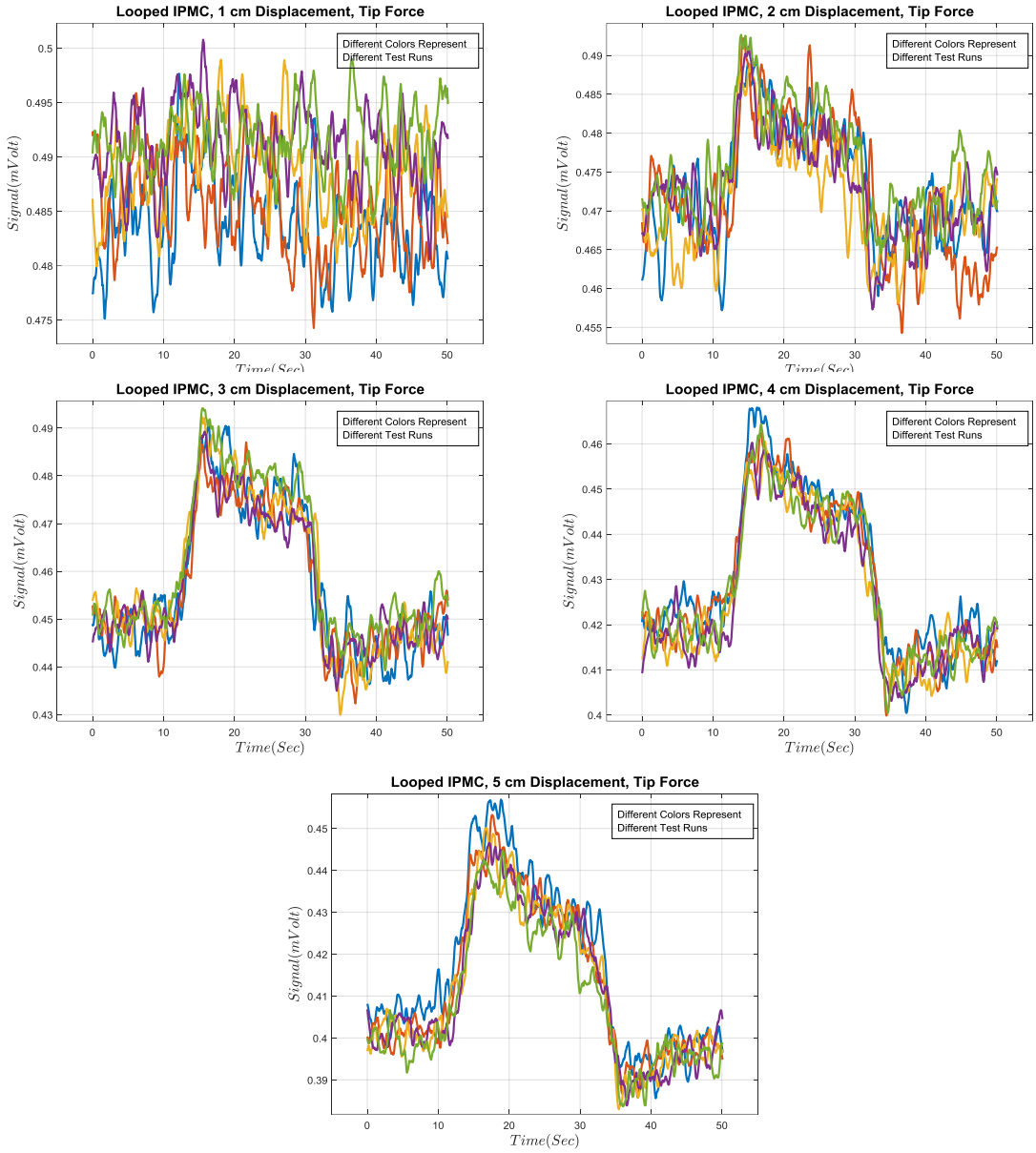

Fig. 6.10 Looped sensor stable responses of tip point deformations

Based on the above test results, depicted in Fig. 6.7, Fig. 6.8, and Fig. 6.9, the consistency of the received signal provides a good basis to consider and search for a linear relationship between the generated output signal and the applied displacement. The initial voltage variation and the deformation can be simplified in

Table 6.1((generated voltage vs. displacement). Based on these results, there is a linear relation for the applied tip displacement and the generated signal for this configuration.

Table 6.1, Generated Voltage Vs Deformation or Tip Displacement

Deformation (cm):	5 cm	4 cm	3 cm	2 cm	1 cm
Charge Variation (mV):	5 mV	4 mV	3 mV	2 mV	1 mV

Experiments were also conducted for the looped IPMC sensors experiencing a flat tip pushing the IPMC looped sensor. In this experiment, a linear actuator with a flat tip or flat surface pushed the looped sample Fig. 6.11. The final deformation of the sample showed more bending than the test done by pointed tip pushing the looped IPMC, and it is expected to generate more significant signals.

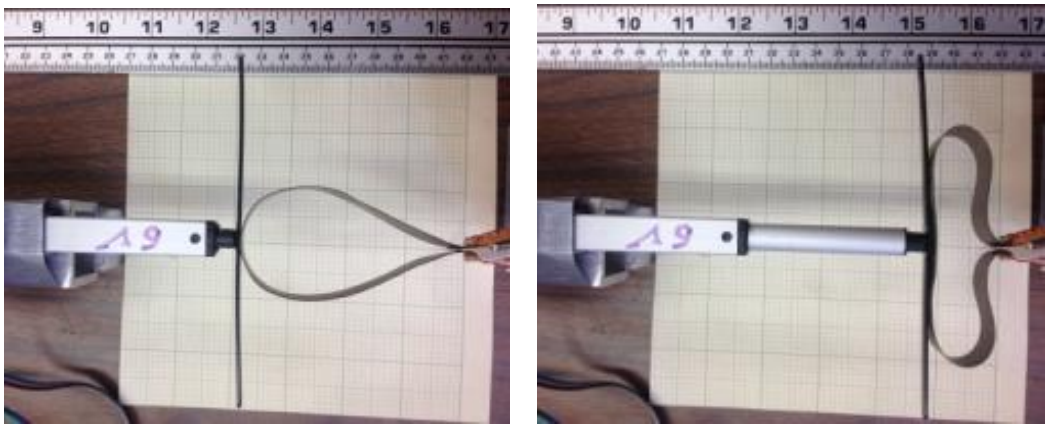

Fig. 6.11 Looped IPMC being pushed by a linear actuator on a flat surface

In Fig. 6.12, test results of the deformations for various applied displacement are reported. In Fig. 6.11, Looped IPMC being pushed by a Linear Actuator with A Flat

Surface. On the left side, the tip touching the loop. On right side deformation of IPMC due to the extended actuator by 5 cm is shown.

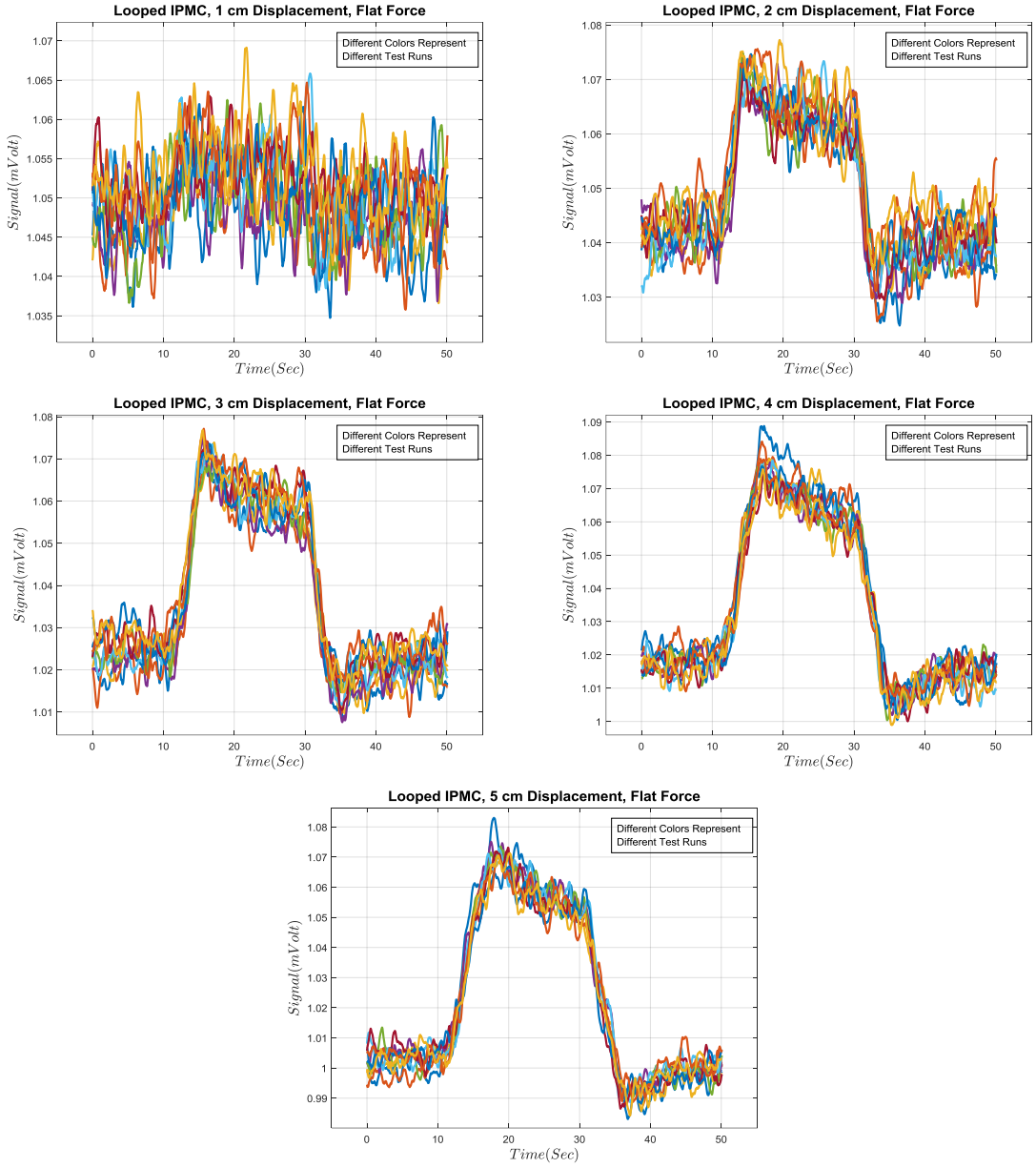

Fig. 6.12 Looped sensor stable response of Flat-tip deformation

In this experiment for each test setup, ten tests performed, and the results presented a consistency for each configuration. Variations of the generated signal vs. deformation presented in Fig. 6.13.

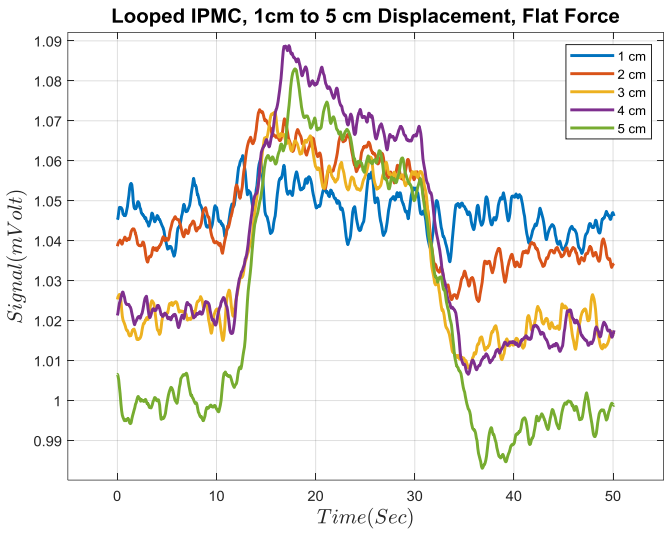

Fig. 6.13 Looped IPMC response voltage signal to Flat point force

The charge variations and the deformations for this test setup are summarized in Table below:

Table 6.2, Generated Voltage Vs Deformation, Flat Front Displacement

Deformation (cm)	5cm	4cm	3cm	2cm	1cm
Charge Variation (mV)	6.5 mV	6mV	5mV	3mV	1mV

Based on the above test result, the best polynomial fit to the voltage produced by the imposed displacement on the loop is given by:

$$mV = -0.3D^2 + 3D - 2 \qquad (6.9)$$

where V is in Volts (mV), and D is displacement (cm).

As demonstrated in Fig. 6.14, the general response of the test with a flat tip actuator has more consistency response.

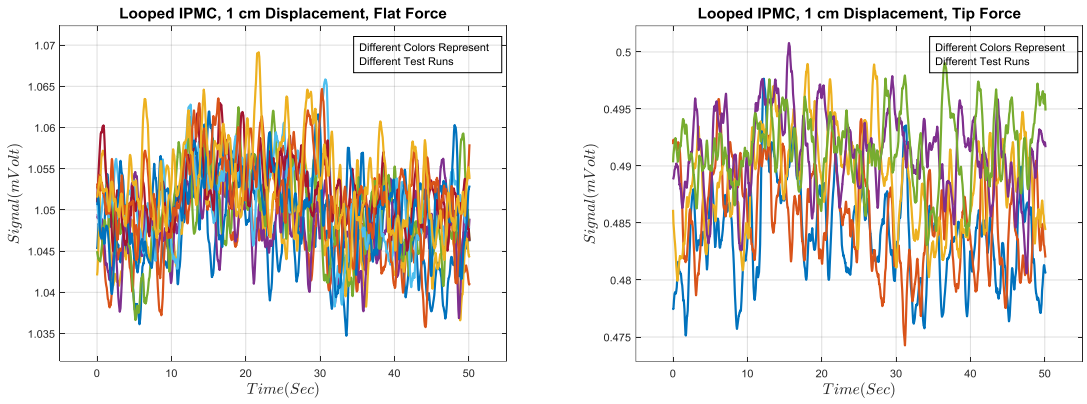

Fig. 6.14 Looped sensor consistency of the response

The last part of this series of the experiment is on side sensing of the looped sensor. In Fig. 6.15, Looped IPMC being pushed by a Linear Actuator with from side. This test is to mimic the side interaction of the looped sensor. On the left side, the tip touching the loop. The middle picture, the actuator is pushing the loop sensor. On right side deformation of IPMC due to the extended actuator by 5cm is shown.

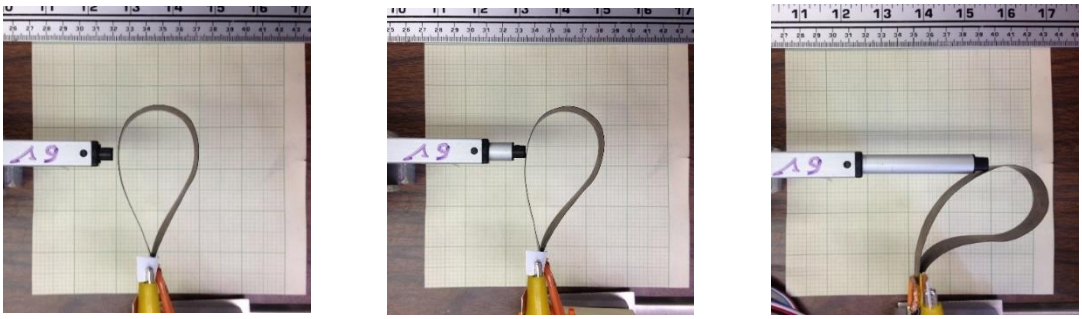

Fig. 6.15 Looped sensor test setup of side deformation

In this experiment for each test setup, ten tests performed. Fig. 6.16 presented the results presented as they have consistency.

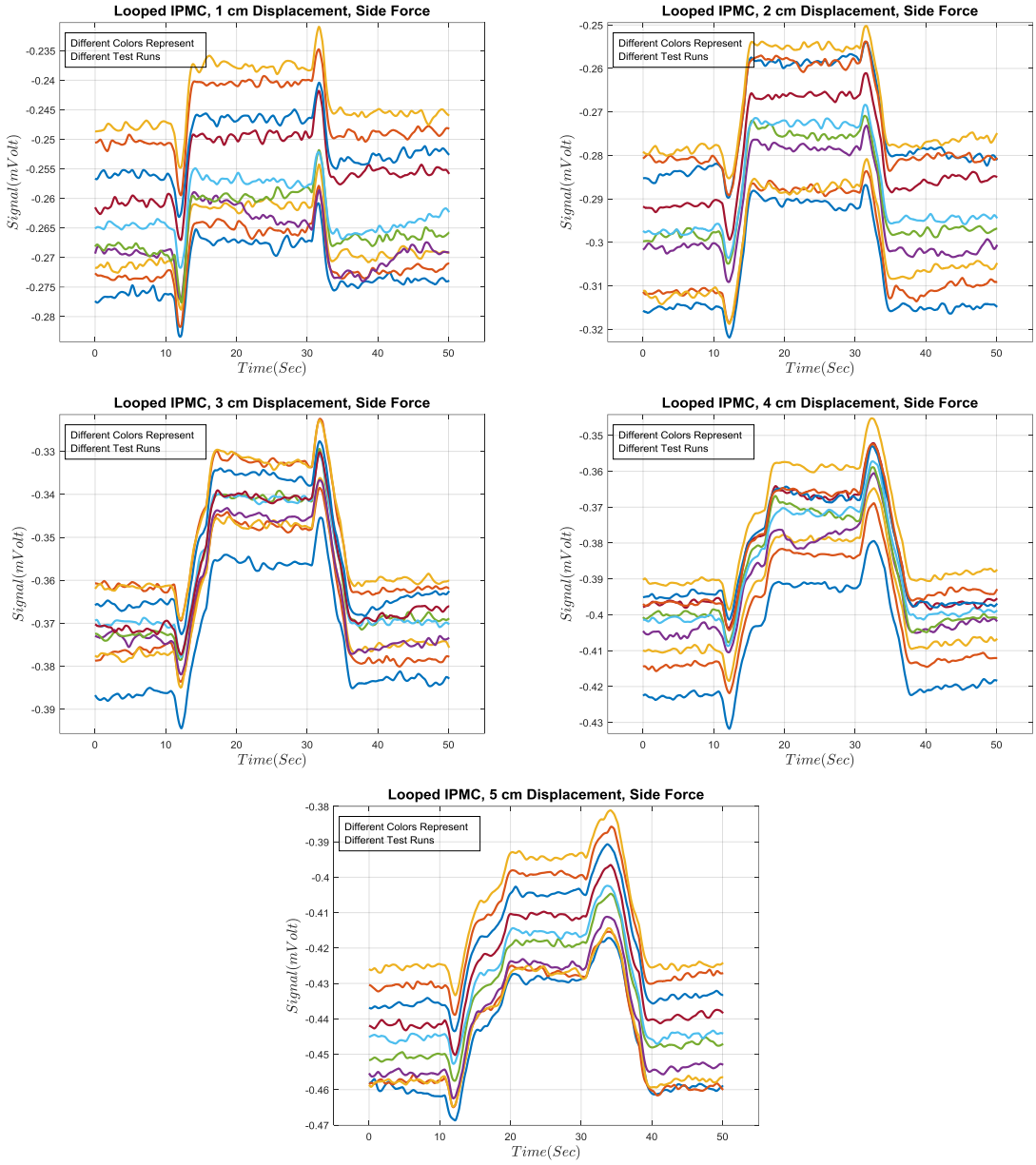

Fig. 6.16 Looped sensor stable response of side deformation

Summary of this configuration test results is in Table 6.3.

Table 6.3 Summary of the test results for the looped haptic feedback sensor

Deformation (cm) For Side	Voltage (mV)
5cm	0.05 mV
4cm	0.038 mV
3cm	0.035 mV
2cm	0.025 mV
1cm	0.01 mV

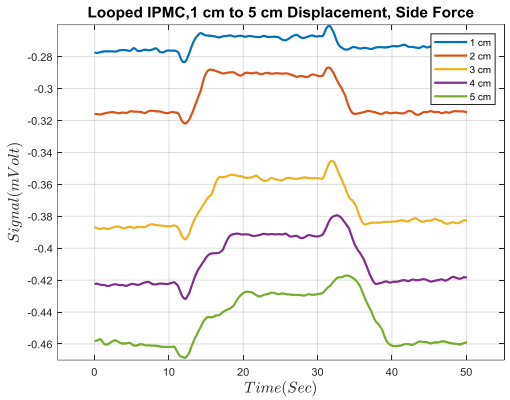

Deformation (cm) For front tip point	Voltage (mV)
5cm	5 mV
4cm	4 mV
3cm	3 mV
2cm	2 mV
1cm	1 mV

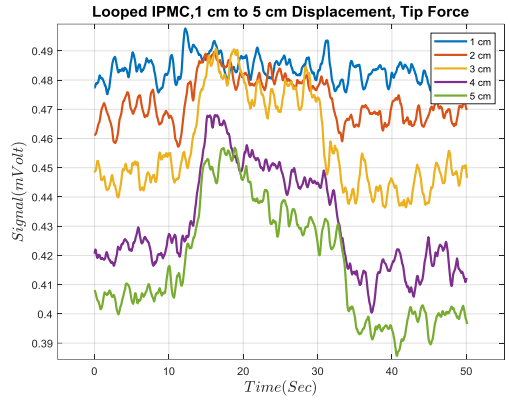

Deformation (cm) For front flat point	Voltage (mV)
5cm	6.5 mV
4cm	6 mV
3cm	5 mV
2cm	3 mV
1cm	1 mV

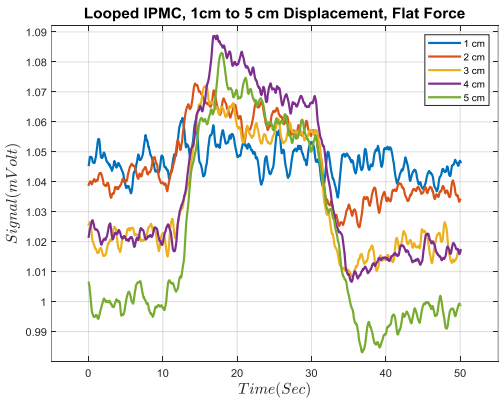

6.3.1 Looped IPMC temporary deformation

During testing the looped IPMC sample, a temporary deformation appeared in the loop. Following is the report for testing the temporary deformations of the looped sensor in response to applied deformation and length of being deformed in Fig. 6.17 through Fig. 6.20.

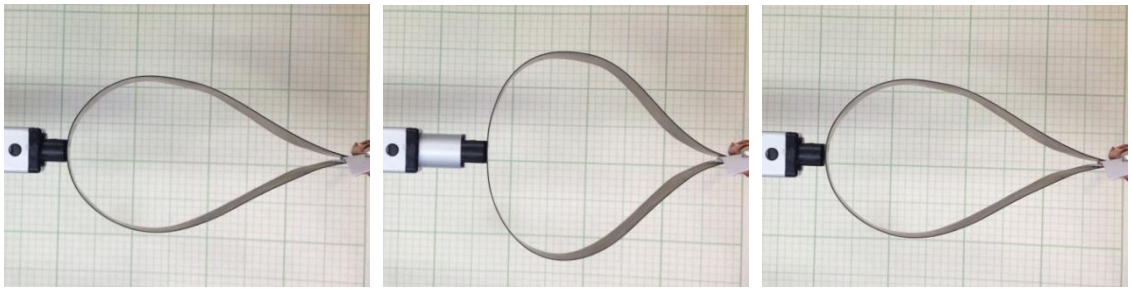

The initial gap between the actuator and the loop | Holding for 1 min at 1 cm Displacement | Final Gap for 1 cm Displacement

Fig. 6.17 Looped sensor temporary deformation for 1cm deformation

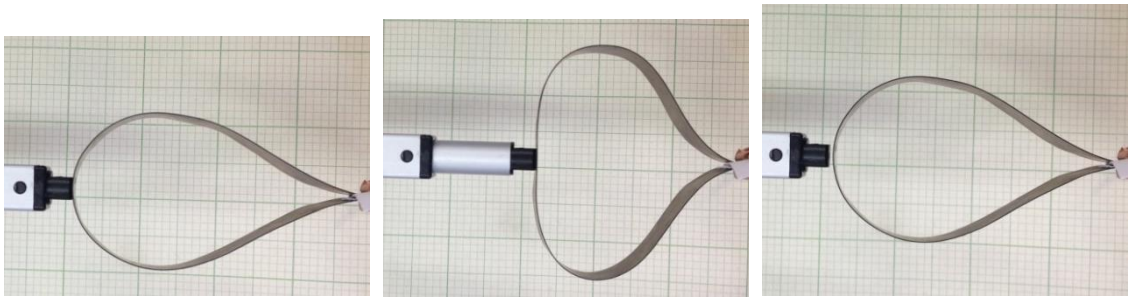

The initial gap between the actuator and the loop | Holding for 1 min at 2 cm Displacement | Final Gap for 2 cm Displacement

Fig. 6.18 Looped sensor temporary deformation for 2cm deformation

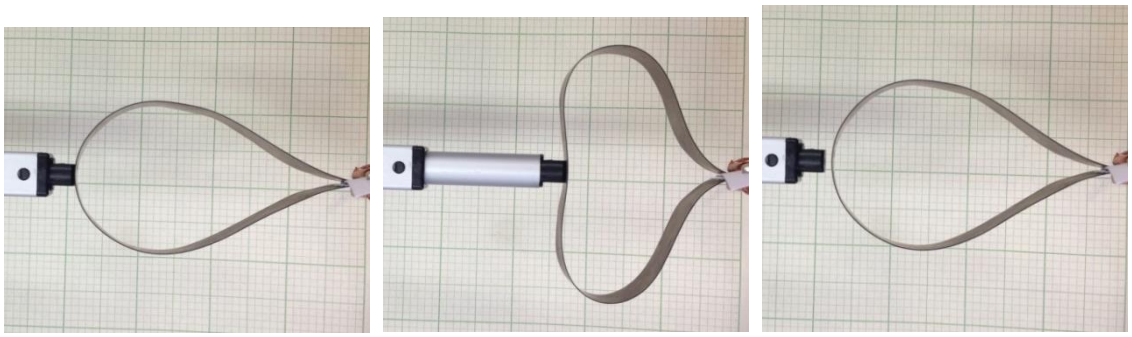

The initial gap between the actuator and the loop | Holding for 1 min at 3cm Displacement | Final Gap for 3cm Displacement

Fig. 6.19 Looped sensor temporary deformation for 3cm deformation

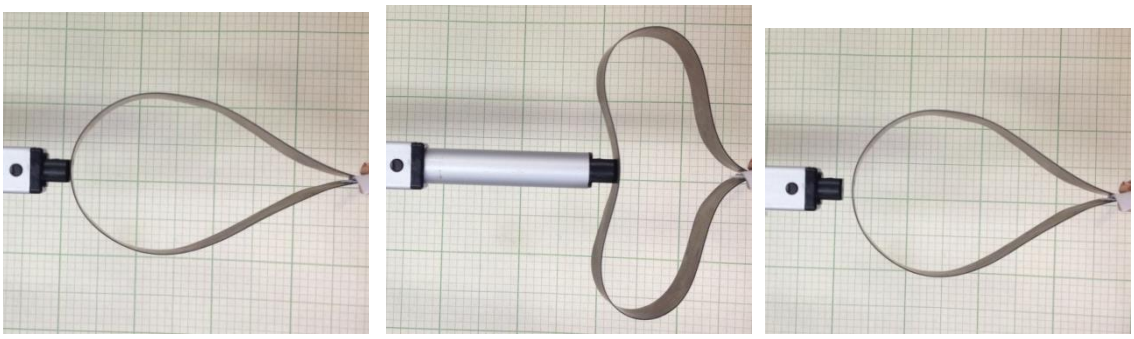

The initial gap between the actuator and the loop | Holding for 1 min at 4cm Displacement | Final Gap for 4cm Displacement

Fig. 6.20 Looped sensor temporary deformation for 4cm deformation

As it is clear from the above figures, there is an increment in the gap as the length of the deformation increases. The other observation is the amount of the gap as its almost one-tenth of the length of applied deformation.

As demonstrated in Fig. 6.21 the gap did not increase as the time of deformed shape increased. Also, after 5 minutes' delay, the maximum gap which was for the 5 cm deformation disappeared totally.

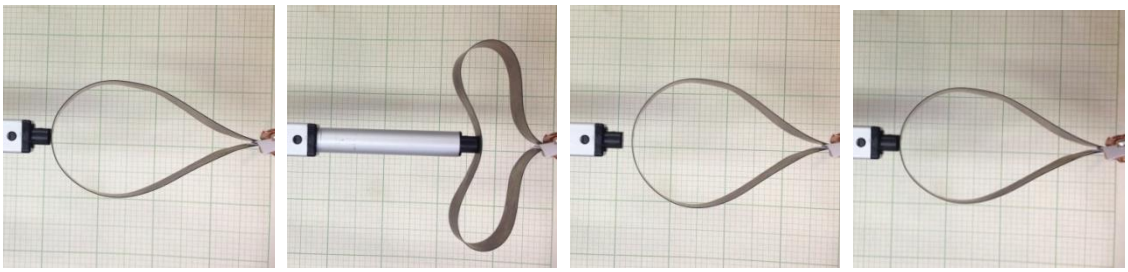

The initial gap between the actuator and the loop | Holding for 1 min at 5cm Displacement | Final Gap for 5cm Deformation | Final Gap for 5cm Deformation after 7min.

Fig. 6.21 Looped sensor temporary deformation for 5cm deformation

6.3.2 Looped IPMC Free End vs. Attached End

The temporary deformation raises the interest in knowing the response of the system if the loop is attached to the actuator and at the end of retraction of the linear actuator, the device poled backward.

Tests durations for each experiment was 60sec. for each test. In the first 20 Sec. the material is at rest. At t = 20sec the actuator pushes 5cm forward. At t = 40 sec. the actuator retracts. For the last 10 Sec. the material will be at rest. The following graphs are the results of the test for the free end of the actuator, and the one clamped to the looped sensor.

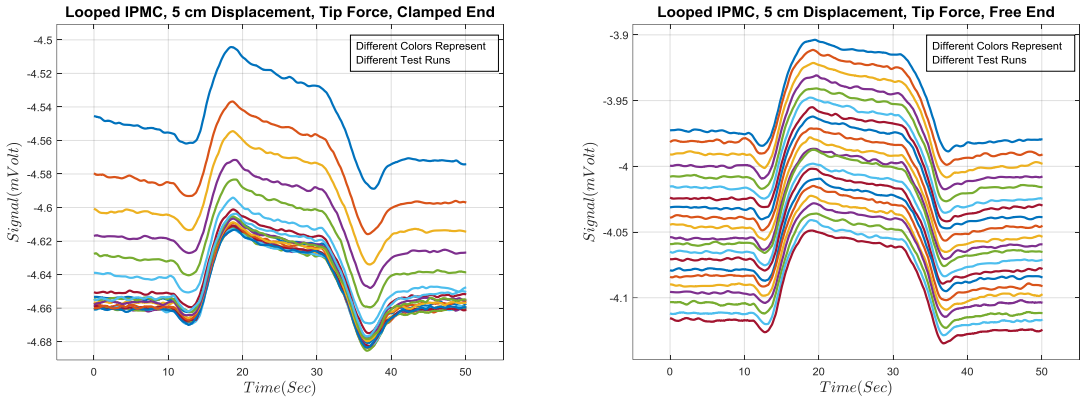

Fig. 6.22 Looped sensor generated signal for 5cm deformation

One observation from this test result is that there is a good level of consistency on the generated electrical charge for this sample. As for each single curve variation of charge is similar to others. The other observation is that the charge balance is not the same as the one at the beginning of each test. In Fig. 6.23 a better description of overall charge variation is demonstrated.

In a comparison between the free end and the one attached to the actuator, the one attached to the actuator reached a stable condition after a few test runs.

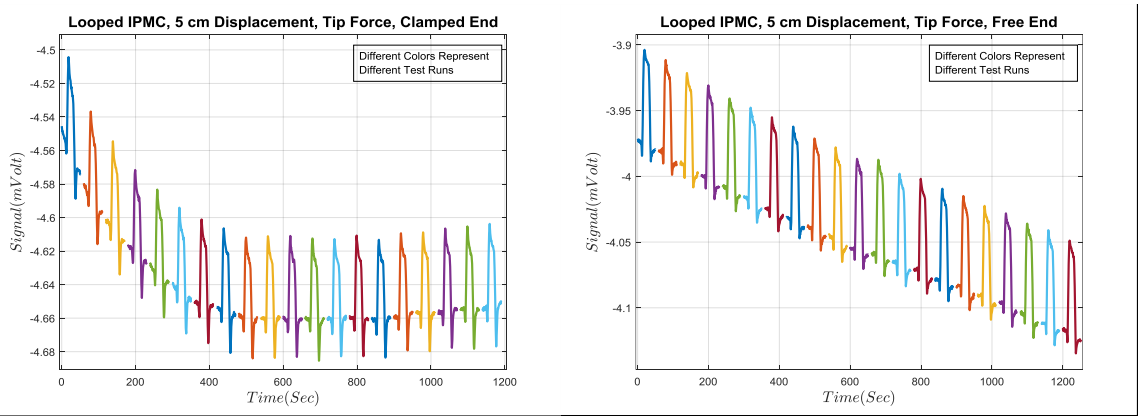

Fig. 6.23 Variation in an overall voltage level of the sample

6.3.3 Looped IPMC, Force-Displacement Report

The test on the sensing signal is based on the applied deformation on the looped sensor. Here is a report of deformation vs. applied load on this loop sensor. The test setup considered for this was using the gravity force to apply load. For this test, the effect of the weight of the sensor on its shape ignored. In this test, a slider and guide were printed using a 3D printing machine. Position of the loop sensor and the printed device presented in Fig. 6.24. penny coins were used as the weight placed on the top of the slider as a way of increasing the load on the IPMC loop sensor. Slider weight is 3.24 grams, and each coin is 2.5 grams.

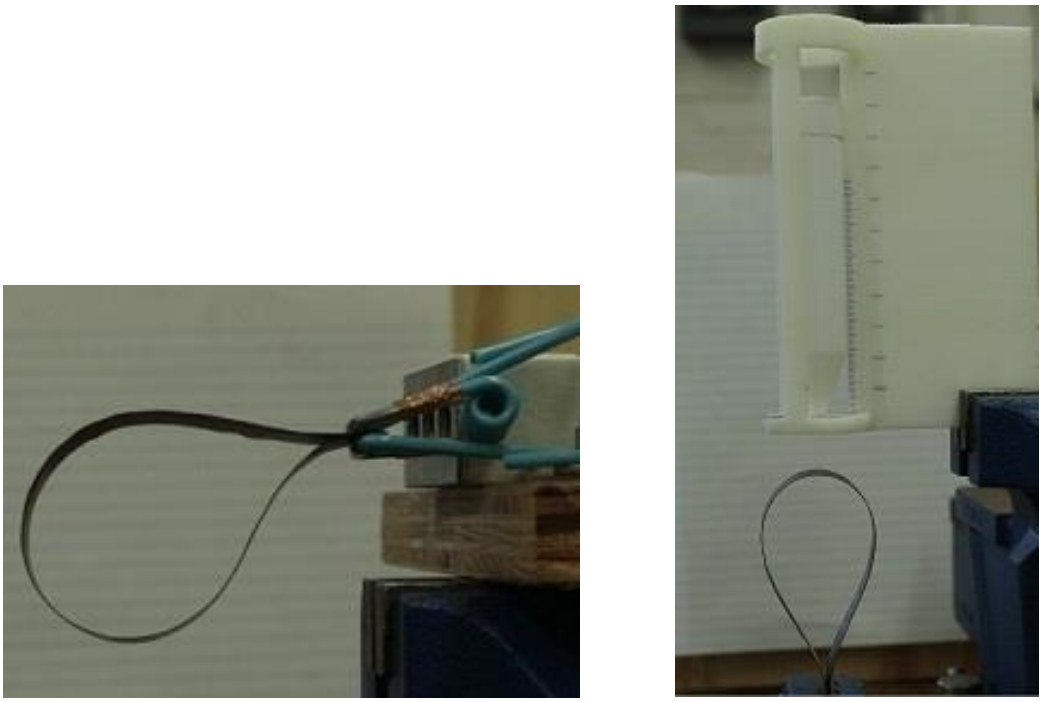

Fig. 6.24 test setup for Looped sensor for the force-displacement

In Fig. 6.25, two configurations of the load application represented. The left side is the pointed tip force and the right side in the flat tip force. The size of the pointed tip force is similar to the size of the tip of the linear actuator.

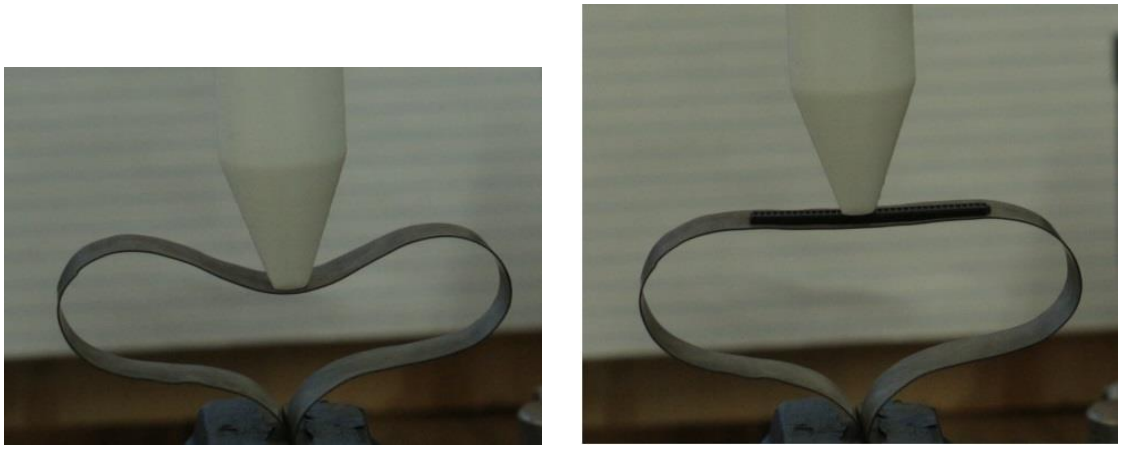

Fig. 6.25 Looped sensor configuration max. load tests

Test results are presented in Fig. 6.26 and Fig. 6.27. The graph demonstrates as if the sensor as more resistance on a flat tip displacement. The other observation is that there is an almost linear relationship between the applied load and the recorded displacement. Also, the gap at the end of the test is similar to that observed in previous tests, while the gap for the flat force is less than half of the tip force.

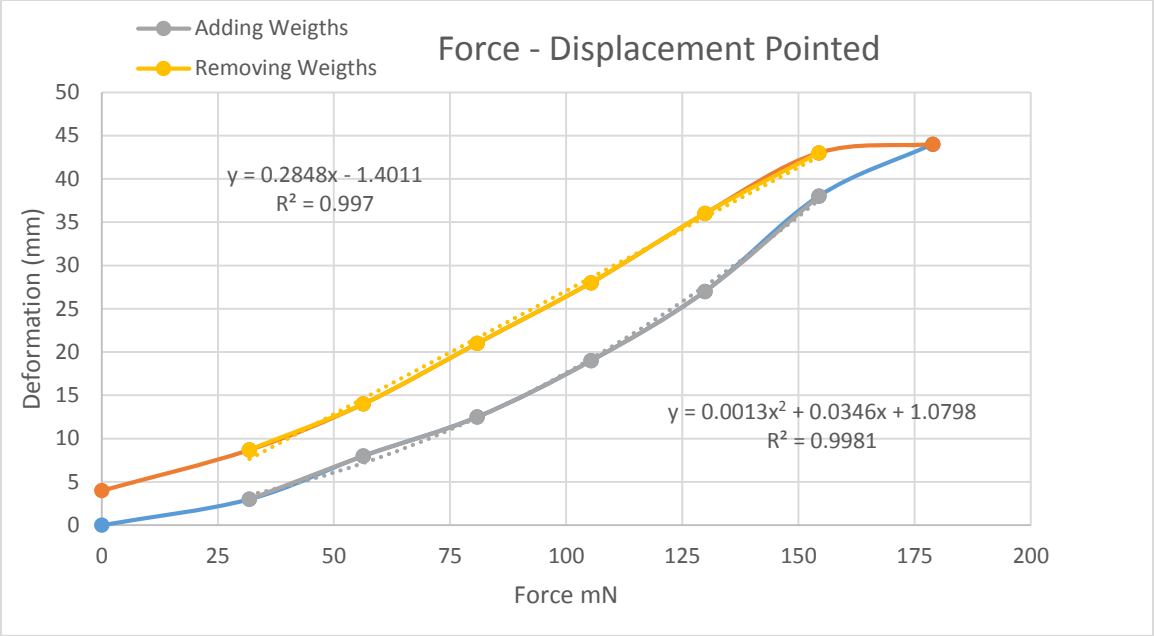

Fig. 6.26 Looped sensor configuration max. load tests

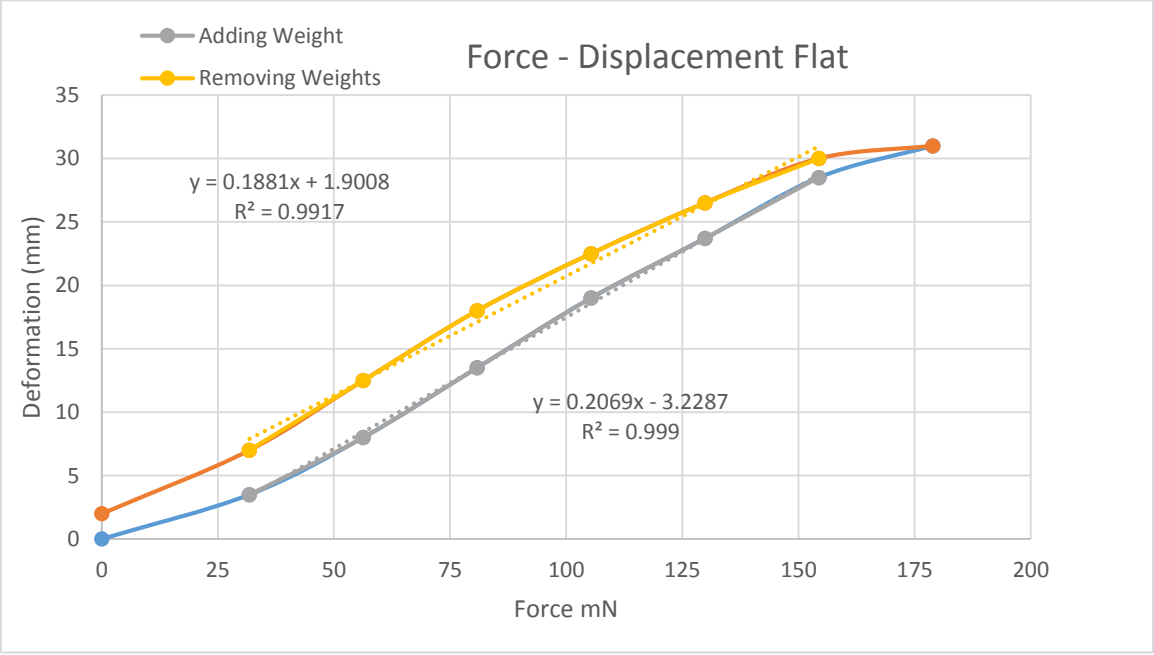

Fig. 6.27 Looped sensor configuration max. load tests

6.4 Looped IPMC, Smaller Scale test report

One of the considerations for this loop haptic loop sensor is for biomedical applications such as in robotic surgery. As demonstrated in Fig. 6.28, this IPMC looped haptic sensor resembles a concept of a device or robotic end-effector to detect the kinesthetic haptic feedback interaction and haptic forces with the body organs. In this figure, a surgical robotic end effector and the enlarged tip to measure kinesthetic haptic force feedback are demonstrated.

Fig. 6.28 Surgical robotic end effector and the enlarged

In order to justify the smaller scale of the introduced loop sensor, similar to the original sample, a much smaller sample with the length 7 mm is tested based on the configuration presented in Fig. 6.29.

Fig. 6.29 IPMC haptic feedback sensor for surgical end-effector test setup

In Fig. 6.29, left side picture demonstrates the test setup for the surgical robotic end effector IPMC haptic feedback sensor and the right side demonstrate the applied deformation/displacement of the end-effector. Test results presented in Fig. 6.30. The test results demonstrate the promising application of IPMC as end effector haptic feedback tools.

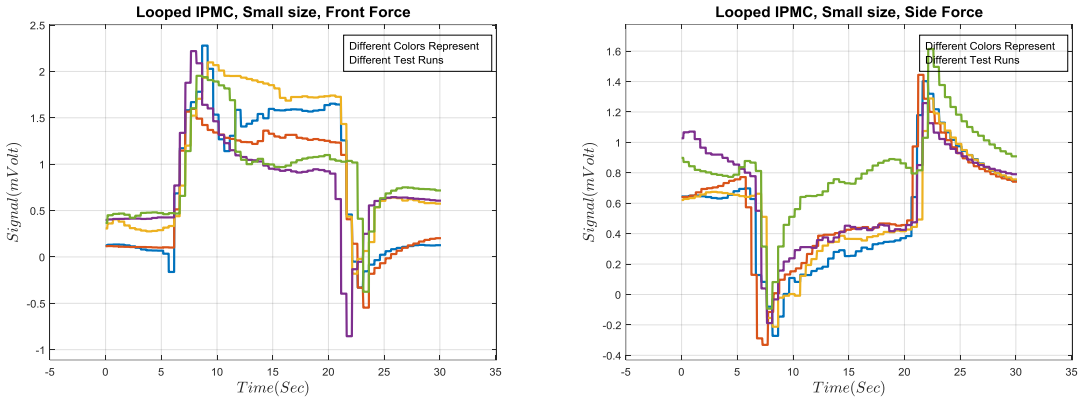

Fig. 6.30 Results of IPMC haptic feedback sensor for surgical end-effector

6.5 Looped IPMC Actuators and Sensors, Design Improvement

The earlier version of the loop sensor was made of a single strip of IPMC. Checking the geometry of deformation of the loop actuators and sensors, one may consider other alternatives, as shown in Fig. 6.31 and Fig. 6.32 by incorporating a second material.

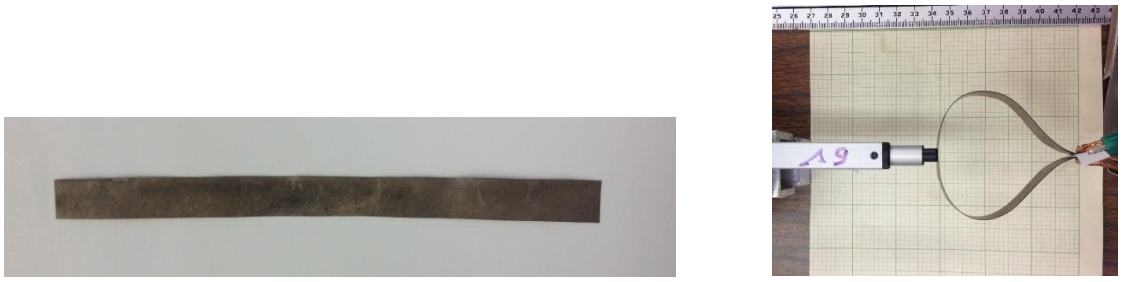

Fig. 6.31 Strip of IPMC in flat form and looped form

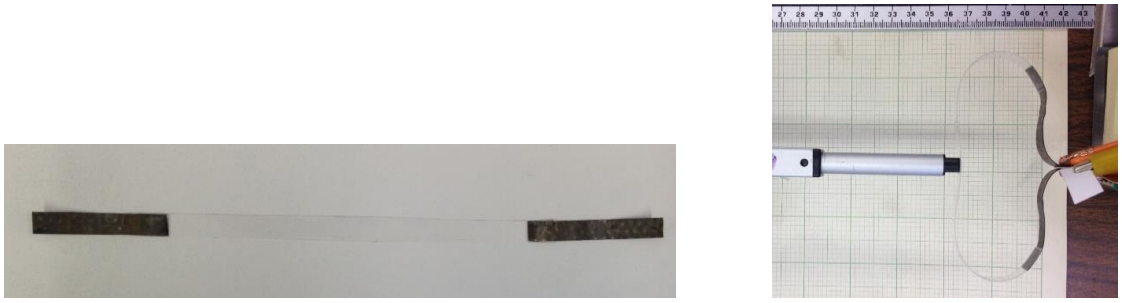

Fig. 6.32 New version of an IPMC haptic feedback sensor

Similar to the previous test configuration, this model was also tested several times, and its operation was verified successfully, Fig. 6.33. These tests result demonstrate smother feedback signal from sensor.

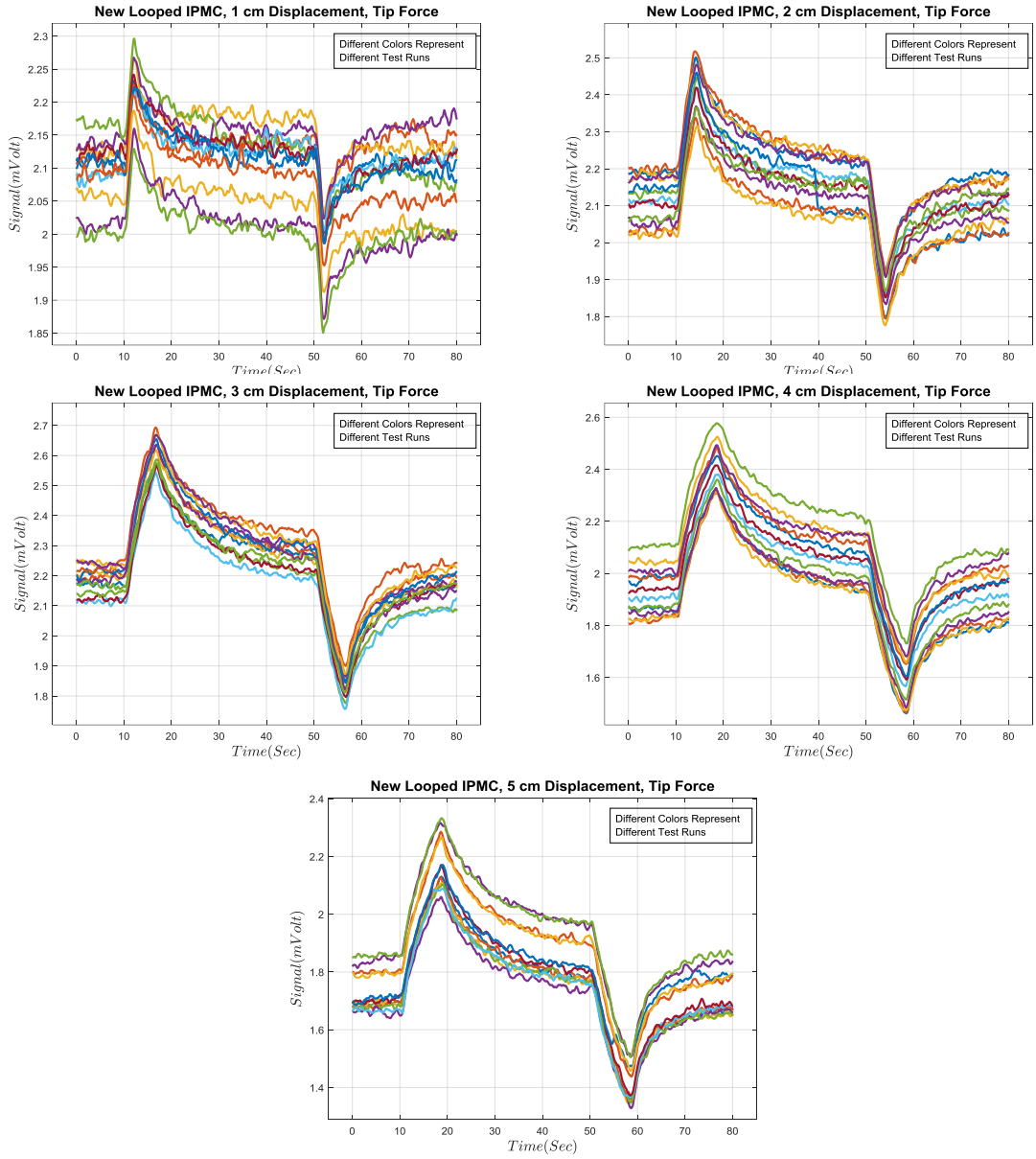

Fig. 6.33 New Looped sensor stable response of Point tip deformation

In Fig. 6.34, a comparison char of the above results demonstrated. A simple comparison for the received signal of 4 cm and 5cm applied deformation shows that the received feedback for this form of sensor and deformation reached a limit. As the applied deformation may not bend the active part of the sensor any more. This

limitation related to the geometry of loop as the midpoint bend toward its connection. In this case free length of the loop sensor was 34cm and maximum applied displacement/deformation on the tip of the looped sensor was 5cm.

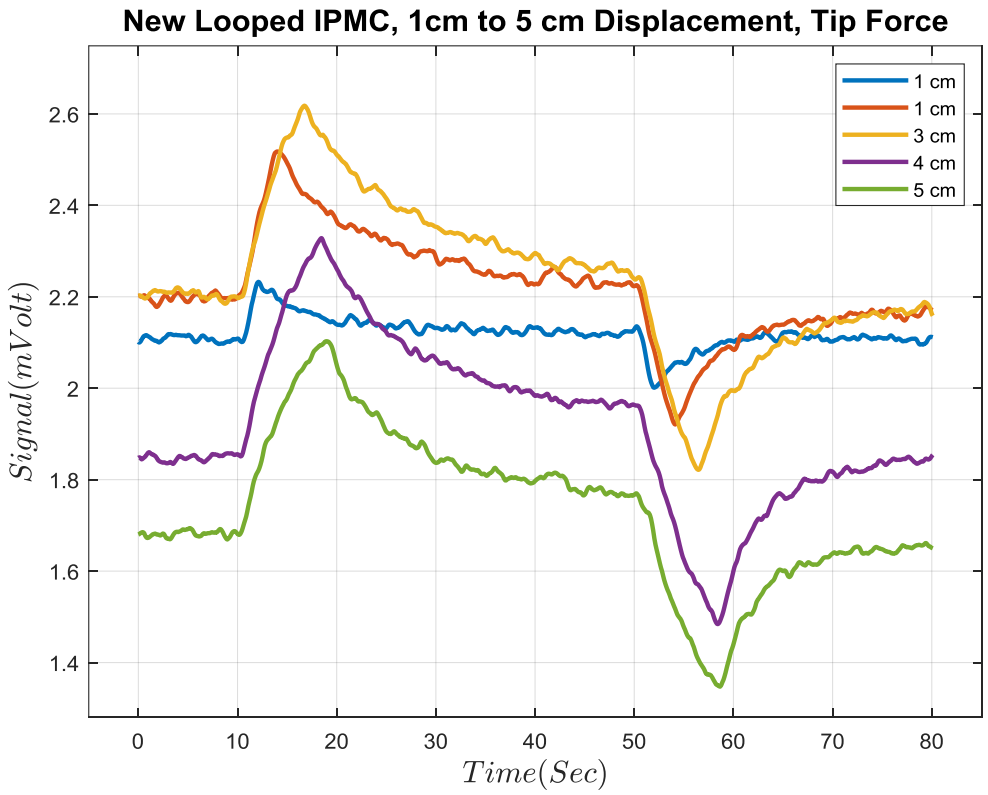

Fig. 6.34 Test results of the new IPMC haptic feedback sensor

Another observation in comparison between the new form of the looped sensor and the original proposed formation is the stability of the generated signal. In this formation level of the noise is much less than the original formation, which means by applying a better filter one may be able to receive more clear results. A sample generated signal demonstrated in Fig. 6.35.

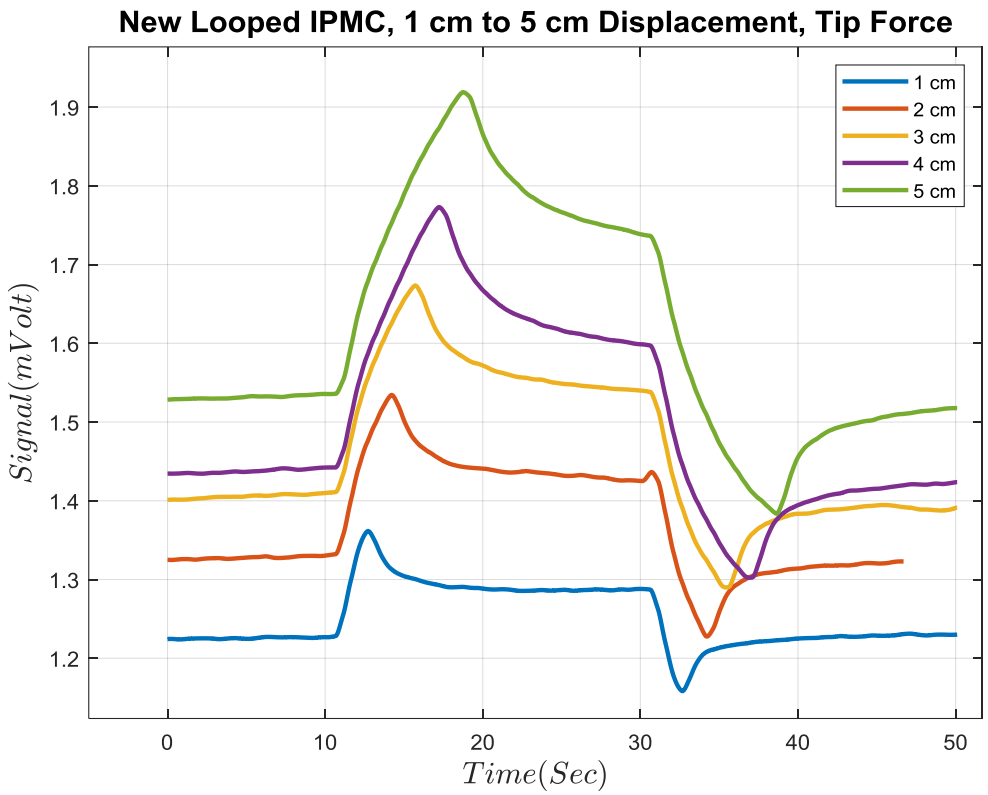

Fig. 6.35 Smother test results of the new IPMC haptic feedback sensor

6.6 Looped IPMC, Future Work

During the test, some jump in generated signals happened, when the material starts to deform. These jumps happened for all of the test, and they are in opposition to the direction charge movements. This is a character that needs some more attention to be understood.

Also, the newly introduced form needs more investigation as it presented to be a more practical model in comparison with the original version.

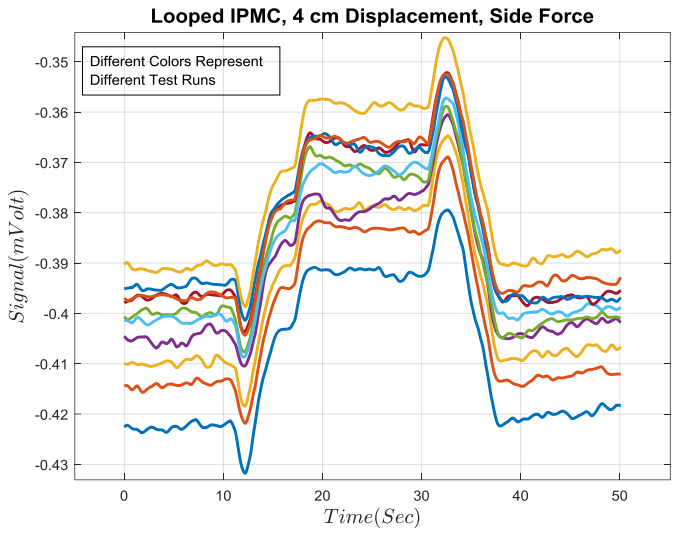

Fig. 6.36 signal of side test on haptic feedback of a loop sensor

The new form of looped haptic feedback sensor has its alternative as the one presented in Fig. 6.37. This form needs to be investigated and characterized.

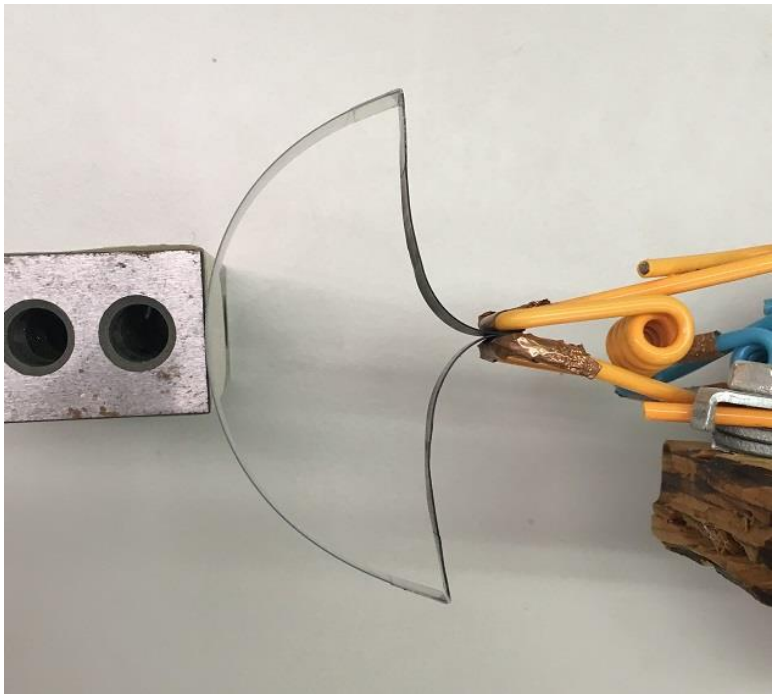

Fig. 6.37 Alternate form of New version of an IPMC haptic feedback sensor

CHAPTER 7

7 DEVICES MODELS MADE OF IONIC POLYMER-METAL COMPOSITES (IPMCs)

7.1 Self-Induced contact oscillatory motions of IPMC Strips

The contact oscillation of IPMCs is based on the fact that if they are originally in a resilient configuration in equilibrium, such as a beam in a cantilever form (Fig. 7.1) with one electrode attached to anode, once touched by the cathode by a brief loose contact they tend to move away from the cathode towards the anode. Interestingly, as the IPMC cantilever moves away from the cathode, it bends or deforms elastically and store potential energy in it to move back, after reaching the maximum amplitude of dynamic elastic deformation due to the imposed electrical field, and contact the cathode again to then move away from it again and thus continue to oscillate back and forth.

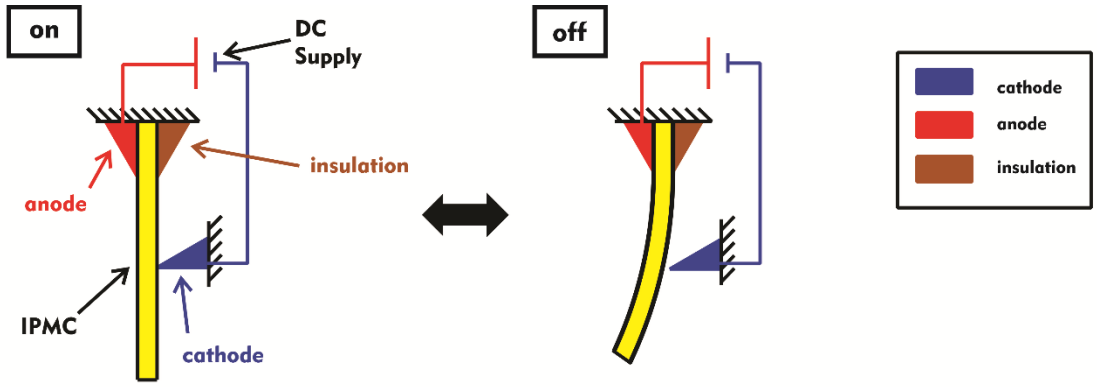

Fig. 7.1 Oscillation of IPMC with static input

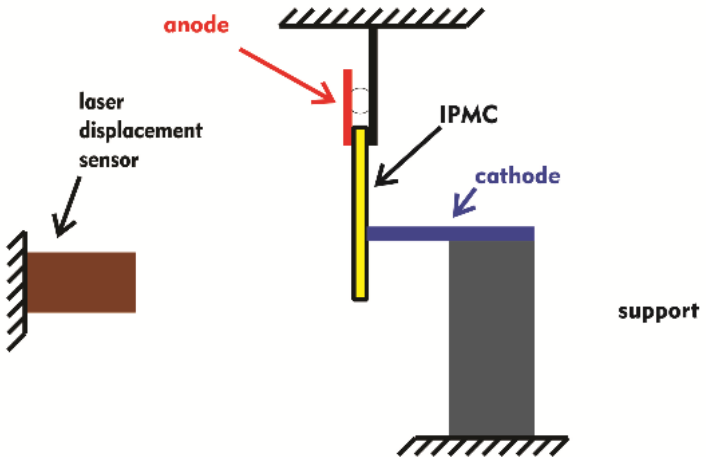

Fig. 7.2 Static Oscillatory IPMC, Test setup

Using one or both of the contact in a way to have touch contact will introduce oscillatory behavior to these materials. The fixed contact will activate the material when it reached a certain point sent, the actuation pulls to the material body. The pulls cause the ion movement inside the material structure and as the deformation reached a certain point the contact will release but due to the moment of the ion it is expected the motion will not stop there and continued to some extent. In Fig. 7.3, the concept of oscillator gripper presented. The device may be used for dispersing particle when soft interaction is required.

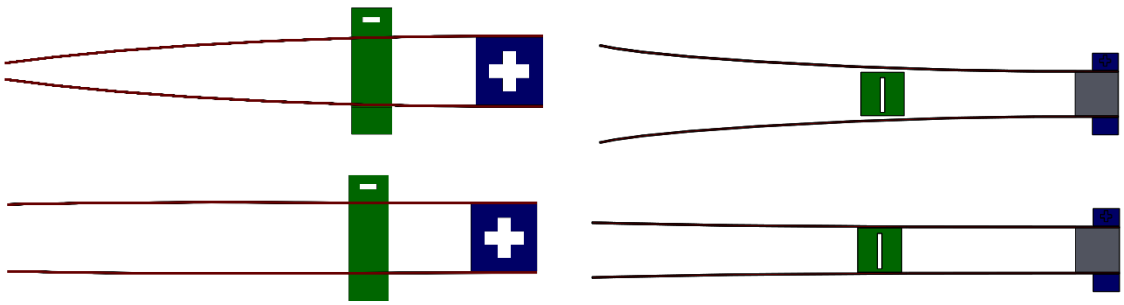

Fig. 7.3 Oscillatory griper/ mixer

In Fig. 7.4 through Fig. 7.8 concepts of oscillatory IPMC with static input presented. Characteristics of these formations are good subjects to be studied.

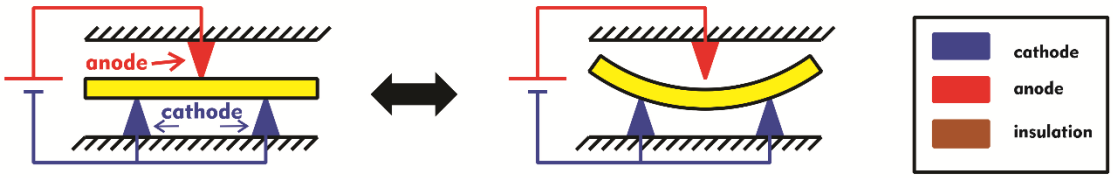

Fig. 7.4 Oscillatory IPMC with pointe electrodes

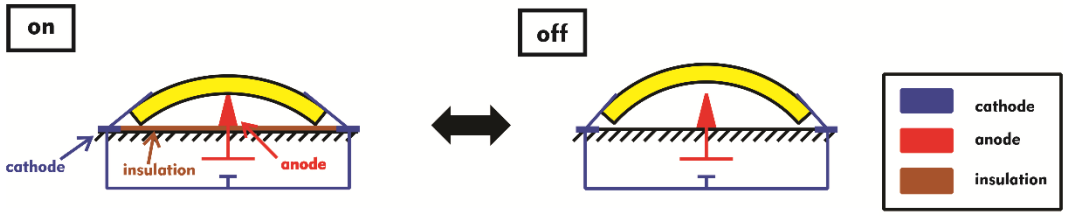

Fig. 7.5 Oscillatory IPMC in a dome shape configuration

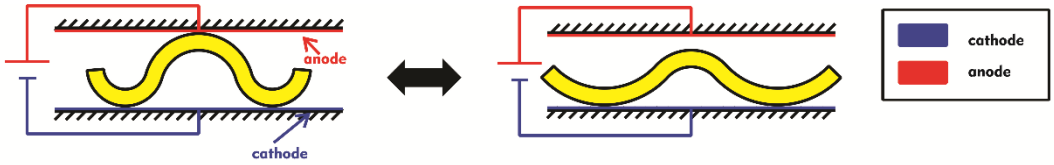

Fig. 7.6 Oscillatory IPMC in a straight contact channel

Fig. 7.7 Test setup for Oscillatory IPMC in a straight contact channel

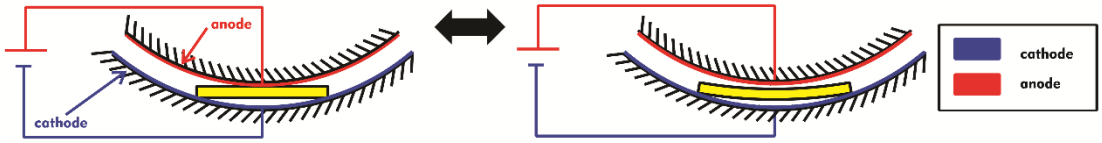

Fig. 7.8 Oscillatory IPMC in a curved electrode

7.2 Tubular Actuators/Sensors and Peristaltic Pump Configuration

In this section, some novel configurations for IPMC actuators and sensors/energy harvesters will be introduced. These configurations are expected to be practical, referring to the basic mechanism in IPMC defined earlier, which is based on ionic movement as shown in Fig. 7.9. These configurations will be based on the introduced sensors/actuators and extending their capability to some degrees. In these proposed designs, to shape the models, sine and cosine functions with a simplified form of the boundary connections are used as they are easier for demonstration. These configurations may be extended using other types of

boundary condition and boundary connections. In Fig. 7.9, left side is a scheme of distribution of cations for IPMC in actuation mode in a perpendicular cross-section. The middle side is a scheme of distribution of cations for IPMC in actuation mode in the perpendicular plane. The right side is a scheme of semi-spherical IPMC deformation in actuation mode.

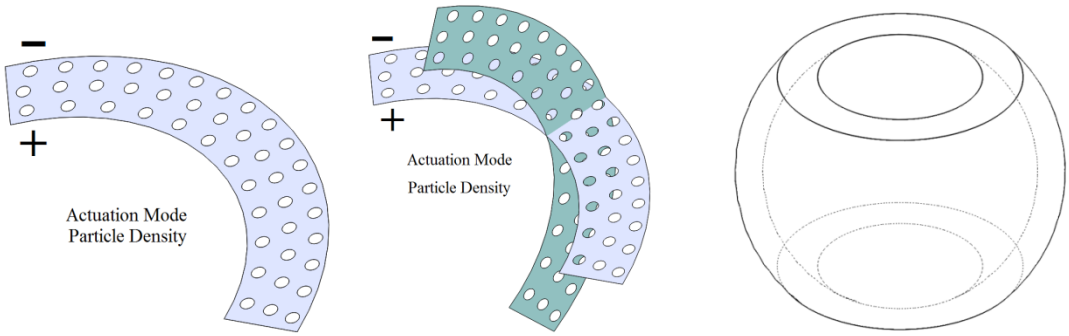

Fig. 7.9 Scheme of distribution of cations for IPMC in actuation mode

In actuation, the IPMC sample is like a cylindrical tube under axial force. In the sensing mode, the axial force on both ends forces the cylinder to shrink the length and expand the radius. As a result, the material will accommodate the deformation. From an actuation point of view, an applied electric field causes the cylinder to contract/expand axially/laterally, as demonstrated in Fig. 7.10. As shown in this figure, the imposed electric field can expand and contract the cylindrical tube made with IPMC[141].

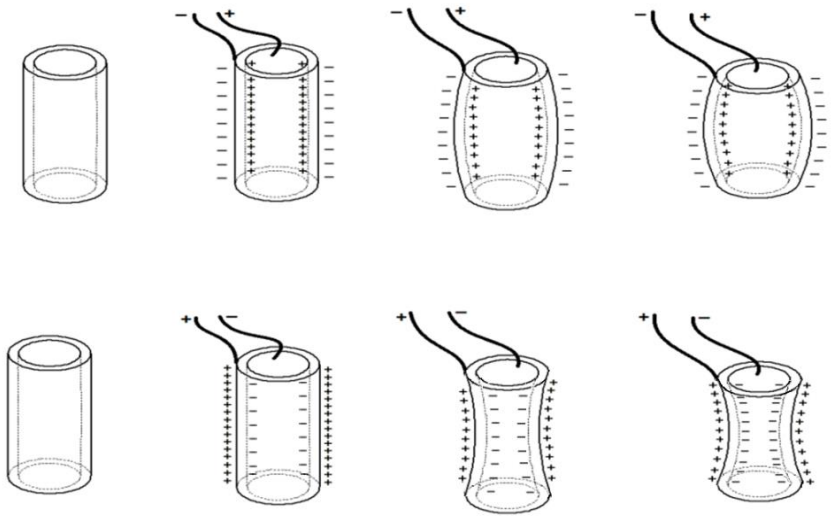

Fig. 7.10 Expansion and contraction of cylindrical tubular IPMC

This applied field will gradually deform the cylinder to become more like a sphere. A possible application for this type of actuation is a pump with no rotary or movable components. In Fig. 3.11, tubular IPMC as the main component of a pumping device the clamps on each end contains a one-way valve. The expansion and contraction of long tubular IPMC act as a pump chamber.

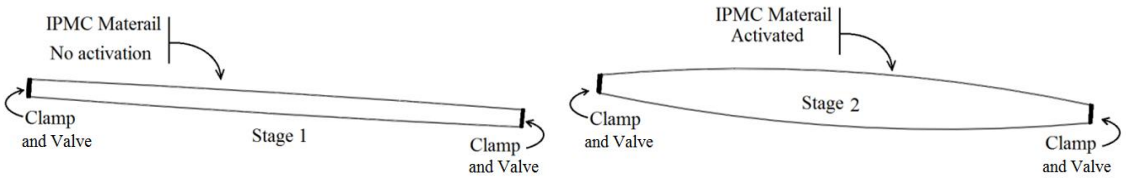

Fig. 7.11 Tubular IPMC as the main component of a pumping device

Next category will be by slicing along the tubular form of the already introduced configurations in Fig. 3.11, to create a slit cylindrical/tubular IPMC actuators and sensors. Following are the arrangements and concepts based on this cylindrical slit configuration.

These configurations are based on the arrangement of several IPMC membrane around a circular object. The assembly by itself can act as a linear actuator and sensor as deformation of each member is discussed in earlier chapters as actuator and sensor/energy harvester.

Expansion and contraction of the assembly will cause the variation of occupied space by the assembly. This phenomenon can be utilized as a pumping chamber by encapsulating the inner space of the assembly and having one-way valves on each side. This idea will be explained more in the next configuration assembly of the actuator, sensor/energy harvester IPMC membrane.

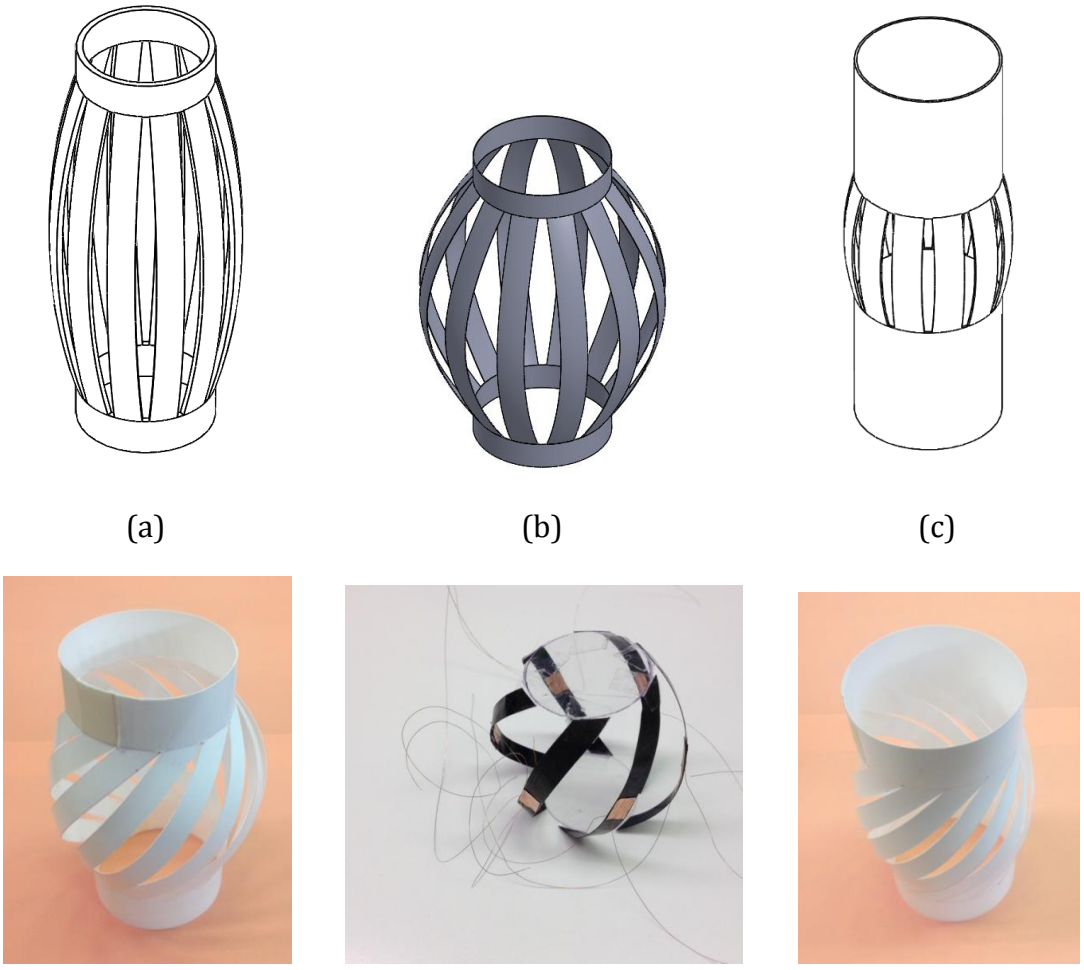

(a) (b) (c)

(d) (e) (f)

Fig. 7.4 Tubular Cylindrical/Helical silt IPMC actuator/sensor.

Another configuration for the boundary connection of the IPMC strips is demonstrated in Fig. 7.13. In this form, due to boundary conditions, the material is already deformed, or it might be bent to fit the assembly requirements. In these configurations, the IPMC membranes have different fixed connections angle at the boundaries.

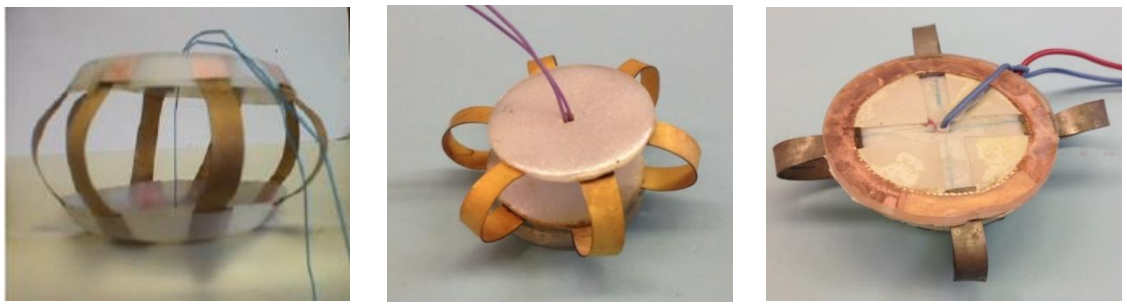

(a) (b) (c)

Fig. 7.13 Tubular silted IPMC linear actuator/sensor, device

These configurations may act better as a more active pump or even an underwater biomimetic robotic jellyfish. In this configuration, the mechanism works as taking water in expansion or swelling and producing the jet of water exiting in contraction or body shrinkage, as shown in Fig. 7.14.

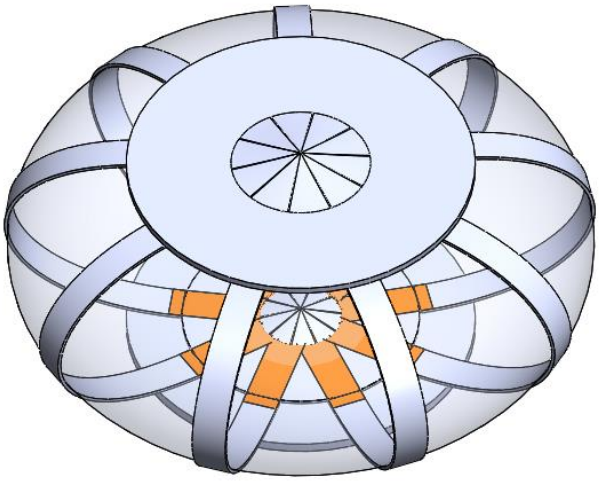

Fig. 7.14 Tubular actuator act as a water pump for underwater application

Considering the form presented in Fig. 7.14. This configuration if rearranged in the following form presented in Fig. 7.15 also act as a four-legged walking spider robot. The spider robot needs a program to move each leg individually. Also, these platforms can also be used as a Stewart platform with undulating legs.

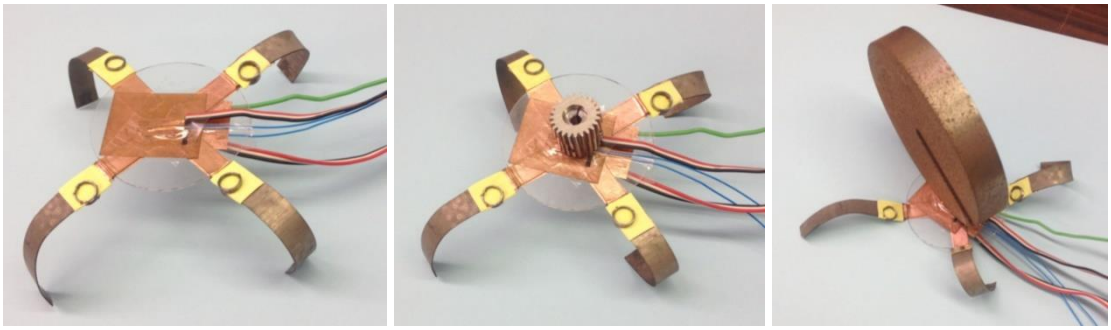

Fig. 7.15 Stewart platform robot with IPMC legs being able to carry weight

As it introduced in the earlier chapter, placing the IPMC membrane at an angle will generate rotary and extension at the same time. The first form of the device considered for the cylindrical concepts is a combination of axial displacement, and rotary will produce a tool to rotate objects step by step. By combining these two movements, as shown in Fig. 7.16.

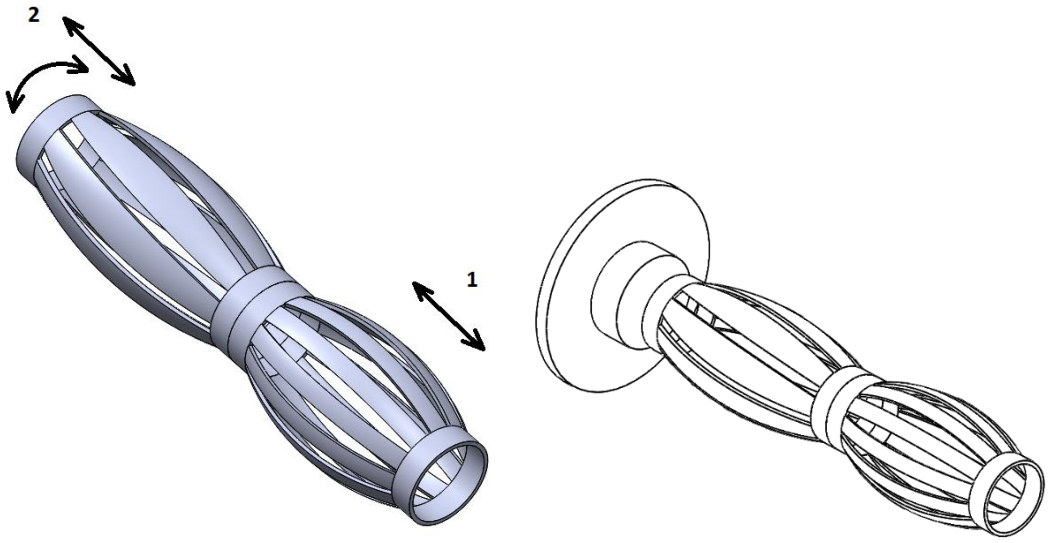

Fig. 7.16 A simple concept for an IPMC Rotary Device

In the form presented in Fig. 7.16, object #1 has axial displacement and object #2 has a combination of rotation and axial movement. Combination of this two will generate step rotation as object #1 will cover the axial movement of the object #2 in the opposite direction.

Extending this concept to involve more of these basic units will be able to create a biomimetic robotic arm capable of expansion, contraction, bending, rolling, twirling, and twisting, as shown in Fig. 7.17.

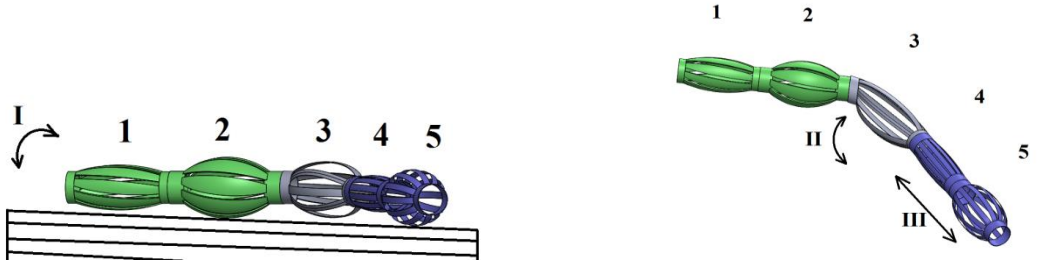

Fig. 7.17 Robot arm concept made of tubular IPMC actuators

In Fig. 7.17, a variety of control strategies can be applied to the assembly to move the biomimetic soft robot. For the rotation in the direction I, actuators 1 and 2 are rotatory and have more range of rotation in the opposite direction and aligned with the central axis. The actuator number 3 has unsymmetrical voltage to generate planar movement in the direction II.

The simplest change for the device is that while #2 and # 5 are touching the floor, #3 and #4 will work accordingly to move #3 forward toward direction III and then contact the ground and let others be released.

In this configuration, the actuation of IPMC strips of the components is independent so that the arm can move to the desired directions.

7.3 Linear Actuators/Sensors and Peristaltic Pump Configuration

Considering the IPMC configuration shown in Fig. 7.18. This format in the first place acts stronger as actuator and in sensing based on the electrical connection will have higher sensitivity and stability for the received displacement.

From another point, if the chamber occupied by expansion and shrinkage encapsulate with two flexible valves on each side, a new biomimetic underwater device will be possible.

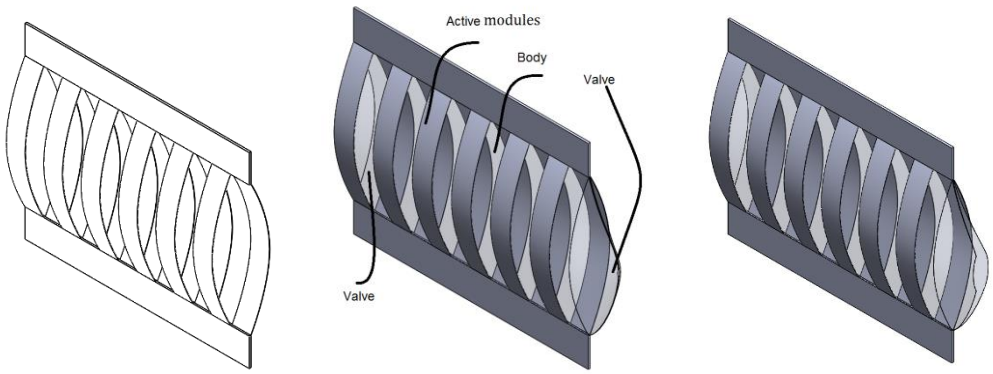

Fig. 7.18 Assembly of the linear actuators with higher capacity

In Fig. 7.18, Left side is an example of the controllable assembly of the linear actuators/sensor with higher capacity. Middle-Side and Right-side are two stages of an underwater mobile device/Peristaltic Pump using IPMC actuators.

Similar to the helical formation, as it was demonstrated in previous chapters, the assembly arrangement of the IPMC strips at an angle with respect to the base, will generate two directions for the actuation or sensing. Using this capability with a linear actuator provide the capability for a walking robot. The combination of these types of actuation presented in Fig. 7.19.

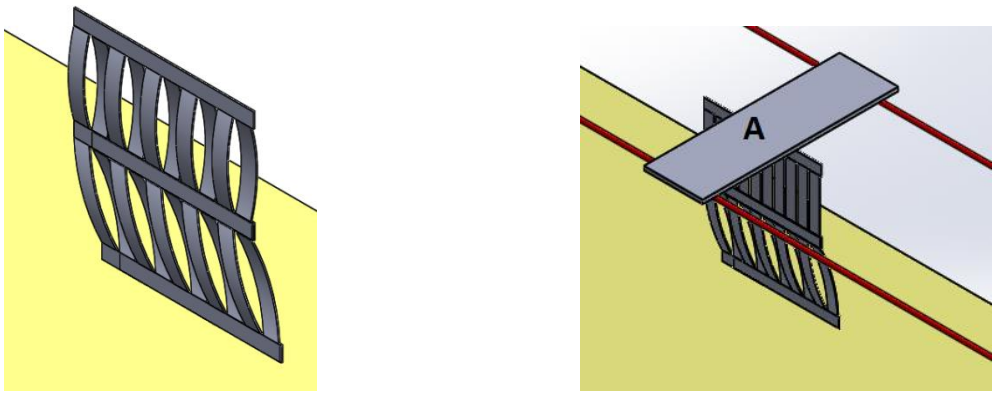

Fig. 7.19 Assemblies of the two types of actuators for a robotic leg

In Fig. 7.19-Left side, The assembly consists of a straight and angled arrangement assemblies of IPMC actuators. The straight one will provide expansion and contraction while the angled actuator provides additional forward direction. These components are attached to the platform “A” which is placed on the red bars in Fig. 7.19-Right side. While the Platform A is on bars and the other side of the actuator assembly touches the floor and platform, the following procedure for a single forward step considered:

1- Expansion of the angled actuator will move the platform upward and forward.
2- Contraction of the straight assembly will bring the platform to the bars.
3- Contraction of the angled actuator will lift the assembly from the floor and forward.
4- Expansion of the straight assembly will bring the assembly to the floor.

Rearranging these two types of assemblies of the IPMC actuator/sensor in a parallel configuration will provide the possibility to rotate a table around the defined horizontal and vertical axis. This table may be used as a reflective table as the top surface can act as an undulating mirror (Fig. 7.20).

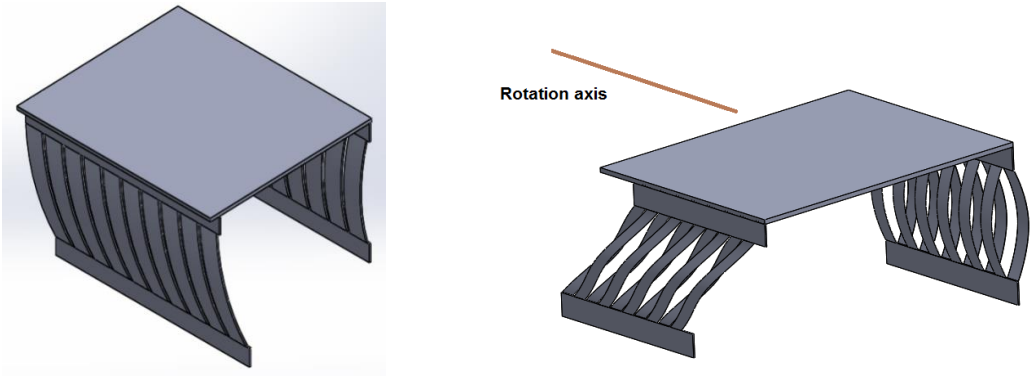

Fig. 7.20 the rotatory table made by IPMC actuator

In Fig. 7.20, the table have rotatory movement while moving down with a combination of straight and the sloped version of the IPMC actuator.

As it was demonstrated in earlier chapters, a single form of a paired actuator/sensor membrane would give control over the motion and force of the tip of the assembly (Fig. 7.21). The actuators in these figures have a linear function in generating movements or tip blocking force.

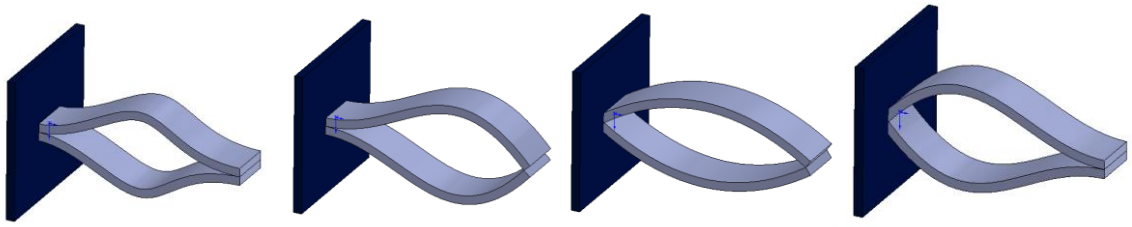

Fig. 7.21 Symmetric form of paired IPMC actuator sensor

In Fig. 7.22, asymmetric function of the different boundary conditions at the attached ends demonstrated. The actual position of the endpoint depends on the force balance of each membrane and related boundary conditions. The analysis will be having two IPMCs with attached endpoints and different boundary conditions.

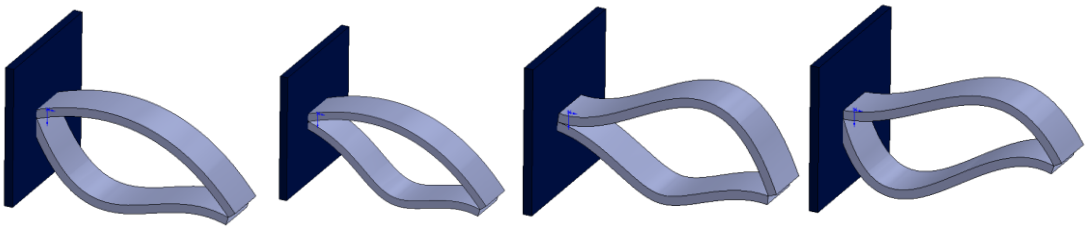

Fig. 7.22 Asymmetric form of paired IPMC actuators/sensors

7.4 A single walking form of the IPMC actuator/sensor

Using a single strip of IPMC also have lots of potential capacity. Using two IPMC, strips with alternating electrodes, as demonstrated in Fig. 7.23 will give the walking capability for a robot with two IPMC legs like a biped. However, the concept will have more load carrying limitations and stability issues, and the pattern coating seems to be necessary for this formation.

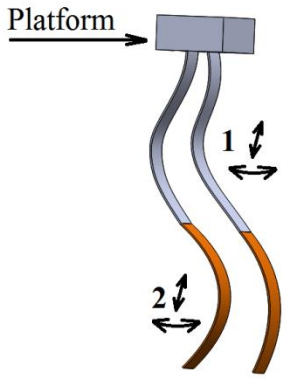

Fig. 7.23 Walking biped with tow strip of IPMCs for each leg

In case of attaching several strips of IPMCs or having a long strip of IPMC with separated conductive coating area, it is possible to make a snake like robot. In this case, a non-restricted movement consists of a combination of several circular curved motions. A similar formation introduced by Kamamichi et al. (2005)[45]. The originality here is that in this configuration, the whole will act as an active element. These movements are able to create snake-like movements to move the whole system.

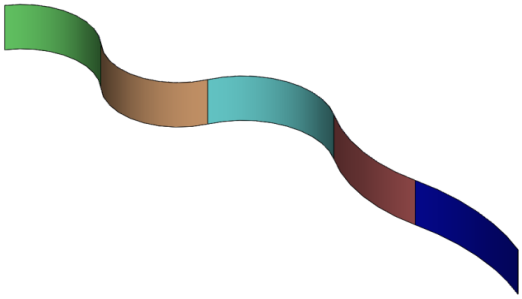

Fig. 7.24 Attachment of several IPMC strips to form a snake-like-robot

7.5 Non-conventional forms and devices

Using the concept of the helical actuator sensor for a soft screwdriver in Fig. 7.25. In this device, the forward force by the handle will cause the driver to turn the tip while its expansion gives feedback to the system to push the screwdriver inward. Knowing the relationship between the turn of the screwdriver and the axial force, one can calibrate the sensing feedback signal from the helical sensor knowing the limits of the applied load and torque.

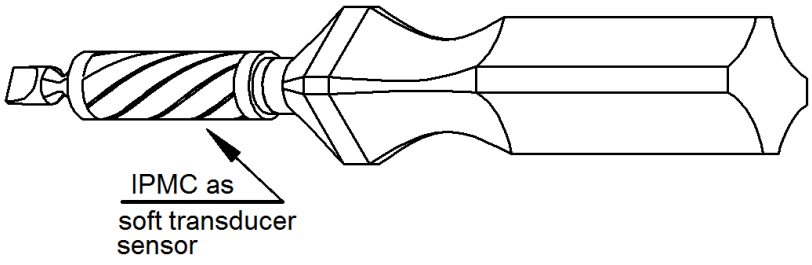

Fig. 7.25 Application concept of slit cylindrical helical IPMC

The other application for this material, as IPMC material, is soft curvature control. An example of these types of undulating structures is illustrated in Fig. 7.26.

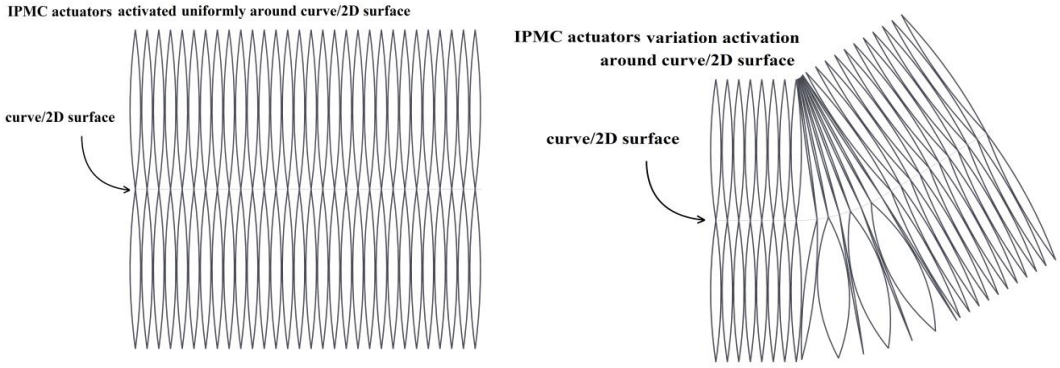

Fig. 7.26 Smooth curvature controller

This formation can be expanded to 3D scope manipulation to have a metamaterial or a robotic arm. Fig. 7.27 illustrates such 3-D undulating soft robots. Another example of this concept was introduced in Fig. 7.4, Fig. 7.14, Fig. 7.16, and Fig. 7.17.

Fig. 7.27 3D curve controller made by pairs assemblies of IPMC strips

Another concept for a preformed strip is a rolled IPMC sample as in a shaft with an angle controller, as shown in Fig. 7.28. In this application, the pre-rolled IPMC is attached to a shaft and by receiving input voltage is able to rotate the shaft.

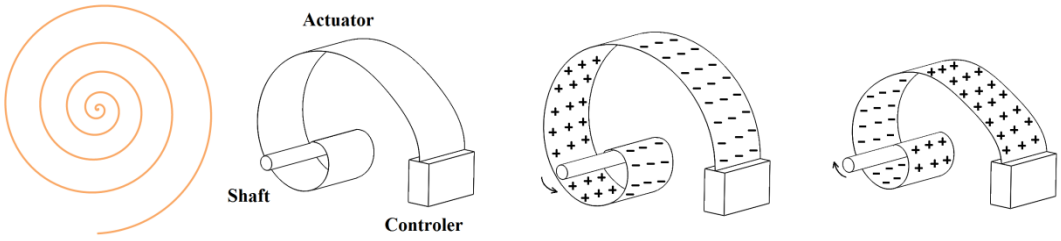

Fig. 7.28 Using IPMC as a shaft Controller to rotate a shaft

One of the characteristics of these groups of material as used in other formats and configurations is their volume expansion and contraction. This characteristic is interesting in creating novel mechanical and robotic metamaterials, as shown in Fig. 7.29 through Fig. 7.32.

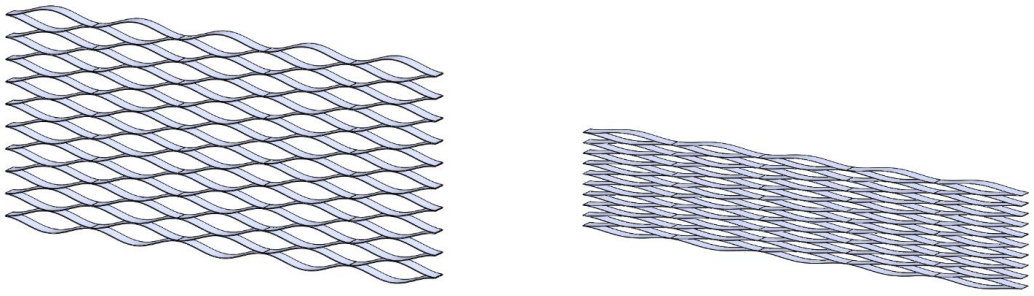

Fig. 7.29 2D metamaterials made with an assembly of pairs of IPMC strips

This concept can also be extended to a 3D mechanical metamaterials made with assemblies of IPMC strips, as shown in Fig. 7.30.

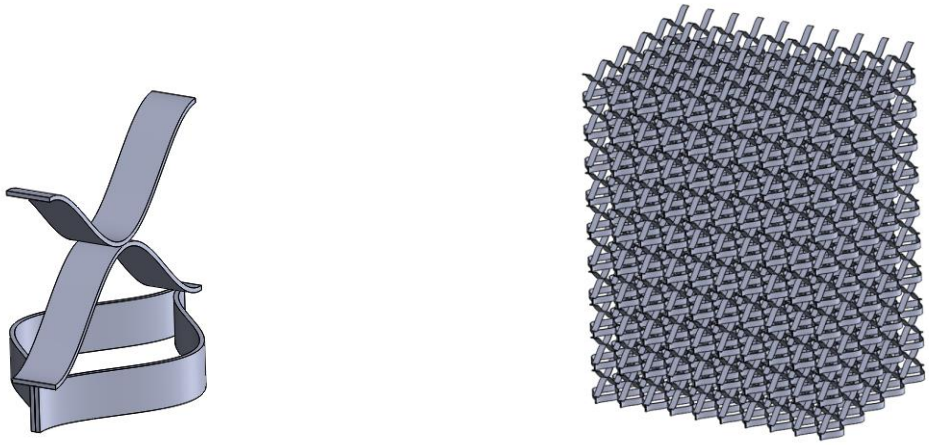

Fig. 7.30 3D metamaterial element made with pairs of IPMC strips

Some other possible configurations for robotic 2D mechanical metamaterials are presented in Fig. 7.31 and Fig. 7.32.

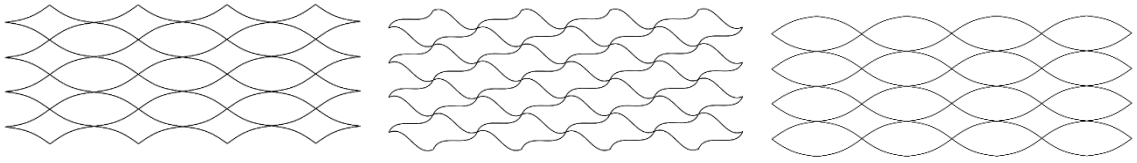

Fig. 7.31 2D metamaterial made with IPMC in a different formation

Formation in Fig. 7.31 and Fig. 7.32 generated by actuation of IPMC strip elements in the structure.

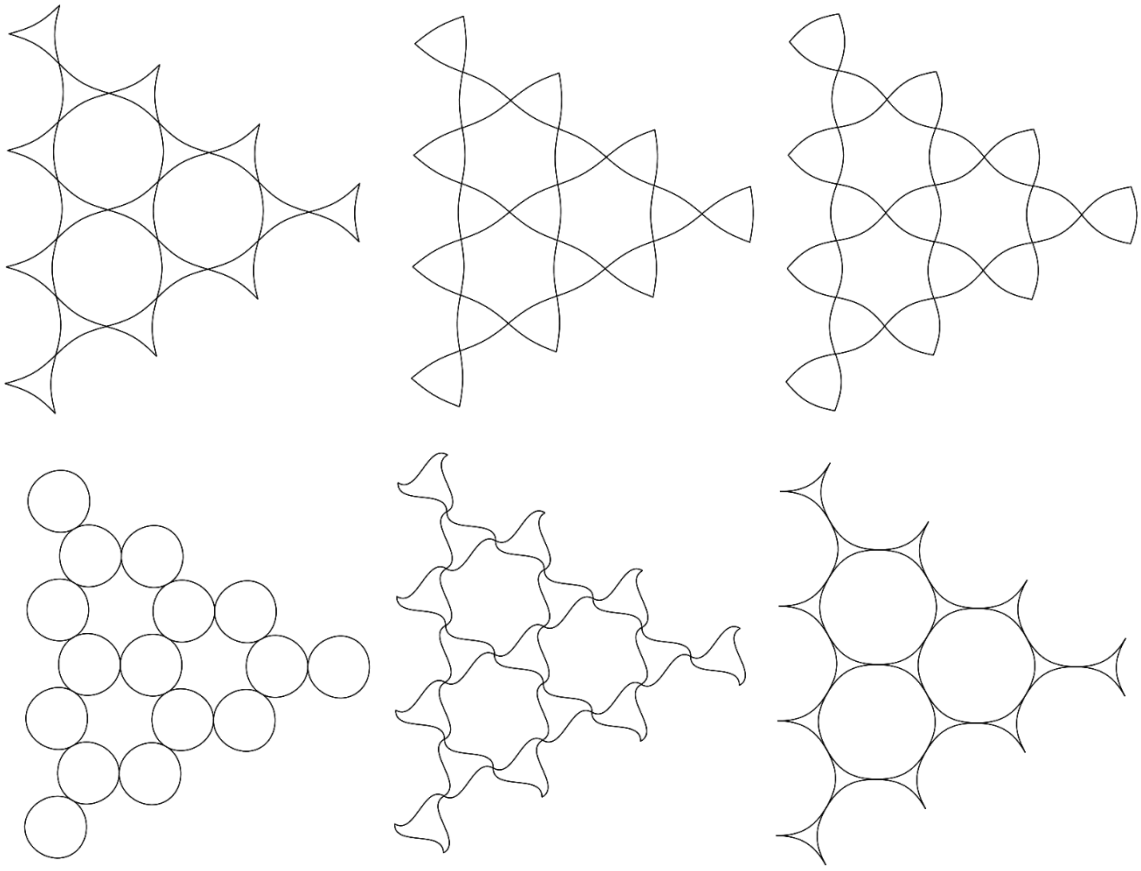

Fig. 7.32 Robotic 2D mechanical metamaterial

CHAPTER 8

8 CONCLUSION

This dissertation described IPMCs in terms of their chemical structure and characteristics as well as their manufacturing process. The applications of these materials in the form of actuator, sensor, and energy harvester were discussed thoroughly in a literature review. The literature review also includes electromechanical modeling as well as some of the experimental results and test reports. The selected test reports are towards the application of IPMCs.

In order to introduce the configurations, modeling of IPMC in sensing mode and actuation mode were studied first. As the deformations are large, nonlinear beam theory is considered to be the proper modeling approach. These mechanical models define the shapes of the fundamental elements for the configurations. For the IPMC assembly, new parameters were considered and were addressed by introducing a decision-making algorithm. These configurations are in the form of looped, flat assembly, slit cylindrical, tubular, and helical.

A mathematical model for each of the configurations or their fundamental elements was provided. A series of experimental tests were carried out to show the actuation and sensing signals of some of the configurations and the rest considered for future studies.

The combination of these IPMC actuators and sensors were shown to make biomimetic soft robotic devices. These configurations give more insights to the applications of IPMCs in robotic surgery, soft robotics, biomimetic soft robots, and medical implants. Also, the extension of the presented configurations to mechanical metamaterials and future research was presented.

BIBLIOGRAPHY

1. Fallahi A, Bahramzadeh Y, Tabatabaie SE, Shahinpoor M. A novel multifunctional soft robotic transducer made with poly (ethylene-co-methacrylic acid) ionomer metal nanocomposite. *Int J Intell Robot Appl*. 2017;1(2):143-156. doi:10.1007/s41315-017-0013-y

2. Mojarrad M, Shahinpoor M. Ion-exchange-metal composite sensor films. In: Claus RO, ed. *Smart Sensing, Processing, and Instrumentation*. ; 1997:52-60. doi:10.1117/12.275724

3. Grodzinsky AJ, Melcher JR. Electromechanical Transduction with Charged Polyelectrolyte Membranes. *IEEE Trans Biomed Eng*. 1976;BME-23(6):421-433. doi:10.1109/TBME.1976.324600

4. Mojarrad M. Characterization and modeling of ionic polymeric smart materials as artificial muscles and robotic swimming structures. 2001.

5. Hong W, Zhao X, Suo Z. Large deformation and electrochemistry of polyelectrolyte gels. *J Mech Phys Solids*. 2010;58(4):558-577. doi:10.1016/j.jmps.2010.01.005

6. Shahinpoor M, Bar-Cohen Y, Simpson JO, Smith J. Ionic polymer-metal composites (IPMCs) as biomimetic sensors, actuators and artificial muscles - a review. *Smart Mater Struct*. 1998;7(6):R15-R30. doi:10.1088/0964-1726/7/6/001

7. Shahinpoor M. Ionic polymer-conductor composites as biomimetic sensors, robotic actuators and artificial muscles - A review. *Electrochim Acta*. 2003;48(14-16 SPEC.):2343-2353. doi:10.1016/S0013-4686(03)00224-X

8. Tadokoro S, Yamagami S, Takamori T, Oguro K. An actuator model of ICPF for robotic applications on the basis of physicochemical hypotheses. *Int Conf Robot Autom*. 2002;(April):1340-1346. doi:10.1109/robot.2000.844784

9. Shahinpoor M, ed. *Ionic Polymer Metal Composites (IPMCs)*. Vol 2. The Royal Society of Chemistry; 2016. doi:10.1039/9781782627234

10. Baek S, Srinivasa AR. Modeling of the pH-sensitive behavior of an ionic gel in the presence of diffusion. *Int J Non Linear Mech*. 2004;39(8):1301-1318. doi:10.1016/j.ijnonlinmec.2003.10.001

11. Heitner-Wirguin C. Recent advances in perfluorinated ionomer membranes: structure, properties and applications. *J Memb Sci*. 1996;120(1):1-33. doi:10.1016/0376-7388(96)00155-X

12. Kolde JA, Bahar B, Wilson MS, Zawodzinski TA, Gottesfeld S. Advanced Composite Polymer Electrolyte Fuel Cell Membranes. *ECS Proc Vol*. 2019;1995-23:193-201. doi:10.1149/199523.0193pv

13. Bahramzadeh Y, Shahinpoor M. A Review of Ionic Polymeric Soft Actuators and Sensors. *Soft Robot*. 2014;1(1):38-52. doi:10.1089/soro.2013.0006

14. Seidi M, Hajiaghamemar M, Tabatabaie E, Shahinpoor M. Ionic Polymer-Metal Composites (IPMCs) as Impact Sensors. In: *Volume 1: Development and Characterization of Multifunctional Materials; Mechanics and Behavior of Active Materials; Modeling, Simulation and Control of Adaptive Systems*. ASME; 2015:V001T02A002. doi:10.1115/SMASIS2015-8842

15. Shahinpoor M, Tabatabaie E. Soft Biomimetic Robotic Looped Haptic Feedback Sensors Mohsen. *J Robot Eng Automa- tionTechnology*. 2018;2018(01). doi:10.29011/JREAT-102/100002

16. Gupta P, Vermani K, Garg S. Hydrogels: from controlled release to pH-responsive drug delivery. *Drug Discov Today*. 2002;7(10):569-579. doi:10.1016/S1359-6446(02)02255-9

17. Sung Wan Kim, Chaul Min Paii, Kimiko M, et al. Self-regulated glycosylated insulin delivery. *J Control Release*. 1990;11(1-3):193-201. doi:10.1016/0168-3659(90)90132-D

18. Mika AM, Childs RF, Dickson JM. Salt separation and hydrodynamic permeability of a porous membrane filled with pH-sensitive gel. *J Memb Sci*. 2002;206(1-2):19-30. doi:10.1016/S0376-7388(01)00474-4

19. HAMLEN RP, KENT CE, SHAFER SN. Electrolytically activated contractile polymer [15]. *Nature*. 1965;206(4989):1149-1150. doi:10.1038/2061149b0

20. TANAKA T, NISHIO I, SUN S-T, UENO-NISHIO S. Collapse of Gels in an Electric Field. *Science (80-)*. 1982;218(4571):467-469. doi:10.1126/science.218.4571.467

21. Siddique J, Ahmed A, Aziz A, Khalique C. A Review of Mixture Theory for Deformable Porous Media and Applications. *Appl Sci*. 2017;7(9):917. doi:10.3390/app7090917

22. De Gennes PG, Okumura K, Shahinpoor M, Kim KJ. Mechanoelectric effects in ionic gels. *Europhys Lett*. 2000;50(4):513-518. doi:10.1209/epl/i2000-00299-3

23. Porfiri M. An electromechanical model for sensing and actuation of ionic polymer metal composites. *Smart Mater Struct*. 2009;18(1):015016. doi:10.1088/0964-1726/18/1/015016

24. Nemat-Nasser S, Li JY. Electromechanical response of ionic polymer-metal composites. *J Appl Phys*. 2000;87(7):3321-3331. doi:10.1063/1.372343

25. Swaminathan N, Qu J, Sun Y. An electrochemomechanical theory of defects in ionic solids. Part II. Examples. *Philos Mag*. 2007;87(11):1723-1742. doi:10.1080/14786430601102981

26. Tiwari R, Kim KJ. Disc-shaped ionic polymer metal composites for use in mechano-electrical applications. *Smart Mater Struct*. 2010;19(6). doi:10.1088/0964-1726/19/6/065016

27. Asaka K, Oguro K. Active Microcatheter and Biomedical Soft Devices Based on IPMC Actuators. In: Carpi F, Smela E, eds. *Biomedical Applications of Electroactive Polymer Actuators*. Chichester, UK, UK: John Wiley & Sons, Ltd; 2009:121-136. doi:10.1002/9780470744697.ch6

28. Lee SJ, Han MJ, Kim SJ, Jho JY, Lee HY, Kim YH. A new fabrication method for IPMC actuators and application to artificial fingers. *Smart Mater Struct*. 2006;15(5):1217-1224. doi:10.1088/0964-1726/15/5/008

29. Bonomo C, Bottino M, Brunetto P, et al. Tridimensional ionic polymer metal composites: optimization of the manufacturing techniques. *Smart Mater Struct*. 2010;19(5):055002. doi:10.1088/0964-1726/19/5/055002

30. Trabia S, Hwang T, Kim KJ. A fabrication method of unique Nafion® shapes by painting for ionic polymer–metal composites. *Smart Mater Struct*. 2016;25(8):085006. doi:10.1088/0964-1726/25/8/085006

31. Kim KJ, Shahinpoor M. Development of three-dimensional polymeric artificial muscles. In: Bar-Cohen Y, ed. *Electroactive Polymer Actuators and Devices*. ; 2001:223. doi:10.1117/12.432650

32. Kim KJ, Shahinpoor M. A novel method of manufacturing three-dimensional ionic polymer-metal composites (IPMCs) biomimetic sensors, actuators and artificial muscles. *Polymer (Guildf)*. 2001;43(3):797-802. doi:10.1016/S0032-3861(01)00648-6

33. Kim KJ, Shahinpoor M. Ionic polymer metal composites: II. Manufacturing techniques. *Smart Mater Struct*. 2003;12(1):65-79. doi:10.1088/0964-1726/12/1/308

34. Noonan C, Tajvidi M, Tayeb AH, Shahinpoor M, Tabatabaie SE. Structure-Property Relationships in Hybrid Cellulose Nanofibrils/Nafion-Based Ionic Polymer-Metal Composites. *Materials (Basel)*. 2019;12(8):1269. doi:10.3390/ma12081269

35. Hwang T, Palmre V, Nam J, Lee D, Kim KJ. A new ionic polymer–metal composite based on Nafion/poly(vinyl alcohol- co -ethylene) blends. *Smart Mater Struct*. 2015;24(10):105011. doi:10.1088/0964-1726/24/10/105011

36. Shahinpoor M, Kim KJ. Novel ionic polymer-metal composites equipped with physically loaded particulate electrodes as biomimetic sensors, actuators and artificial muscles. *Sensors Actuators, A Phys*. 2002;96(2-3):125-132. doi:10.1016/S0924-4247(01)00777-4

37. Punning A, Kruusmaa M, Aabloo A. Surface resistance experiments with IPMC sensors and actuators. *Sensors Actuators, A Phys*. 2007;133(1):200-209. doi:10.1016/j.sna.2006.03.010

38. Zhao D, Li D, Wang Y, Chen H. Improved manufacturing technology for producing porous Nafion for high-performance ionic polymer–metal composite actuators. *Smart Mater Struct*. 2016;25(7):075043. doi:10.1088/0964-1726/25/7/075043

39. Rinne P, Põldsalu I, Johanson U, et al. Encapsulation of ionic electromechanically active polymer actuators. *Smart Mater Struct*. 2019. doi:10.1088/1361-665X/ab18c0

40. Barramba J, Silva J, Costa Branco PJ. Evaluation of dielectric gel coating for encapsulation of ionic polymer-metal composite (IPMC) actuators. *Sensors Actuators, A Phys*. 2007;140(2):232-238. doi:10.1016/j.sna.2007.06.035

41. Duncan AJ, Leo DJ, Long TE. Beyond Nafion: Charged Macromolecules Tailored for Performance as Ionic Polymer Transducers. *Macromolecules*. 2008;41(21):7765-7775. doi:10.1021/ma800956v

42. Osborn AM, Moore RB. *Morphology of Proton Exchange Membranes*. Vol 10. Elsevier B.V.; 2012. doi:10.1016/B978-0-444-53349-4.00288-0

43. Lei H, Li W, Tan X. Encapsulation of ionic polymer-metal composite (IPMC) sensors with thick parylene: Fabrication process and characterization results. *Sensors Actuators, A Phys*. 2014;217:1-12. doi:10.1016/j.sna.2014.05.013

44. Punning A, Anton M, Kruusmaa M, Aabloo A. A Biologically Inspired Ray - like Underwater Robot with Electroactive Polymer Pectoral Fins. *Int IEEE Conf mechatronics Robot*. 2004:241-245.

45. Yamakita M, Kamamichi N, Kozuki T, Asaka K, Luo ZW. A snake-like swimming robot using IPMC actuator and verification of doping effect. *2005 IEEE/RSJ Int Conf Intell Robot Syst IROS*. 2005:3333-3338. doi:10.1109/IROS.2005.1545485

46. Paquetre JW, Kim KJ, Yim W. Aquatic robotic propulsor using ionic polymer-metal composite artificial muscle. In: *2004 IEEE/RSJ International Conference on Intelligent Robots and Systems (IROS) (IEEE Cat. No.04CH37566)*. Vol 2. IEEE; 2005:1269-1274. doi:10.1109/IROS.2004.1389570

47. Sadeghipour K, Salomon R, Neogi S. Development of a novel electrochemically active membrane and "smart" material based vibration sensor/damper. *Smart Mater Struct*. 1992;1(2):172-179. doi:10.1088/0964-1726/1/2/012

48. Ferrara L, Shahinpoor M, Kim KJ, et al. Use of ionic polymer-metal composites (IPMCs) as a pressure transducer in the human spine. In: Bar-Cohen Y, ed. *Electroactive Polymer Actuators and Devices*. ; 1999:394-401. doi:10.1117/12.349704

49. Martin BR. Energy Harvesting Applications of Ionic Polymers. *Mech Eng*. 2005.

50. Millet P, Durand R, Pineri M. Preparation of new solid polymer electrolyte composites for water electrolysis. *Int J Hydrogen Energy*. 1990;15(4):245-253. doi:10.1016/0360-3199(90)90043-X

51. Esmaeli E, Ganjian M, Rastegar H, Kolahdouz M, Kolahdouz Z, Zhang GQ. Humidity sensor based on the ionic polymer metal composite. *Sensors Actuators, B Chem*. 2017;247:498-504. doi:10.1016/j.snb.2017.03.018

52. Lei H, Lim C, Tan X. Humidity-dependence of IPMC sensing dynamics: characterization and modeling from a physical perspective. *Meccanica*. 2015;50(11):2663-2673. doi:10.1007/s11012-015-0164-6

53. Chen W-H, Lu J-S, Su G-DJ. Ionic polymer metal composite for an optical zoom in a compact camera. *Opt Express*. 2015;23(10):13265. doi:10.1364/oe.23.013265

54. Smoukov SK, Wang T, Farajollahi M, et al. Electroactive polymers for sensing. *Interface Focus*. 2016;6:1-19. doi:10.1098/rsfs.2016.0026

55. Nakabo Y, Mukai T, Asaka K. *Biomimetic Soft Robots Using IPMC*.; 2007. doi:10.1007/978-1-84628-372-7_7

56. Abdulsadda AT, Tan X. An artificial lateral line system using IPMC sensor arrays. *Int J Smart Nano Mater*. 2012;3(3):226-242. doi:10.1080/19475411.2011.650233

57. Ando B, Baglio S, Beninato A, Graziani S, Pagano F, Umana E. A Seismic Sensor Based on IPMC Combined With Ferrofluids. *IEEE Trans Instrum Meas*. 2013;62(5):1292-1298. doi:10.1109/TIM.2012.2232473

58. Paola B, Fortuna L, Giannone P, Graziani S, Strazzeri S. IPMCs as vibration sensors. *Conf Rec - IEEE Instrum Meas Technol Conf*. 2008:2065-2069. doi:10.1109/IMTC.2008.4547388

59. Bonomo C, Brunetto P, Fortuna L, Giannone P, Graziani S, Strazzeri S. A tactile sensor for biomedical applications based on IPMCs. *IEEE Sens J*. 2008;8(8):1486-1493. doi:10.1109/JSEN.2008.920723

60. Brunetto P, Fortuna L, Giannone P, Graziani S, Pagano F. A small scale viscometer based on an IPMC actuator and an IPMC sensor. *2010 IEEE Int Instrum Meas Technol Conf I2MTC 2010 - Proc*. 2010:585-589. doi:10.1109/IMTC.2010.5488156

61. Ming Y, Yang Y, Fu RP, et al. IPMC Sensor Integrated Smart Glove for Pulse Diagnosis, Braille Recognition, and Human–Computer Interaction. *Adv Mater Technol*. 2018;3(12):1-8. doi:10.1002/admt.201800257

62. Hong W, Almomani A, Montazami R. Electrochemical and morphological studies of ionic polymer metal composites as stress sensors. *Meas J Int Meas Confed*. 2017;95:128-134. doi:10.1016/j.measurement.2016.09.036

63. Lei H, Sharif MA, Tan X. Dynamics of omnidirectional IPMC sensor: Experimental characterization and physical modeling. *IEEE/ASME Trans Mechatronics*. 2016;21(2):601-612. doi:10.1109/TMECH.2015.2468080

64. Tsugawa MA. Development of a Tube-Shaped Ionic Polymer-Metal Composite Actuator with Integrated Sensing. 2014;(December).

65. Gudarzi M, Smolinski P, Wang QM. Compression and shear mode ionic polymer-metal composite (IPMC) pressure sensors. *Sensors Actuators, A Phys*. 2017;260:99-111. doi:10.1016/j.sna.2017.04.010

66. Gudarzi M, Smolinski P, Wang QM. Bending mode ionic polymer-metal composite (IPMC) pressure sensors. *Meas J Int Meas Confed*. 2017;103:250-257. doi:10.1016/j.measurement.2017.02.029

67. Shahinpoor M, Kim KJ. Ionic polymer-metal composites: III. Modeling and simulation as biomimetic sensors, actuators, transducers, and artificial muscles. *Smart Mater Struct*. 2004;13(6):1362-1388. doi:10.1088/0964-1726/13/6/009

68. Bahramzadeh Y, Shahinpoor M. Dynamic curvature sensing employing ionic-polymer-metal composite sensors. *Smart Mater Struct*. 2011;20(9). doi:10.1088/0964-1726/20/9/094011

69. Song DS, Han DG, Rhee K, Kim DM, Jho JY. Fabrication and characterization of an ionic polymer-metal composite bending sensor. *Macromol Res*. 2017;25(12):1205-1211. doi:10.1007/s13233-017-5156-z

70. Cellini F, Pounds J, Peterson SD, Porfiri M, Por M. Underwater energy harvesting from a turbine hosting ionic polymer metal composites. *Smart Mater Struct*. 2014;23(8). doi:10.1088/0964-1726/23/8/085023

71. Patel M, Mukherjee S. Modelling and analysis of ionic polymer metal composite based energy harvester. *Mater Today Proc*. 2018;5(9):19815-19827. doi:10.1016/j.matpr.2018.06.345

72. Sharif MA, Lei H, Al-rubaiai MK, Tan X. Ionic polymer-metal composite torsional sensor: Physics-based modeling and experimental validation. *Smart Mater Struct*. 2018;27(7). doi:10.1088/1361-665X/aac364

73. Giacomello A, Porfiri M. Underwater energy harvesting from a heavy flag hosting ionic polymer metal composites. *J Appl Phys*. 2011;109(8). doi:10.1063/1.3569738

74. Oguro K, Takenaka H, Kawami Y, et al. ACTUATOR ELEMENT. 1932;2(12).

75. Shahinpoor M, Mojarrad M. Ionic Polymer Sensors and Actuators. 2002;2(12).

76. Shahinpoor M, Kim KJ. METHOD OF FABRICATING A DRY ELECTRO-aCTIVE POLYMERIC SYNTHETIC MUSCLE. 2007. https://linkinghub.elsevier.com/retrieve/pii/0375650585900112.

77. Doi M, Matsumoto M, Hirose Y. Deformation of Ionic Polymer Gels by Electric Fields. *Macromolecules*. 1992;25(20):5504-5511. doi:10.1021/ma00046a058

78. Osada Y, Okuzaki H, Hori H. A polymer gel with electrically driven motility. *Nature*. 1992;355(6357):242-244. doi:10.1038/355242a0

79. Bonomo C, Fortuna L, Giannone P, Graziani S. A sensor-actuator integrated system based on IPMCs. *Proc IEEE Sensors, 2004*. 2006:489-492. doi:10.1109/icsens.2004.1426207

80. Fang BK, Lin CCK, Ju MS. Development of sensing/actuating ionic polymer-metal composite (IPMC) for active guide-wire system. *Sensors Actuators, A Phys*. 2010;158(1):1-9. doi:10.1016/j.sna.2009.12.001

81. Shahinpoor M. Conceptual design, kinematics and dynamics of swimming robotic structures using ionic polymeric gel muscles. *Smart Mater Struct*. 1992;1(1):91-94. doi:10.1088/0964-1726/1/1/014

82. Guo S, Fukuda T, Asaka K. A new type of fish-like underwater microrobot. *IEEE/ASME Trans Mechatronics*. 2003;8(1):136-141. doi:10.1109/TMECH.2003.809134

83. Katz SL, Jordan CE. A case for building integrated models of aquatic locomotion that couple internal and external forces. *... Untethered Submers Tech Proc Sp Ses ...*. 1997. http://www.dtic.mil/cgi-bin/GetTRDoc?AD=ADA330550#page=139%0Apapers3://publication/uuid/E667C91F-6971-4565-9553-9B248F96E2BD.

84. Kim B, Kim DH, Jung J, Park JO. A biomimetic undulatory tadpole robot using ionic polymer-metal composite actuators. *Smart Mater Struct*. 2005;14(6):1579-1585. doi:10.1088/0964-1726/14/6/051

85. Jung J, Tak Y, Kim B, Park J-O, Lee S-K, Pak J. Tadpole Robot (TadRob) using ionic polymer metal composite (IPMC) actuator. *Smart Struct Mater 2003 Electroact Polym Actuators Devices*. 2003;5051(October):272. doi:10.1117/12.484299

86. Chu WS, Lee KT, Song SH, et al. Review of biomimetic underwater robots using smart actuators. *Int J Precis Eng Manuf*. 2012;13(7):1281-1292. doi:10.1007/s12541-012-0171-7

87. Arena P, Bonomo C, Fortuna L, Frasca M, Graziani S. Design and control of an IPMC wormlike robot. *IEEE Trans Syst Man, Cybern Part B Cybern*. 2006;36(5):1044-1052. doi:10.1109/TSMCB.2006.873188

88. Guo S, Fukuda T, Arai F, Oguro K, Negoro M, Nakamura T. Micro active guide wire catheter system. In: *Proceedings 1995 IEEE/RSJ International Conference on Intelligent Robots and Systems. Human Robot Interaction and Cooperative Robots*. Vol 2. IEEE Comput. Soc. Press; 2002:172-177. doi:10.1109/IROS.1995.526156

89. Lumia R, Shahinpoor M. IPMC microgripper research and development. *J Phys Conf Ser*. 2008;127. doi:10.1088/1742-6596/127/1/012002

90. Ford S, Macias G, Lumia R. Single active finger IPMC microgripper. *Smart Mater Struct*. 2015;24(2):025015. doi:10.1088/0964-1726/24/2/025015

91. Gonzalez C, Lumia R. An IPMC microgripper with integrated actuator and sensing for constant finger-tip displacement. *Smart Mater Struct*. 2015;24(5):055011. doi:10.1088/0964-1726/24/5/055011

92. Aw KC, McDaid AJ. Bio-applications of ionic polymer metal composite transducers. *Smart Mater Struct*. 2014;23(7):074005. doi:10.1088/0964-1726/23/7/074005

93. Wang Y, Liu J, Zhu D, Chen H. Active Tube-Shaped Actuator with Embedded Square Rod-Shaped Ionic Polymer-Metal Composites for Robotic-Assisted Manipulation. *Appl Bionics Biomech*. 2018;2018:1-12. doi:10.1155/2018/4031705

94. Mojarrad M, Shahinpoor M. Biomimetic robotic propulsion using polymeric artificial muscles. In: *Proceedings of International Conference on Robotics and Automation*. Vol 3. IEEE; 2002:2152-2157. doi:10.1109/ROBOT.1997.619281

95. Shahinpoor M. Ionic polymeric conductor nanocomposites (IPCNCs) as distributed nanosensors and nanoactuators. *Bioinspir Biomim*. 2008;3(3):035003. doi:10.1088/1748-3182/3/3/035003

96. Olsen ZJ, Kim KJ. A reduced dimensional mapping approach for modeling IPMCs with computational efficiency and rapid design development applications. *Smart Mater Struct*. 2018;27(12). doi:10.1088/1361-665X/aae8fc

97. Moghadam AAA, Kouzani A, Torabi K, Kaynak A, Shahinpoor M. Development of a novel soft parallel robot equipped with polymeric artificial muscles. *Smart Mater Struct*. 2015;24(3). doi:10.1088/0964-1726/24/3/035017

98. Najem J, Sarles SA, Akle B, Leo DJ. Biomimetic jellyfish-inspired underwater vehicle actuated by ionic polymer metal composite actuators. *Smart Mater Struct*. 2012;21(9). doi:10.1088/0964-1726/21/9/094026

99. Yeom S-W, Oh I-K. A biomimetic jellyfish robot based on ionic polymer metal composite actuators. *Smart Mater Struct*. 2009;18(8):085002. doi:10.1088/0964-1726/18/8/085002

100. Chen Z, Um TI, Bart-smith H. Sensors and Actuators A : Physical A novel fabrication of ionic polymer – metal composite membrane actuator capable of 3-dimensional kinematic motions. *Sensors Actuators A Phys*. 2011;168(1):131-139. doi:10.1016/j.sna.2011.02.034

101. Yamakita M, Kamamichi N, Kaneda Y, Asaka K, Luo ZW. Development of an artificial muscle linear actuator using ionic polymer-metal composites. *Adv Robot*. 2004;18(4):383-399. doi:10.1163/156855304773822473

102. Chen Z. A review on robotic fish enabled by ionic polymer–metal composite artificial muscles. *Robot Biomimetics*. 2017;4(1):24. doi:10.1186/s40638-017-0081-3

103. Nguyen KT, Ko SY, Park JO, Park S. Terrestrial Walking Robot with 2DoF Ionic Polymer-Metal Composite (IPMC) Legs. *IEEE/ASME Trans Mechatronics*. 2015;20(6):2962-2972. doi:10.1109/TMECH.2015.2419820

104. Kim MH, Kim KY, Lee JH, et al. An experimental study of force control of an IPMC actuated two-link manipulator using time-delay control. *Smart Mater Struct*. 2016;25(11):117001. doi:10.1088/0964-1726/25/11/117001

105. Shahinpoor M, Thompson MS. The Venus Flytrap as a model for a biomimetic material with built-in sensors and actuators. *Mater Sci Eng C*. 1995;2(4):229-233. doi:10.1016/0928-4931(95)00105-0

106. Shahinpoor M. Biomimetic robotic Venus flytrap (Dionaea muscipula Ellis) made with ionic polymer metal composites. *Bioinspiration and Biomimetics*. 2011;6(4):046004. doi:10.1088/1748-3182/6/4/046004

107. Shi L, Guo S. Development and evaluation of a Venus flytrap-inspired microrobot. *Microsyst Technol*. 2016;22(8):1949-1958. doi:10.1007/s00542-015-2484-9

108. Chang XL, Chee PS, Lim EH, Chong WC. Radio-frequency enabled ionic polymer metal composite (IPMC) actuator for drug release application. *Smart Mater Struct*. 2019;28(1). doi:10.1088/1361-665X/aaefd3

109. Cheong HR, Lai KC, Chee PS. A wireless powered electroactive polymer using magnetic resonant coupling. *IOP Conf Ser Mater Sci Eng*. 2018;409:012002. doi:10.1088/1757-899X/409/1/012002

110. Cheong HR, Teo CY, Leow PL, Lai KC, Chee PS. Wireless-powered electroactive soft microgripper. *Smart Mater Struct*. 2018;27(5):055014. doi:10.1088/1361-665X/aab866

111. Jackson J, Hubbard U. Design and Characterization of Sectored (Patterned) IPMC Actuators for Propulsion and Maneuvering in Bio-Inspired Underwater Systems. 2011;(August).

112. Tadokoro S, Fuji S, Fushimi M, et al. Development of a distributed actuation device consisting of soft gel actuator elements. In: *Proceedings. 1998 IEEE International Conference on Robotics and Automation (Cat. No.98CH36146)*. Vol 3. IEEE; 1998:2155-2160. doi:10.1109/ROBOT.1998.680640

113. Shuxiang Guo, Hata S, Sugumoto K, Fukuda T, Oguro K. Development of a new type of capsule micropump. In: *Proceedings 1999 IEEE International Conference on Robotics and Automation (Cat. No.99CH36288C)*. Vol 3. IEEE; 2003:2171-2176. doi:10.1109/ROBOT.1999.770428

114. Du Y, Zhao G, Sun Z, Gu Y. Bionic structure of shark's gill jet orifice based on artificial muscle. *J Cent South Univ*. 2018;25(4):855-865. doi:10.1007/s11771-018-3789-5

115. Sherif HMF. The artificial ventricle: A conceptual design for a novel mechanical circulatory support system. *Minim Invasive Ther Allied Technol*. 2009;18(3):178-180. doi:10.1080/13645700902921773

116. Shahinpoor M. Implantable Heart-Assist and Compression Devices Employing an Active Network of Electrically-Controllable Ionic Polymer–Metal Nanocomposites. In: *Biomedical Applications of Electroactive Polymer Actuators*. Chichester, UK: John Wiley & Sons, Ltd; 2009:137-159. doi:10.1002/9780470744697.ch7

117. Chatterjee D, Hanumaiah N, Bahramzadeh Y, Shahinpoor M. Actuation and Sensing Studies of a Miniaturized Five Fingered Robotic Hand Made with Ion Polymeric Metal Composite (IPMC). *Adv Mater Res*. 2013;740:492-495. doi:10.4028/www.scientific.net/AMR.740.492

118. Tadokoro S, Yamagami S, Ozawa M, Kimura T, Takamori T, Oguro K. Multi-DOF device for soft micromanipulation consisting of soft gel actuator elements. In: *Proceedings 1999 IEEE International Conference on Robotics and Automation (Cat. No.99CH36288C)*. Vol 3. IEEE; 2003:2177-2182. doi:10.1109/ROBOT.1999.770429

119. Steve T, Scott RW, Larry AR, Al S, David PM, Ned F. A MEMS-based flexible sensor and actuator system for space inflatable structures. *Smart Mater Struct*. 2001;10(6):1230. http://stacks.iop.org/0964-1726/10/i=6/a=312.

120. Chang L, Yu L, Li C, et al. Ionic polymer with single-layered electrodes: A novel strategy for ionic actuator design. *Smart Mater Struct*. 2018;27(10). doi:10.1088/1361-665X/aae00a

121. Kanno R, Tadokoro S, Hattori M, Takamori T, Costaftis M, Oguro K. Dynamic model of ICPF (ionic conducting polymer film) actuator. In: *1995 IEEE International Conference on Systems, Man and Cybernetics. Intelligent Systems for the 21st Century*. Vol 1. IEEE; 2002:177-182. doi:10.1109/ICSMC.1995.537754

122. Farinholt K, Leo DJ. Modeling of electromechanical charge sensing in ionic polymer transducers. *Mech Mater*. 2004;36(5-6):421-433. doi:10.1016/S0167-6636(03)00069-3

123. Shahinpoor M. Micro-Electro-Mechanics of Ionic Polymeric Gels As Electrically Controllable Artificial Muscles. *J Intell Mater Syst Struct*. 1995;6(3):307-314. doi:10.1177/1045389X9500600302

124. Asaka K, Oguro K. Bending of polyelectrolyte membrane platinum composites by electric stimuli. *J Electroanal Chem*. 2000;480(1-2):186-198. doi:10.1016/S0022-0728(99)00458-1

125. Porfiri M. Charge dynamics in ionic polymer metal composites. *J Appl Phys*. 2008;104(10). doi:10.1063/1.3017467

126. Aureli M, Porfiri M. Nonlinear sensing of ionic polymer metal composites. *Contin Mech Thermodyn*. 2013;25(2-4):273-310. doi:10.1007/s00161-012-0253-x

127. Nemat-Nasser S, Wu Y. Comparative experimental study of ionic polymer–metal composites with different backbone ionomers and in various cation forms. *J Appl Phys*. 2003;93(9):5255-5267. doi:10.1063/1.1563300

128. Tiwari R, Kim KJ. IPMC as a mechanoelectric energy harvester: Tailored properties. *Smart Mater Struct*. 2013;22(1). doi:10.1088/0964-1726/22/1/015017

129. Newbury K. Characterization , Modeling , and Control of Ionic Polymer Transducers by Characterization , Modeling , and Control of Ionic Polymer Transducers. *Mech Eng*. 2002;(September). https://vtechworks.lib.vt.edu/handle/10919/29012.

130. Bonomo C, Fortuna L, Giannone P, Graziani S, Strazzeri S. A model for ionic polymer metal composites as sensors. *Smart Mater Struct*. 2006;15(3):749-758. doi:10.1088/0964-1726/15/3/010

131. Nemat-Nasser S. Micromechanics of actuation of ionic polymer-metal composites. *J Appl Phys*. 2002;92(5):2899-2915. doi:10.1063/1.1495888

132. Branco PJC, Dente JA. Derivation of a continuum model and its electric equivalent-circuit representation for ionic polymer-metal composite (IPMC) electromechanics. *Smart Mater Struct*. 2006;15(2):378-392. doi:10.1088/0964-1726/15/2/019

133. Chang L, Liu Y, Niu Q, et al. Rough interface in IPMC: modeling and its influence analysis. *Smart Mater Struct*. 2018;27(7):075055. doi:10.1088/1361-665x/aaca59

134. Shen Q, Stalbaum T, Minaian N, Oh I, Kim KJ. A robotic multiple-shape-memory ionic polymer–metal composite (IPMC) actuator: modeling approach. *Smart Mater Struct*. 2019;28(1):015009. doi:10.1088/1361-665X/aaeb83

135. Vunder V, Hamburg E, Johanson U, Punning A, Aabloo A. Effect of ambient humidity on ionic electroactive polymer actuators. *Smart Mater Struct*. 2016;25(5):055038. doi:10.1088/0964-1726/25/5/055038

136. Ansaf B, Duong TH, Jaksic NI, et al. Influence of Humidity and Actuation time on Electromechanical Characteristics of Ionic Polymer-Metal Composite Actuators. *Procedia Manuf*. 2018;17:960-967. doi:10.1016/j.promfg.2018.10.148

137. Zhu Z, Horiuchi T, Kruusamäe K, et al. The effect of ambient humidity on the electrical response of ion-migration-based polymer sensor with various cations. *Smart Mater Struct*. 2016;25(5):055024. doi:10.1088/0964-1726/25/5/055024

138. Shahinpoor M, Kim KJ. Ionic polymer–metal composites: IV. Industrial and medical applications. *Smart Mater Struct*. 2005;14(1):197-214. doi:10.1088/0964-1726/14/1/020

139. Dominik I, Kwaśniewski J, Kaszuba F. Ionic polymer-metal composite displacement sensors. *Sensors Actuators, A Phys*. 2016;240:10-16. doi:10.1016/j.sna.2016.01.047

140. Palmre V, Kim SJ, Pugal D, Kim K. Improving electromechanical output of IPMC by high surface area Pd-Pt electrodes and tailored ionomer membrane thickness. *Int J Smart Nano Mater*. 2014;5(2):99-113. doi:10.1080/19475411.2014.914108

141. Tabatabaie SE, Mohsen Shahinpoor. Novel Configurations of Slit Tubular Soft Robotic Actuators and Sensors made with Ionic Polymer Metal Composites (IPMCs). *Robot Autom Eng J*. 2018;3(4):1-10. doi:10.19080/raej.2018.03.555616

142. Shen Q, Stalbaum T, Minaian N, Oh I. A robotic multiple-shape-memory ionic polymer – metal composite (IPMC) actuator : modeling approach. 2019.

143. Lughmani WA, Jho JY, Lee JY, Rhee K. Modeling of bending behavior of IPMC beams using concentrated ion boundary layer. *Int J Precis Eng Manuf*. 2009;10(5):131-139. doi:10.1007/s12541-009-0104-2

144. Mehran Mojarrad MS. lon-Exchange-Metal composite sensor films. *Smart Struct Mater*. 1997:52-60.

145. Nayfeh AH, Emam SA. Exact solution and stability of postbuckling configurations of beams. *Nonlinear Dyn*. 2008;54(4):395-408. doi:10.1007/s11071-008-9338-2

146. Moeinkhah H, Rezaeepazhand J, Akbarzadeh A, Oh I-KK. Accurate Dynamic Modeling of Helical Ionic Polymer-Metal Composite Actuator Based on Intrinsic Equations. *IEEE/ASME Trans Mechatronics*. 2015;20(4):1680-1688. doi:10.1109/TMECH.2014.2347356

147. Li SL, Kim WY, Cheng TH, Oh IK. A helical ionic polymer-metal composite actuator for radius control of biomedical active stents. *Smart Mater Struct*. 2011;20(3). doi:10.1088/0964-1726/20/3/035008

148. Nategh MJ, Tabatabaie SE. An enhanced methodical approach to machine tool design procedure. *Proc Inst Mech Eng Part B J Eng Manuf*. 2008;222(2):309-318. doi:10.1243/09544054JEM760

149. Shoup TE, McLarnan CW. On the Use of the Undulating Elastica for the Analysis of Flexible Link Mechanisms. *J Eng Ind*. 1971;93(1):263. doi:10.1115/1.3427884

BIOGRAPHY OF THE AUTHOR

Seyed Ehsan Tabatabaie was born in Iran, July 1978. He spent elementary school in several cities around the country. He stayed with his family up to end of the college when he was admitted for a Mechanical Engineering program through national entrance exam to Mazandaran University in 1997. Graduating with a Bachelor of Science Degree in Mechanical Engineering-Manufacturing and Production, He was admitted to the Modares University in 2003 to pursue a Master of Science degree in Mechanical Engineering-Manufacturing and Production. He graduated from the Modares University in 2006. He continued working part-time in different engineering fields mostly related to design and manufacturing before starting to work as a research and developer engineer at CROUSE (P.J.S) Co. in Automotive Industry. He was working fulltime for three years in this field on different projects and innovations. He then was admitted into the Ph.D. program at The University of Maine in 2013 for the doctoral program in the Department of Mechanical Engineering. He is a candidate for the Doctor of Philosophy degree in Mechanical Engineering from The University of Maine in August 2019.